

**Remodeling of Zinc Homeostasis
In Differentiated Mammary Epithelial Cells**

by

Yu Han

M.S., Chinese Academy of Sciences, 2011

B.E., Ocean University of China, 2008

A thesis submitted to the

Faculty of the Graduate School of the University of Colorado

in partial fulfillment of the requirements for the degree of Doctor of Philosophy

College of Arts & Sciences

Department of Biochemistry

2018

This thesis entitled:

“Remodeling of Zinc Homeostasis In Differentiated Mammary Epithelial Cells”

written by Yu Han

has been approved for the College Arts & Sciences Department of Biochemistry

Amy. E. Palmer

Natalie Ahn

Date _____

The final copy of this thesis has been examined by the signatories, and we find that both the content and the form meet acceptable presentation standards of scholarly work in the above mentioned discipline.

Han, Yu (Ph.D., Biochemistry)

“Remodeling of Zinc Homeostasis In Differentiated Mammary Epithelial Cells”

Thesis directed by Prof. Amy E. Palmer

Zinc is the second most abundant transition metal in mammals and an essential nutrient required for growth. Coupled with the biological significance of zinc, zinc homeostasis needs to be tightly controlled because too little zinc leads to zinc deficiency and too much zinc is toxic. Unfortunately, most of our understanding of zinc homeostasis regulation to date was obtained using non-physiological manipulation *via* external supplementation or depletion of zinc, which can cause non-specific side effects. A systematic study of zinc homeostasis regulation under physiological condition is needed for a better understanding of how mammalian cells balance zinc distribution to fulfill biological functions. In this study, I hypothesized that the mammary epithelial cells (MECs) distribute and utilize zinc differently during cell differentiation to meet the altered need for zinc among subcellular compartments, as well as to actively secrete zinc into mother’s milk on a daily basis. Using a mouse MEC cell line (HC11) as a model system, the differential expression of zinc-dependent and zinc-homeostasis genes during cell differentiation was systematically examined using RNAseq. My findings reveal an increase of lysosomal Zn^{2+} and cytosolic Zn^{2+} at the early and late stage of differentiation, respectively. Importantly, I discovered that the induced expression of ZIP14, a cortisol-induced zinc transporter responsible for importing Zn^{2+} into cytosol, was crucial for the production of the most important milk protein (WAP), which suggested a link between zinc homeostasis and milk production.

Dedication

To my great grandparents and parents, without whom I would not be who I am.

Acknowledgement

Firstly, I would like to thank my grandparents, Yunhu Zhang and Weiqing Yu, for the countless care and love I received throughout my childhood. They were imprinted in my earliest memories. I will not forget the delicious meals made by my grandma and the chess games I played with my grandpa. I will not forget that my grandpa took my cousin and me to swimming everyday in summer, with me sitting in the front and my cousin sitting in the back of his bicycle. I will also not forget the stories my grandma told me that as a nurse how she took care of injured soldiers during wartime or how funny it was to her when her students humiliated her during a Chinese political movement. I did not fully understand the hardship they went through until I became a mom and tried to get my Ph.D. at the same time. It is their spirit and love that fostered my courage to embrace new challenges.

Secondly, I want to thank my mom, Li Yu and Baoan Han for 32 years of continuous love. As a single child, I received all the attention and love in the family but luckily, I did not turn out to be a spoiled child. Thanks to my mom for being a great role model, I have always worked hard and put responsibilities the first in my life. They took care of me as parents and nowadays they fly 7,000 miles to America to take care of my children as grandparents. Thousands of words will be too short to show my gratitude to them. If anyone deserves all honors from my achievement, that would be my parents.

Next, I want to thank my husband, my babies and my parents in law. Because of them, I have a family in America. This is incredibly precious for an immigrant. Not only they support me, I also learned to grow up and became a wife and a mom.

Finally, I would like to thank my colleagues. Everyone in the Palmer lab is incredibly nice and supportive. I am especially thankful to Lynn Sanford for helping me with RNAseq analysis and David Simpson for making cloning constructs for me when I took my maternal leave. I also want to thank Theresa in the cell culture facility for all the support she gave as a working mom. I would not have made this far without them.

Last but not least, I want to thank my advisor Amy, for accepting me working in her lab when I started as a volunteer and recommended me to get in this program. She has been a wonderful mentor for the past 6 years. Moreover, I am grateful for her proofreading of my publication and thesis.

Contents

Chapter

1 Introduction

1.1 Publication status and author contributions	1
1.2 Importance of zinc in human health	1
1.2.1 Zinc as an essential factor for protein structure and function	1
1.2.2 Zn ²⁺ as a second messenger	2
1.2.3 Zinc in the mammary gland and lactation	3
1.3 Regulation of zinc homeostasis in mammalian cells	4
1.4 The expression and functional modification of zinc homeostasis genes	9
1.4.1 The expression and functional modification of Zinc transporters	9
1.4.2 The expression and functional modification of metallothioneins (MTs)	11
1.4.3 The expression and functional modification of MTF1	12
1.5 The regulation of zinc homeostasis by glucocorticoid hormones	13
1.6 The regulation of zinc homeostasis by prolactin	17

1.7 Common techniques to measure total zinc.....	18
1.8 Common Techniques To Measure Labile Zn ²⁺	19
2 Remodeling of Zinc Homeostasis In Differentiated Mammary Epithelial Cells.....	21
2.1 Abstract.....	22
2.2 Publication status.....	23
2.3 Introduction	23
2.4 Experimental methods	26
2.4.1 Chemicals and reagents.....	26
2.4.2 Cell culture	27
2.4.3 Lentiviral transduction	28
2.4.4 shRNA knockdown (KD) of ZIP14	29
2.4.5 Reverse transcription polymerase chain reaction (RT-PCR) and quantitative reverse transcription PCR (RT-qPCR)	29
2.4.6 Western blotting	30
2.4.7 Immunofluorescence	31
2.4.8 RNAseq.....	32
2.4.9 Inductively coupled plasma mass spectrometry (ICP-MS).....	33
2.4.10 Measurement of labile cytosolic Zn ²⁺ using NES-ZapCV2.....	34
2.4.11 Promoter reporter assay.....	35
2.5 Results.....	37
2.5.1 Characterization of HC11 cell differentiation	37
2.5.2 Changes in global gene expression at 24 hr and 6 days post hormone treatment.	40

2.5.3 Differential expression of zinc-dependent genes in differentiated cells.....	43
2.5.4 Differential expression of zinc homeostasis genes	46
2.5.5 Cortisol increases the steady-state level of ZIP14, MT1 and MT2 mRNAs. .	48
2.5.6 Measurement of total zinc and labile cytosolic Zn ²⁺ over the progression of cell differentiation	52
2.5.7 ZIP14 is responsible for increased cytosolic Zn ²⁺ at day 6 post hormone treatment and is important for the upregulation of WAP mRNA.....	55
2.6 Discussion	59
2.7 Future direction.....	65
2.7.1 The regulation of ZIP14, MT1 and MT2 mRNA expression by lactogenic hormones	65
2.7.2 Protein expression of ZIP14 at day6 post hormone treatment.....	66
2.7.3 Zn ²⁺ transport into cytosol by ZIP14 enriched in a peri-nuclear region in differentiated cells	66
2.7.4 The regulation of WAP mRNA expression by ZIP14.....	66
3 Superiority of SpiroZin2 Versus FluoZin-3 For Monitoring Vesicular Zn ²⁺ Allows Identification of Lysosomal Zn ²⁺ Accumulation In Lactating Mammary Cells.....	68
3.1 Abstract.....	68
3.2 Publication status and author contributions	69
3.3 Introduction	69
3.4 Methods	72
3.4.1 Chemicals.....	72
3.4.2 Molecular cloning	73

3.4.3 Cell culture	73
3.4.4 Cell loading with zinc probes and calibration	73
3.4.5 Live cell imaging.....	74
3.4.6 Responses of probes to Zn ²⁺ perturbation in HC11 cells	75
3.4.7 Variability of fluorescence Intensities of zinc probes.....	76
3.4.8 Colocalization Assay of Zinc Probes with Vesicular Markers.....	77
3.4.9 Cytosolic distribution of zinc probes	78
3.4.10 Lysosomal pH measurement.....	79
3.4.11 Monitoring cytosolic Zn ²⁺ using a genetically-encoded Zn ²⁺ FRET sensor .	79
3.4.12 Measurement of lysosomal Zn ²⁺ level during lactation.....	80
3.5 Results.....	81
3.5.1 Titration of probes in HC11 cells	81
3.5.2 SpiroZin2 staining yields consistent signals after normalization to TPA treatment while FluoZin3-stained cells have highly variable signals	84
3.5.3 Colocalization assay of zinc probes with vesicular markers.....	87
3.5.4 A population of FluoZin-3 localizes to the cytosol	91
3.5.5 SpiroZin2 reveals changes in lysosomal Zn ²⁺ upon perturbation.....	93
3.5.6 A substantial increase in lysosomal Zn ²⁺ was detected in SpiroZin2-stained mammary epithelial cells at 24 hr post hormone treatment.....	96
3.7 Discussion	98
3.8 Future Direction	101
4 Implications in Zinc Homeostasis and Cell Signaling.....	103
Bibliography.....	106

Appendix A.....124

Appendix B.....129

Appendix C.....133

Appendix D.....137

Tables

Table 1.1 Subcellular localization of zinc transporters.....	6
Table 2.1 Top downregulated and upregulated zinc genes.....	44

Figures

Figure 2.1 Characterization of HC11 cell differentiation upon hormone treatment.....	39
Figure 2.2 Global gene expression changes at 24 hr and 6 days post hormone treatment.....	42
Figure 2.3 Differential expression of zinc-dependent genes at day 6 post hormone treatment compared to the resting state.....	45
Figure 2.4 Differential expression of zinc homeostasis genes.....	47
Figure 2.5 Hydrocortisone increases the steady-state level of ZIP14, MT1 and MT2 mRNAs.....	51
Figure 2.6 Measurement of total zinc and labile cytosolic Zn ²⁺ over the progression of cell differentiation.....	54
Figure 2.7 Functional studies of ZIP14.....	58
Figure 3.1 Titration of probes in HC11 cells.....	83
Figure 3.2 SpiroZin2 staining yields consistent signals after normalization to TPA treatment while FluoZin3-stained cells have highly variable signals.....	86
Figure 3.3 Co-localization analysis of SpiroZin2 and three vesicular markers demonstrates that SpiroZin2 resides in lysosomal vesicles.....	89
Figure 3.4 Co-localization analysis of FluoZin-3 and three vesicular markers demonstrates that FluoZin-3 non-specifically localizes to lysosomal, Golgi, and secretory vesicles.....	90
Figure 3.5 A population of FluoZin-3 localizes to the cytosol.....	92
Figure 3.6. SpiroZin2 reveals changes in lysosomal Zn ²⁺ upon perturbation.....	95

Figure 3.7. A substantial increase in lysosomal Zn^{2+} was detected in SpiroZin2-stained mammary epithelial cells at 24 hr post hormone treatment.....97

Chapter 1

Introduction

1.1 Publication status and author contributions

Han, Y. and Palmer, A. E. Recent advances in the hormonal regulation of zinc homeostasis. *Critical Reviews in Biochemistry and Molecular Biology*. Invited review. Manuscript in preparation.

1.2 Importance of zinc in human health

1.2.1 Zinc as an essential factor for protein structure and function

Zinc is the second most abundant trace metal element in human body after iron¹. Zinc is redox-inert in biological systems and functions as a Lewis acid, which makes zinc an important structural and catalytic cofactor of proteins in biological reactions². Zinc coordinates proteins *via* binding to oxygen, nitrogen and sulfur donors from the side chains of histidine, glutamate/aspartate, and /or cysteine. For example, in the classical Cys2His2 zinc-finger motif, zinc stabilizes the folded motif by interacting with 2 cysteine (Cys) and 2 histidine (His) residues. Zinc-finger containing proteins are essential in many molecular processes such as DNA-protein binding, protein folding and assembly, RNA packaging, etc³. As a catalytic cofactor, zinc dynamically coordinates water, substrate complexes, and/or transient reaction intermediates in the active site of enzymes⁴. In fact, zinc is present as a catalytic cofactor in 4 main enzyme classes⁴⁻⁶, illustrating a central role of zinc in catalysis.

1.2.2 Zn²⁺ as a second messenger

In cell signaling cascades, extracellular first messengers, such as hormones, antigens and neurotransmitters, bind and activate signaling receptors, leading to the production or a transient increase of concentration of small-molecule intracellular second messengers^{7,8}. Second messengers then activates downstream targets to amplify signals in signaling pathways. Classical examples of second messengers are cyclic 3'5'-adenosine monophosphate (cAMP), diacylglycerol (DAG), inositol trisphosphate (IP3) and calcium (Ca²⁺)^{7,8}. For example, upon ion channel activation by external stimuli, Ca²⁺ release from ER to cytosol results in a transient increase of cytosolic labile Ca²⁺ concentration from 100 nM to 500-1000 nM^{9,10}. Ca²⁺ signal is detected by calmodulin (CaM), an endogenous Ca²⁺ sensor. Ca²⁺-binding induces a conformational change of CaM allowing interaction of CaM with over 300 partner proteins¹¹.

Zn²⁺ has been suggested as a second messenger / signaling transducer^{12,13}. A transient or stable/homeostatic change in intracellular Zn²⁺ level (zinc signal) can be induced by external stimulus. For example, a intracellular Zn²⁺ increase was detected in primary monocytes after minutes of treatment with Escherichia coli, LPS, Pam3CSK4, TNF- α , or insulin^{14,15}. Upon treatment with a steroid hormone to induce cell differentiation, intracellular Zn²⁺ levels in HL-60 cells (a myeloid cell line) diminished at 24 hr post hormone treatment and declined even further at 48 hr and 72 hr¹⁶. Targets of Zn²⁺ signals have been suggested to include phosphodiesterases (PDE)^{17,18}, phosphatase (PTP)^{19,20} and protein tyrosine kinase (PTK)^{21,22}, all of which are central players of cell signaling processes. However, the role of Zn²⁺ as a second messenger

remains inconclusive because firstly, a Zn^{2+} -binding messenger molecule that can amplify Zn^{2+} signals, like calmodulin in calcium signaling, has not been identified²²; secondly, there is no strong evidence showing endogenous Zn^{2+} released upon external stimuli directly regulates downstream targets in signaling pathways. Current understanding of the role of Zn^{2+} as an intracellular second messenger is acquired from *in vitro* assay or mammalian cell studies in which cells were supplemented with Zn^{2+} / Zn^{2+} ionophore (pyrithione)^{17-20,23}. However, Ho²³ showed that the addition of pyrithione along with Zn^{2+} was essential for the inhibition of ERK2 phosphorylation in mouse hippocampal neuronal cells (HT22), whereas Zn^{2+} had no effect. Collectively, the role of Zn^{2+} as a second messenger is still questionable and requires stronger evidence.

1.2.3 Zinc in the mammary gland and lactation

Zinc plays important biological roles in the normal function of major organs in human body (e.g. prostate, pancreas, endocrine, exocrine, brain)^{24,25}. Here, I focused on the importance of Zinc in the mammary gland and lactation because it is closely related with my thesis research. The mammary gland undergoes intense morphological and functional changes during pregnancy and lactation, and many of those processes are Zinc dependent. For example, LIM-ONLY-4 (LMO 4) is a LIM-domain-containing zinc finger protein and transcription factor²⁶. Lmo4 promotes mammary gland proliferation and negatively regulates mammary cell differentiation in a temporal fashion, with its level peaking in late pregnancy but withdrawing through lactation²⁷. Lmo4^{-/-} mice developed immature mammary gland proliferation and reduced milk production²⁷. GATA3 is also a zinc-binding transcription factor and plays crucial roles in modulating mammary gland morphogenesis and maintaining luminal cell differentiation in

lactation^{28,29}. Additional evidence of the importance of zinc in regulating mammary gland morphology is the role of the zinc-dependent matrix metalloproteinases (MMPs). The mammary gland expands extensively during pregnancy and lactation, which involves the degradation and remodeling of extracellular matrix tissue by MMPs. It has been shown that MMP3 and MMP7 are upregulated during mammary gland expansion^{30,31}. In conclusion, zinc-dependent proteins are essential in the remodeling of mammary gland during pregnancy and lactation.

Zinc is also an essential nutrient for newborns. Some breast-fed newborns with zinc deficiency can develop severe dermatitis, diarrhea and hair loss³²⁻³⁴. Neonatal zinc deficiency has been attributed to the aberrant expression of some members of the Zn transporter (ZnT) family. For example, ZnT2 mutants with single-nucleotide mutations have been identified in women with low milk zinc concentration³⁴⁻³⁶. In addition, reduced mRNA expression of ZnT5 and ZnT6 were identified in breastfeeding women producing zinc-deficient milk³⁷. A ZnT4 nonsense-mutation in lethal milk mice resulted in low zinc concentration in milk, and pups exclusively fed with the lethal milk die even before weaning³⁸. These studies suggest that the ZnT transporters play important roles in the secretion of zinc into mother's milk during lactation. However, the underlying detailed mechanism by which zinc is secreted into milk is still poorly understood.

1.3 Regulation of zinc homeostasis in mammalian cells

Intracellular zinc level needs to be tightly controlled because too little zinc leads to zinc deficiency and too much zinc is toxic. Mammalian cells contain hundreds of μM total zinc with the majority of zinc stably bound to proteins and a small pool of labile

Zn^{2+} that is buffered by small-molecules, peptides and proteins³⁹. Measuring labile Zn^{2+} using genetically encoded fluorescent sensors revealed the uneven distribution of labile Zn^{2+} with low hundreds of pM in nucleus and cytosol and 0.1-1 pM in mitochondria, ER and Golgi³⁹.

The precise control of zinc levels (i.e. zinc homeostasis) is regulated at least in part by zinc transporters, zinc buffering (metallothioneins) and the metal-responsive transcription factor 1 (MTF1)²². In this study, these key players of zinc homeostasis are defined as zinc homeostasis genes. Zinc transporters localize to cell and organelle membranes to regulate the distribution and transport of zinc among subcellular compartments. Twenty-four zinc transporters have been identified in humans, including 14 Zrt-, Irt-like protein (ZIP) family transporters and 10 Zn transporter (ZnT) family transporters². The functions of ZIPs and ZnTs are opposite: ZIPs transport Zn^{2+} into cytosol whereas ZnTs mobilize Zn^{2+} out of cytosol². The expression and intracellular localization of zinc transporters are regulated dynamically during different cellular processes. The subcellular localization of zinc transporters was summarized in Table 1.1. ZnT9 was not included because it is supposed to not have zinc transport activity, due to the lack of a crucial histidine in the zinc-binding site².

Table 1.1 Subcellular localization of zinc transporters

Transporter	Subcellular localization	Transporter	Subcellular localization
ZIP1	Plasma membrane ^{40,41}	ZIP13	Golgi apparatus ⁴² , vesicles ⁴³
ZIP2	Plasma membrane ⁴⁴	ZIP14	Plasma membrane ⁴⁵⁻⁴⁷
ZIP3	Plasma membrane ⁴⁸ , vesicles ⁴⁹	ZnT1	Plasma membrane ^{50,51} , vesicles ^{52,53}
ZIP4	Plasma membrane ⁵⁴	ZnT2	Endosome/lysosome ^{55,56} , ER ⁵⁷ , zymogene granules ^{58,59} , plasma membrane ⁶⁰
ZIP5	Plasma membrane ⁶¹	ZnT3	Synaptic vesicles ^{62,63}
ZIP6	Plasma membrane ⁶⁴	ZnT4	Endosome/lysosome ⁶⁵ , <i>Trans</i> -Golgi network (TGN) ⁶⁶
ZIP7	ER ⁶⁷ , Golgi apparatus ⁶⁸	ZnT5	Golgi apparatus ⁶⁹ , secretory vesicles ⁷⁰
ZIP8	Plasma membrane ⁷¹ , lysosome ^{72,73}	ZnT6	Golgi apparatus ⁷⁴
ZIP9	<i>Trans</i> -Golgi network (TGN) ⁷⁵ , plasma membrane ⁷⁶	ZnT7	Golgi apparatus ⁷⁷ , secretory vesicles ⁷⁰
ZIP10	Plasma membrane ⁷⁸	ZnT8	Insulin granules ⁷⁹
ZIP11	Golgi apparatus ⁸⁰ , nucleus ⁸¹	ZnT10	Golgi apparatus ⁸² , early endosome ⁸³
ZIP12	Plasma membrane ⁸⁴		

Thionein (T) is a small protein (61-68 amino acids) that binds up to 7 zinc ions with high affinity ($K_d = 0.32 \text{ pM}$ at pH 7.4)⁸⁵, whereby zinc binding leads to the formation of metallothionein (MT). Despite its high Zn^{2+} binding affinity, MTs also transfer Zn^{2+} to apoproteins and apoenzymes. With its dual functions, T/MT serves as a Zn^{2+} reservoir that can bind excess Zn^{2+} and release Zn^{2+} under conditions of Zn^{2+} depletion^{86,87}. Indeed, MT1 and MT2 null mice are more sensitive to zinc deficiency and zinc toxicity compared to control mice⁸⁸. The intracellular Zn^{2+} buffering capacity of MTs was supported by the evidence that the ratio of MT to T increased with the total and free Zn^{2+} concentrations in human colon cancer cells⁸⁹. An increase in Zn^{2+} also induced the expression of thionein which provides the cell with a greater capacity to buffer Zn^{2+} ⁸⁹. Zn^{2+} release from MTs to apoproteins is triggered by intracellular redox-active reagents (e.g. disulfide and selenium compounds), and affected by the redox state of cells⁹⁰. Zn^{2+} release from MTs by glutathione disulfide (GSSG) has been well characterized and will be used as an example to illustrate the principle here. GSSG was first identified as the cellular ligand to interact with rabbit MT2 coupled with Zn^{2+} release by Maret⁹¹. Jiang⁸⁷ further showed that GSSG-induced Zn^{2+} release from human MT1 and MT2 to zinc-depleted sorbitol dehydrogenase operated in a similar manner. GSSG enhanced the rate of Zn^{2+} release and increased the number of released Zn^{2+} atoms⁸⁷. The effect of GSSG was dependent on its concentration and augmented by the presence of GSH, even though GSH inhibited MT- Zn^{2+} release in the absence of GSSG⁸⁷. This suggests that the cellular GSG/GSSH ratio potentially serves as a driving force for the mobilization and transfer of MT- Zn^{2+} to apoenzymes⁸⁷. Subsequent to these studies, the oxidative stress-induced MT- Zn^{2+} release has been

demonstrated in neuronal cells⁹²⁻⁹⁵. To date, the list of cellular reactive species that can activate MT-Zn²⁺ release has been expanded to disulfide^{87,91}, selenium^{87,96}, oxidative reagents^{93,97,98} and nitric oxide^{99,100}.

MTF1 is a zinc-sensing transcription factor that is conserved from insects to animals and plays important roles in the regulation of gene expression upon stimulation with heavy metal and oxidative stress¹⁰¹. MTF1 senses increases in cytosolic Zn²⁺ *via* a zinc-sensing motif and then translocates to the nucleus, where MTF1 binds short consensus DNA sequences called metal response elements (MREs) to regulate the transcription of downstream genes. Eighteen genes have been identified in human and/or mouse as major direct targets of MTF1-induced transcription activation *via* MTF1-MREs binding in their promoters¹⁰¹. The major functions of the 18 genes are metal transport and homeostasis, redox homeostasis, liver development and cell differentiation¹⁰¹. It is noteworthy that MTF1 is essential for life, as MTF1-KO (knockout) mice die at an embryonic stage because of liver degeneration^{102,103}. Among zinc homeostasis genes, most MTs and 3 zinc transporters (ZnT1, ZnT2, Zip10) contain MREs in their promoters, and have been shown to be regulated by MTF1^{58,78,104}. Most genes with MREs, including MTs, ZnT1 and ZnT2, are transcriptionally upregulated by MTF1; however, ZIP10 transcription was repressed by excess zinc and MTF1, possibly because its MRE is located 17 bp downstream of the transcription start site leading to RNA Pol II stalling⁷⁸. Even though only a small pool of genes is directly regulated by MTF1, more genes are affected by the indirect regulation of MTF1¹⁰⁵. A recent study revealed that the expression of ~130 genes was affected by MTF1 knockdown but MRE sequence was not enriched in their promoters¹⁰⁵. Furthermore, this study showed that

MTF1-regulated gene expression of MTs and ZnT1 is on top of a hierarchy of zinc homeostasis regulation: MTF1 increases the expression of MTs and ZnT1 in response to elevated Zn^{2+} and then MTs and ZnT1 buffer or transport intracellular Zn^{2+} to curtail the effect of Zn^{2+} increase on the expression of other genes¹⁰⁵. In summary, mammalian cells have developed sophisticated networks to regulate zinc homeostasis, in order to maintain the appropriate zinc level for cell function and vitality.

In spite of all the studies mentioned above, our understanding of zinc homeostasis regulation is still very limited with many hypotheses that need to be addressed in future. For example, how cells regulate zinc homeostasis systematically to handle fluctuations of endogenous Zn^{2+} , and how cells utilize the Zn^{2+} signals to fulfill biological functions remain to be addressed.

1.4 The expression and functional modification of zinc homeostasis genes

1.4.1 The expression and functional modification of zinc transporters

Numerous studies have demonstrated that the steady-state expression (mRNA or protein) of zinc transporters can be upregulated in response to several stimuli, such as ER stress, cytokine, hormone and hypoxia^{47,106–110}. Regulation of expression can occur at the transcriptional level^{58,111–114}, or at the post-transcriptional level *via* alternative splicing, as observed with ZnT2 in mouse mammary epithelial cells⁶⁰ and ZnT5 in Chinese hamster ovary cells¹¹⁵. The protein translated from those mRNA variants localized to different intracellular compartments, suggesting unique function of each variant^{60,115}. In addition, microRNA silencing has been shown to repress ZIP5 and ZIP8 expression^{116,117}. In the case of ZIP8, it is a direct target of a microRNA-488 and ZIP8 silencing resulted in reduced cartilage degradation¹¹⁷. Compared to normal

cartilage, the microRNA-488 level was significantly lowered in osteoarthritis (OA) patient cartilage, which caused cartilage degradation¹¹⁷. Combined, these studies reveal that there are multiple layers of regulation of zinc transporter mRNA. While there are examples of transcriptional regulation, alternative splicing, and microRNA targeting for a handful of transporter genes, the picture is far from completed as there is little to no information on many of the transporters.

Zinc transporters can also be regulated by post-translational modification including glycosylation, phosphorylation and ubiquitination. Glycosylated variants of human ZIP4^{118,119} and ZIP8¹²⁰ have been reported; however, the function of glycosylation in ZIP8 is not necessary for zinc transport¹²⁰. The functional implication of glycosylation in ZIP4 has not been identified. Zinc transporters can also be phosphorylated at one or more sites, as seen with ZnT1, ZnT3, ZnT6, ZIP3, ZIP6, ZIP7, ZIP8 and ZIP10¹²¹. For example, phosphorylation of ER-localized ZIP7 on S275, S276, S293 and T294 resulted from activation of protein kinase CK2 (PKCK2), and phosphorylation of all 4 sites was necessary for full activation of downstream signaling pathways including AKT, P13K, MAPK and MTOR¹²². However, whether phosphorylation of ZIP7 induces a release of Zn²⁺ from the ER to cytosol is still inconclusive, as an increase of cytosolic labile Zn²⁺ was not detected using a cytosol-targeted Zn²⁺ FRET sensor upon activation of PKCK2 by treatment with epidermal growth hormone (EGF)¹²³. Zinc transporters can also be post-translationally modified by ubiquitination. When HEK293 cells were challenged with excess Zn²⁺, ZIP4 was shown to be ubiquitinated and targeted for ubiquitin–proteasome degradation (UPD) pathway to protect cells from zinc toxicity¹¹⁸. Similar regulation was also reported for

the yeast Zn²⁺ transporter ZRT1¹²⁴. Finally, dysfunction of ZIP13, which is responsible for the human Ehlers-Danlos syndrome (EDS)¹²⁵, is also associated with ubiquitination. The aberrant ubiquitination of two ZIP13 mutant proteins in human EDS led to the degradation of ZIP13 and altered zinc homeostasis, suggesting the therapeutic potential of targeting UPD of ZIP13¹²⁵. Collectively, various post-translational modifications have been identified in a few zinc transporters and some modifications play important roles in cellular process. It remains unclear that whether all zinc transporters are modified post-translationally and whether the modifications are biologically functional.

1.4.2 The expression and functional modification of metallothioneins (MTs)

There are 4 classes of human MTs (MT 1 to 4) comprising 11 functional isoforms with 8 MT1 isoforms (MT1 A, B, E, F, G, H, M and X), 1 MT2 (also known as MT2A), 1 MT3 and 1 MT4¹²⁶. MT1 and 2 are universally present in many tissues and enriched in liver and kidney¹²⁷. MT3 expression is limited to the brain and male reproductive organs¹²⁷. MT4 is exclusively expressed in stratified squamous epithelia¹²⁸. Various expression patterns of MT1 isoforms have been detected in human cancers¹²⁷. The expression of MTs can be induced by heavy metal treatment *via* the activation of MTF1, oxidative stress, and glucocorticoid hormones^{101,129}. The induction of MTs by glucocorticoid hormones will be discussed later in this chapter. Additionally, MT expression is also controlled by epigenetic regulation. In mouse lymphosarcoma and rat hepatoma cancer cells, MT1 gene expression was silenced because of the DNA methylation in its promoter^{130,131}. Suppression of methylation using a specific inhibitor of DNA methyltransferase (DNMT) activated MT1 expression¹³². Furthermore, Zn²⁺-induced activation of MT1 transcription by MTF1 involves DNA acetylation. A histone

acetyltransferase p300/CBP has been shown to be recruited by MTF1 upon Zn^{2+} treatment, and knockdown of p300/CBP expression significantly suppressed the transcription of MT1 but not ZnT1¹³³. A further study demonstrated that the formation of MTF1 coactivator complex upon Zn^{2+} exposure resulted in a rapid removal of nucleosome at the MT1 promoter to stimulate MT1 transcription¹³⁴.

1.4.3 The expression and functional modification of MTF1

Heavy metals, oxidative stress and hypoxia can increase the steady-state level of MTF1 mRNA or protein^{71,134–141}. The upregulation of MTF1 mRNA was suggested to be mediated by post-transcriptional modification, as transcription from the endogenous MTF1 promoter and a transfected promoter-reporter fusion construct in mouse fibroblast was not induced by heavy metal or oxidative stress¹⁴². MTF1 function is regulated by multiple post-translational steps, such as zinc responsive nuclear accumulation, DNA binding and formation of an MTF1 transcription activation complex¹⁰¹. Human and mouse MTF1 contain two major functional domains: the DNA-binding domain and transactivation domain¹⁰¹. MTF1 constitutively shuttles between the cytoplasm and nucleus and accumulates in the nucleus upon heavy metal treatment and various stresses (heat shock, oxidative stress, low pH, etc)^{143,144}. MTF1 has a nuclear localization signal (NLS) and nuclear export signal (NES). The NLS spans the DNA-binding domain and NES localizes in the transactivation domain. The individual NLS or NES is not zinc responsive, as chimeric proteins with NLS or NES fused to a protein marker were constitutively active independent of zinc treatment, which suggests that the zinc-induced nuclear accumulation of MTF1 relies on the intact MTF1 rather than the NLS or NES alone¹⁰³.

The DNA-binding of MTF1 is also zinc dependent. The DNA-binding domain contains six Cys2His2 zinc fingers, with zinc fingers 2 - 4 comprising the DNA-binding core¹⁴⁵. Zinc sensitivity is mediated by zinc finger 1 as deletion of this motif led to constitutive DNA binding *in vitro*¹⁴⁶. Moreover, fusing MTF1 zinc finger 1 with a truncated transcription factor SP1 generated a chimeric protein, the DNA-binding of which is dependent on zinc treatment¹⁴⁶. The transactivation domain of MTF1 interacts with other transcription factors and mediators to regulate the expression of downstream genes. Nine MTF1 partners have been identified in mouse and/or human including six transcription factors (Sp1, HIF-1 alpha, Nrf1, HSF1 and CEBP alpha, USF1), one transcription activator and histone acetyltransferase (p300/CBP), one phosphatase (PTEN) and one regulator of the Ras signaling transduction pathway (NF1)¹⁰¹, implicating the coordinated regulation of gene expression by MTF1 complex.

1.5 The regulation of zinc homeostasis by glucocorticoid hormones

Glucocorticoids are essential hormones that are synthesized and secreted by the adrenal cortex in response to stress or daily metabolic changes¹⁴⁷. Glucocorticoids act on almost every tissue and organ in human body to maintain or restore homeostasis upon stimuli¹⁴⁷. Glucocorticoids regulate a wide range of biological processes including metabolism, immune system function, skeletal growth, reproduction, cognition and cardiovascular function^{148,149}. Upon cell exposure to glucocorticoids, glucocorticoid activates signal transduction pathways to either enhance or repress the transcription of downstream genes. In the classical nuclear glucocorticoid signaling pathway, glucocorticoids penetrate cells and then bind the glucocorticoid receptor (GR) in the cytosol, leading to a conformational change and nuclear translocation of GR. GR then

binds specific sequences (glucocorticoid response elements, GRE) in the promoter of target genes to modulate gene expression¹⁵⁰. The decision of activation or repression of gene expression depends on the sequences of GRE¹⁵¹. In addition to the classical glucocorticoid receptor-mediated signaling, a growing body of studies in different species have suggested rapid glucocorticoid signaling mediated by putative membrane G protein-coupled receptors (GPCRs) and other signaling cascades downstream of GPCRs¹⁵²⁻¹⁵⁹. For example, the Taker group found out that the activation of a stimulatory G protein (Gs)-coupled membrane receptor facilitated the rapid glucocorticoid-induced synthesis and release of endocannabinoids from neuroendocrine cells^{157,158}. The cAMP signaling pathways, protein kinase A (PKA) and protein kinase C (PKC) are all downstream targets of membrane GPCR. It has been shown that the rapid glucocorticoid inhibition of voltage-gated calcium signals in PC12 cells involved PKA¹⁵⁹ and PKC¹⁵⁷. Moreover, the rapid inhibition of excitatory synaptic inputs by glucocorticoid relied on the activation of cAMP signaling transduction pathway¹⁵⁸.

It is been demonstrated in various species that glucocorticoids can enhance the expression of metallothioneins (MTs), ⁶⁵Zn uptake, and intracellular zinc levels in mammalian cells or *in vivo*^{58,160-165}. This effect can be detected after hours (6-24 hr)^{161,164,165} or days (10 days)¹⁶⁰ of hormone treatment. A glucocorticoid response element (GRE) was found ~7 kb upstream of the MT1 transcription start site (TSS) and ~ 1 kb upstream of the MT2 TSS, respectively^{166,167}, which drives transcription upon binding of activated glucocorticoid receptor. The amount of intracellular total zinc has been shown to increase upon glucocorticoid treatment, as measured by atomic absorption spectrophotometry or radioactivity of hormone-induced ⁶⁵Zn uptake^{160,164}.

Furthermore, intracellular labile Zn^{2+} levels have also been shown to increase upon treatment of mouse hippocampal neuronal cells (HT-22)¹⁶⁵ and rat pancreatic acinar cells (AR42J) with glucocorticoids¹⁰⁶. FluoZin-3 is a small-molecule fluorescence sensor for labile Zn^{2+} , and its resting fluorescence increases upon zinc binding¹⁶⁸. Cellular Zn^{2+} levels can also be determined using this equation $[Zn^{2+}] = Kd \times [(F - F_{min}) / (F_{max} - F)]$ ($Kd = 15 \text{ nM}$)¹⁶⁹. In HT-22 cells, 6 hr of glucocorticoid (10 μM) treatment increased the resting fluorescence of FluoZin-3 by ~35% as measured by flow cytometry¹⁶⁵. Forty-eight hours of glucocorticoid treatment (0.1 μM) increased intracellular labile Zn^{2+} from ~2 nM to ~6 nM in AR42J cells, where fluorescence was measured using flow cytometry and then converted to $[Zn^{2+}]$ with the above equation¹⁰⁶. In both studies, glucocorticoid hormone also augmented the increase in labile Zn^{2+} upon addition of extracellular zinc. The source of the increased labile Zn^{2+} is at least partially suggested to be an intracellular store, as incubation of cells with a cell-impermeable Zn^{2+} chelator did not affect the increase of Zn^{2+} upon short-term (6 hr) hormone treatment¹⁶⁵. Long-term glucocorticoid treatment (> 20 hr) could potentially change the expression profile of zinc homeostasis genes (e.g. zinc transporters) to affect zinc uptake from the extracellular environment and intracellular Zn^{2+} storage. In polarized rainbow trout gill epithelial cells, 20 hr treatment with 1 μM glucocorticoid increased the rate of transepithelial zinc transport from the apical side to the basolateral side¹⁶¹, suggesting the regulation of zinc transport was a long-term effect after hormone treatment.

Unlike the well-established stimulation of MT expression by glucocorticoid, it is poorly understood if hormone treatment also regulates the expression of any of the 24

mammalian zinc transporters, although some of the studies discussed above certainly hint at the possibility of altered zinc transport. So far, only ZnT1 and ZnT2 have been demonstrated to be upregulated by glucocorticoid treatment. The steady-state mRNA level of ZnT1 increased by ~ 2 fold at 20 hr post glucocorticoid treatment (0.25 μ M) in rainbow trout gill epithelium¹⁶¹. Furthermore, glucocorticoid enhanced the effect of zinc addition on ZnT1 mRNA upregulation, which was mediated by the glucocorticoid receptor (GR) signaling pathway, as treatment with a GR antagonist RU486 abolished the enhanced effect of the hormone on ZnT1 mRNA increase¹⁶¹. However, the underlying mechanism of how cortisol induced the ZnT1 mRNA expression is still not understood. The induced expression of ZnT2 by glucocorticoids is better characterized in pancreatic acinar cells. ZnT2 mRNA expression in both primary mouse pancreatic acinar cells and rat pancreatic acinar cell line (AR42J) showed a transient increase at 8-20 hr post glucocorticoid hormone injection or treatment⁵⁸. ZnT2 protein expression was also upregulated in the primary mouse acinar cells, where mRNA induction was mediated by the coordinated activation of GR and STAT5 (signal transducer and activator of transcription 5)⁵⁸. GR and STAT5 were both present on the ZnT2 promoter post glucocorticoid treatment as determined by CHIP (chromatin immunoprecipitation). Both GR and JAK-STAT5 signaling pathways were required for the activation of ZnT2 transcription, as specific inhibitors for GR, JAK and STAT5 all abolished glucocorticoid-induced ZnT2 mRNA expression⁵⁸. STAT5 is the signal transducer of the JAK-STAT signaling pathway and a transcription factor. The requirement of STAT5 in the glucocorticoid-induced ZnT2 mRNA transcription suggests a crosstalk between the JAK-STAT and GR signaling pathways.

In summary, although it is well established that glucocorticoids can activate the expression of metallothioneins (MTs) and induce zinc uptake in mammalian cells, very little is known regarding the regulation of zinc transporters by this hormone.

1.6 The regulation of zinc homeostasis by prolactin

Prolactin (PRL) is a peptide hormone (~150–200 aa) and is present in all vertebrates¹⁷⁰. PRL expression has been found in anterior pituitary gland as well as extrapituitary tissues¹⁷⁰. PRL regulates a wide range of biological processes including growth and development, reproduction, metabolism and immune system function¹⁷¹. PRL is transported by circulatory system and acts on target cells *via* prolactin receptors (PrIR). PRL binding induces the dimerization of PrIR and activation of Janus kinase (JAK)¹⁷². JAK then phosphorylates its substrate STAT5 on tyrosine residues, which results in the dimerization and nuclear-translocation of phosphorylated STAT5¹⁷². STAT5 dimers then bind a specific DNA motif called interferon- γ activation site (GAS) in the promoter region of target genes to drive gene transcription¹⁷².

PRL-activated cell signaling is crucial for differentiation of the mammary gland during pregnancy and milk synthesis throughout lactation¹⁷². Although the expression of many zinc transporters is modulated during lactation⁸⁰, only one zinc transporter, ZnT2, has been shown to be directly regulated by PRL at the transcription level¹⁷³ and post-translational level¹⁷⁴ in mouse mammary epithelial cells. The ZnT2 promoter contains a functional GAS sequence, which is essential for the initiation of ZnT2 transcription in response to PRL treatment, as deletion of this GAS abolished ZnT2 mRNA induction by PRL treatment¹⁷³. STAT5 was present on the GAS element upon PRL treatment¹⁷³, which suggested the transcription activation was mediated by PRL-

induced JAK-STAT5 signaling cascade. PRL also modifies ZnT2 function *via* ubiquitination. The ubiquitination had dual roles in zinc homeostasis: it first caused a transient enrichment of ZnT2 on the membrane of secretory vesicles and a transient increase of zinc secretion; later, the ubiquitinated ZnT2 was then targeted for degradation¹⁷⁴. However, conflicting results were reported in breast cancer cells, where attenuation of PrIR increased ZnT2 protein levels but had no effect in ZnT2 mRNA levels⁵⁷. Collectively, the modulation of ZnT2 and other zinc homeostasis genes by PRL needs to be explored in more detail in normal mammary gland and malignant breast cancer tissue.

1.7 Common techniques to measure total zinc

The common techniques for quantifying total zinc in biological samples will be briefly summarized in this thesis, including (1) atomic absorption spectrometry, (2) inductively coupled plasma mass spectrometry, (3) Mass-spectrometry based imaging and (4) X-ray fluorescence based imaging.

Atomic absorption spectrometry (AAP) is a widely used technique in biology or chemistry laboratories to measure trace metal levels in a variety of samples^{160,175–177}. Samples are first vaporized and then converted to free atoms by flame or electrothermal heating methods¹⁷⁸. The free atoms are then exposed to a light source and the absorption of light is measured¹⁷⁸. Each atom has a unique absorption spectrum and the absorption follows the principle of the Beer's Law, in which the concentration of the analyte metal is proportional to the absorption of the light at a certain wavelength¹⁷⁹. Compared to AAP, inductively coupled plasma mass spectrometry (ICP-MS) has much higher sensitivity (ICP-MS: parts per trillion; AAP: parts per billion)^{179,180}. Moreover,

ICP-MS allows measurement of multiple isotopes in a specimen. During an ICP-MS analysis, samples first are converted to argon plasma by heating^{181,182}. The generated charged ions then pass through a mass detector^{181,182}. Ionized atoms/isotopes can be differentiated by their mass-to-charge ratios (m/z).

Total metal imaging methods not only allow the quantification but also the mapping of metal distribution in a specimen. Depending on the imaging mechanism, the most common total metal imaging methods can be classified into two groups: the mass-spectrometry (MS) based imaging and X-ray fluorescence microscopy (XFM). With MS based imaging, samples are ablated at thousands of spots using a focused laser beam to generate charged ions^{183,184}. The ions are then separated in mass detector based on their m/z and ion counts of each atom are converted into atom concentration for that ablation spot¹⁸⁴. The image of metal distribution across the biological sample can be constructed using the concentration of the analyte metal in each ablation spot. X-ray fluorescence microscopy (XFM) is based on the characteristic X-ray released from atoms upon excitation of a core electron to the continuum by a high energy X-ray beam from a synchrotron source^{183,185}. The emitted X-ray fluorescence intensity is proportional to the concentration of each atom^{183,185}. Because each atom has unique and characteristic emission spectrum, XFM allows simultaneous mapping of multiple atoms^{186,187}.

1.8 Common Techniques To Measure Labile Zn²⁺

The widely used techniques for measuring labile Zn²⁺ can be classified into two groups: small-molecule fluorescence sensors and protein-based fluorescence sensors.

Small molecule Zn^{2+} sensors are comprised of a fluorophore conjugated with an electron-rich metal chelating group. All commercially available small-molecule Zn^{2+} sensors are intensity-based, meaning that the fluorescence intensity of the conjugated fluorophore increases upon Zn^{2+} binding to the metal chelating group. When Zn^{2+} is not bound, fluorescence is quenched by the PET (photoinduced electron transfer) mechanism between the fluorophore and the chelating group. The most popular PET-based probes include TSQ¹⁸⁸, Zinquin¹⁸⁹, FluoZin-3¹⁶⁸ and Newport Green PDX¹⁶⁸. A major disadvantage of PET-based sensors is pH sensitivity. This can be an obstacle in understanding zinc biology as an enrichment of labile Zn^{2+} in acidic vesicular compartments have been suggested to play important biological roles in different types of cells^{190–196}. For this reason, the Lippard group developed two reaction-based vesicular Zn^{2+} sensors, SpiroZin1¹⁹⁷ and SpiroZin2¹⁹⁸. The reaction-based sensor operates *via* a turn-on mechanism where Zn^{2+} binding induces a ring-opening reaction that converts a non-fluorescent spirobenzopyran to a fluorescent cyanine dye. Both sensors are insensitive to changes in pH between pH 3 and 7^{197,198}.

Although small-molecule sensors have many advantages such as high dynamic range, cell permeable, high intensity¹⁸³, their application is limited due to the non-specific intracellular localization and highly variable intensities, which confounds the interpretation of Zn^{2+} measurement¹⁹⁹. Moreover, non-specific accumulation causes high intracellular concentration of dye that buffers and perturbs cytosolic Zn^{2+} ¹⁹⁹. Protein-based sensors are genetically encoded, and therefore can be specifically targeted to subcellular organelles. Most protein-based sensors function by FRET (Förster resonance energy transfer). Sensor constructs are made of a FRET donor

fluorescent protein (FP), a linker sequence containing Zn^{2+} -binding domain(s), and an acceptor FP. Zn^{2+} binding induces a conformational change in the sensor, which results in an increase or decrease in FRET signals. Currently, FRET Zn^{2+} sensors have been targeted to all subcellular compartments including plasma membrane, ER, Golgi apparatus, mitochondria, nucleus and cytosol³⁹. However, one limitation of FRET sensors is that they utilize two FPs, which limits the multi-color imaging of another analyte in the same sample²⁰⁰. Recently-developed single FP-based Zn^{2+} sensors GZnP1²⁰⁰ and GZnP2²⁰¹ incorporate a circularly-permuted green fluorescence protein (cpGFP) and two zinc finger motifs. Upon Zn^{2+} binding, zinc finger motifs interact and this interaction induces a conformational change in cpGFP, which results in an increase of fluorescence^{200,201}. However, one substantial limitation of these sensors is their sensitivity of pH. A pH change from 6.5 to 7.5 resulted in a ~ 3-fold increase of sensor intensity²⁰⁰, which requires awareness of pH change during Zn^{2+} measurement. Despite this flaw, the single-FP Zn^{2+} sensors potentially allow multi-color imaging of Zn^{2+} in different organelles simultaneously.

Chapter 2

Remodeling of Zinc Homeostasis In Differentiated Mammary Epithelial Cells

2.1 Abstract

Zinc is the second most abundant transition metal in humans and is an essential nutrient required for growth and development of newborns. Zinc homeostasis needs to be tightly regulated, as zinc excess and zinc deficiency are associated with human diseases. During lactation, mammary epithelial cells (MECs) differentiate into secretory phenotype and uptake zinc from blood circulation and export zinc into mother's milk. At the cellular level, there are many zinc-dependent cellular processes (e.g. transcription, metabolism of nutrients) that play important roles in the differentiation of MECs. Using mouse mammary epithelial cells as a model system, we investigated the remodeling of zinc homeostasis during differentiation. We identified changes in global gene expression in MECs upon treatment with lactogenic hormones using RNAseq, including zinc-dependent genes and some regulatory genes for zinc homeostasis. Functional enrichment analysis of differentially-regulated zinc-dependent genes demonstrated a shift in the need for zinc during the switch of cell states. We further showed that the increased mRNA levels of three zinc homeostasis genes, *slc39a14* (ZIP14), metallothionein (MT) I and II were induced by cortisol but not by prolactin. The cortisol-induced increase in the steady state mRNA level of three genes was partially mediated by the nuclear glucocorticoid receptor signaling pathways. An increase in the cytosolic labile zinc pool was also detected in lactating mammary cells, consistent with the up-regulated mRNA level of MTs. ZIP14, a major zinc transporter, enriches in a perinuclear region in lactating cells, raising the possibility of a release of free zinc into cytosol from an intracellular organelle. ZIP14 is important for the expression of a major milk protein, whey acid protein (WAP), as knockdown of ZIP14 dramatically decreased

WAP mRNA level. In summary, we used RNAseq to characterize the regulation of the expression of zinc-dependent genes in differentiated mouse mammary epithelial cells. We also identified a ZIP14-mediated connection between zinc homeostasis and milk protein synthesis for the first time, implying the important role(s) of the regulation of zinc homeostasis in lactation.

2.2 Publication status

This manuscript is in preparation and will be submitted this summer 2019.

2.3 Introduction

Zinc is an essential trace element in humans, and both too much and too little zinc have been associated with a variety of health problems or diseases²⁰². The importance of zinc is underscored by the discovery that up to 10% of the proteins encoded by the human genome are predicted to contain a zinc binding site²⁰³. In these proteins, zinc may stabilize the 3-dimensional protein structure or serve as a catalytic cofactor²². Zinc homeostasis refers to a stable state in which organisms acquire, distribute and maintain zinc to ensure a healthy balance. Zinc homeostasis needs to be regulated tightly as suboptimal zinc homeostasis has been associated with many health problems and human diseases²⁰². Patients with nutritional or inherited zinc deficiency developed growth and development retardation, skin abnormalities, diarrhea^{202,204,205}. Zinc homeostasis is also deregulated in cancer. For example, it has been demonstrated that prostate cancer tissues only have 20 – 40% of zinc compared to normal prostate tissue^{206,207}, whereas breast cancer tissues have significantly higher zinc level compared to normal breast tissues^{208,209}. At the cellular level, too much zinc

can induce altered mitochondrial metabolism, mitochondrial apoptogenesis and cell death²¹⁰⁻²¹³.

Intracellular zinc homeostasis is known to be regulated by at least three classes of proteins, including zinc transporters, buffering proteins such as metallothionein (MT)/thionein (T) and the zinc-sensing metal transcription factor 1 (MTF1). Zinc transporters localize to cell and organelle membranes to regulate the distribution of zinc ions (Zn^{2+}) among subcellular compartments. Twenty-four Zinc transporters have been identified in humans including 14 SLC39A or Zrt-, Irt-like protein (ZIP) family transporters and 10 SLC30A or Zn transporter (ZnT) family transporters²¹⁴. Zinc transporters move Zn^{2+} across membranes with ZIPs transporting Zn^{2+} into the cytosol and ZnTs transporting Zn^{2+} out of the cytosol. It is been shown that the expression of some zinc transporters can be regulated by external stimuli at (post)transcriptional and (post)translational levels, including mechanisms such as transcriptional activation, alternative splicing, protein glycosylation and phosphorylation, and protein translocation^{58,60,111,112,114,118,120,121}. However, a full understanding of expression regulation and functional modification of all transporters is still lacking.

The second major class of proteins that regulate Zn^{2+} homeostasis is the class of buffering proteins called metallothionein (MT)/thionein (T) which are small proteins (61-68 amino acids) that can bind up to 7 zinc ions⁸⁵. Thionein (T) binds Zn^{2+} when Zn^{2+} is available, which leads to the formation of metallothionein (MT). The release of Zn^{2+} from MT is triggered by a reaction of the redox-active cysteine sulfur with oxidative species⁹⁰. The released Zn^{2+} is then available to bind cellular Zn^{2+} proteins such as zinc-dependent apoenzymes⁹⁰.

Finally, zinc homeostasis is also controlled by the zinc-MTF1 axis. MTF1 senses increases in cytosolic Zn^{2+} via a zinc-sensing motif and translocates to the nucleus to activate transcription of downstream zinc homeostasis genes, including MT1 and MT2 and zinc transporters ZnT1 and ZnT2^{58,104}. Zn^{2+} buffering by MT1 and MT2, and Zn^{2+} transport out of cytosol by ZnT1 and ZnT2 can protect cells from Zn^{2+} toxicity. MTF1 isn't the only regulator of zinc homeostasis, as a number of studies have shown that the expression of zinc homeostasis genes are modulated in response to external stimuli (e.g. hormone treatment) under different physiological and pathological conditions^{15,46,58,83,215–218}.

Mammary epithelial cells (MECs) undergo dramatic intracellular changes to fulfill their biological function during differentiation and lactation. Among these changes include many zinc-dependent cellular processes that play important roles in the switch of cell state. For example, two zinc-dependent transcription factors, Lmo4 and Zfp389, are upregulated during lactation and are suggested to regulate the proliferation and lactation of MECs^{219–221}. Matrix metalloproteinases (MMPs) are zinc-dependent enzymes that are secreted by MECs to remodel the architecture of the mammary gland and their expression levels are regulated in a temporal fashion throughout lactation²⁵. For example, MMP3³⁰ and MMP7³¹ expression were upregulated during lactation, whereas MMP2²²² and MMP11²²³ were downregulated in the ending stage of lactation. Moreover, MECs actively take up zinc from blood circulation and secrete a large amount of zinc (1-3 mg/day) into mother's milk²²⁴. We hypothesize that zinc homeostasis and zinc-dependent molecular processes are remodeled in MECs during lactation in response to dramatic shifts of cellular needs for zinc. A number of studies have

explored zinc and lactation, but our current understanding is limited to the altered expression or localization of zinc transporters and the involvement of some transporters in exporting zinc into milk or sequestering zinc into subcellular compartments^{49,60,66,80,173,225}. A systematic study is still needed to fully understand the regulation of zinc homeostasis and zinc-dependent processes in lactating MECs. In this study, the transcriptome of differentiated HC11 mouse mammary epithelial cells (MECs) was profiled using RNAseq and differential expression of zinc-dependent and zinc-homeostasis-regulatory genes were analyzed using DESeq2²²⁶. Functional annotation and enrichment of the differentially expressed zinc-dependent genes revealed an increased need for zinc for transport and a few enzyme classes, and decreased need for zinc for DNA/protein binding in secretory/differentiated HC11 cells compared to non-differentiated cells. Furthermore, I found out that 15 out of 19 expressed zinc homeostasis genes were differentially regulated in the differentiated HC11 cells upon lactogenic hormone treatment. Among these genes, the mRNA level of ZIP14 was directly enhanced by cortisol treatment and ZIP14 is responsible for the increase of cytosolic Zn²⁺ level in differentiated HC11 cells. Furthermore, ZIP14 is important for the mRNA expression of whey acid protein, which is a major milk protein, suggesting an important association between zinc homeostasis and milk production.

2.4 Experimental methods

2.4.1 Chemicals and reagents

Tris (2-pyridylmethyl) amine (TPA) was purchased from Sigma-Aldrich (catalog number 723134) and diluted with dimethyl sulfoxide (DMSO) to prepare 20 mM stock

solutions. Stock solutions (5 mM) of 2-mercaptopyridine N-oxide (pyrithione, Sigma-Aldrich, catalog number 188549) were prepared in DMSO. Nuclear staining was achieved with NucBlue Live ReadyProbes Reagent (Thermo Fisher, catalog number R37605) for live cells or Hoechst 33258 (Sigma-Aldrich 861405) for fixed cells. An aqueous ZnCl₂ solution (1 mM) was diluted in phosphate-free HEPES-buffered Hanks' balanced salt solution (HHBSS, 1.26 mM CaCl₂, 1.1 mM MgCl₂, 5.36 mM KCl, 137 mM NaCl, 16.65 mM D-glucose, and 30 mM HEPES, pH 7.4) to make a 200 μM ZnCl₂ stock solution. An insulin stock solution (4 mg/mL) was purchased from Life Technologies (catalog number 12585014). Human recombinant epidermal growth factor (EGF, VWR 47743-566) was prepared as a 10 μg/mL stock solution in water. Prolactin (Sigma-Aldrich L6520) was prepared as a 5 mg/mL stock solution in water. A stock solution (138 μM) of hydrocortisone (Sigma-Aldrich H0888) in absolute ethanol was also prepared. Trace-metal grade nitric acid (65% -70%) was purchased from FLUKA (02650). Y standard solution (10 ppm) was purchased from Inorganic Ventures (IV-stock-53-125 mL). Ga standard solution (1000 ppm) was purchased from Inorganic Ventures (ICP - CGGA1-125ML). For ICP-MS experiments, a Zn standard solution (1000 ppm) was purchased from VWR (Cat. No. RCMSZN1KN-100).

2.4.2 Cell culture

HC11 cells were grown and maintained in the proliferation (P) medium (RPMI supplemented with 10 % (v/v) fetal bovine serum (FBS), 1 % (v/v) penicillin/streptomycin (pen/strep), 10 ng/mL EGF and 5 μg/mL insulin). To induce cell differentiation, 4×10^5 cells were plated in a 35-mm dish (or 1×10^6 cells in a 10-cm

dish) in the proliferation medium. Cells reached confluency after 3 days. Cells were maintained in the resting (R) medium containing RPMI, 2 % FBS (v/v), 1 % pen/strep (v/v), 5 µg/mL insulin for one additional day, then treated with the differentiation (D) medium containing 2% FBS, 1% pen/strep, 5 µg/mL insulin, 5 µg/mL prolactin, and 1 µM hydrocortisone for up to 6 days. The differentiation medium was changed every 2 days. Samples were collected at the following time points for downstream analysis: P day 2 (cells growing in the proliferation media for 2 days since plated), R day 1 or day 6 (cells growing in the resting media for 24 hr or 7 days), D 12 hr, 24 hr, day 3 and day 6 (cells incubated in the differentiation media for the corresponding time).

2.4.3 Lentiviral transduction

HEK293T cells were maintained in RPMI media supplemented with 10 % FBS and transfected with lentiviral packaging plasmids and viral expression plasmids (which encode the promoter reporter constructs or ZIP14 shRNAs) using the TransIT-LT1 (Mirus Bio) reagent following the manufacturer's instruction. The packaging plasmids were a gift from Dr. Hubert Yin (University of Colorado, Boulder), containing pRev, which encodes the reverse transcriptase protein (Rev), pMDL, which encodes the Gag and Pol proteins, and pVSV-G, which encodes the Env protein. Media was changed at 24 hr after transfection. By day 3 after transfection, media was filtered using a 0.22 µm filter and the virus-containing media supplemented with 8 µg/mL of polybrene was added to HC11 cells. After 3 days, puromycin (3 µg/mL) was added to HC11 cells to select for cells with stable expression of exogenous genes. Cells that survived puromycin selection were recovered in the proliferation media and stored in liquid nitrogen for future use.

2.4.4 shRNA knockdown (KD) of ZIP14

Four individual ZIP14-targeted shRNA constructs were stably expressed in HC11 cells using lentiviral transduction (Genecopoeia, Cat. No. LVRU6MP-MSH038111-31,32,33,34). Successful transduction was selected by puromycin and expression of a red fluorescence protein (mCherry) marker using flow cytometry. The efficiency of ZIP14 KD was examined by RT-qPCR.

2.4.5 Reverse transcription polymerase chain reaction (RT-PCR) and quantitative reverse transcription PCR (RT-qPCR)

HC11 cells were trypsinized and harvested. Cell pellets were stored at -80 °C after flash freezing in liquid Nitrogen until use. RNA purification, DNA removal and reverse transcription were performed following manufacturer's protocols. Specifically, RNA was purified with the RNease Mini Kit (QIAGEN, Cat. No. 74106); DNA was removed by DNaseI treatment (Thermo Scientific Cat. No. EN0525); RNA was reverse transcribed to cDNA using oligodT primers (Invitrogen, Cat. No. 18418012) and the Omniscript RT Kit (QIAGEN, Cat. No. 205113). RNase inhibitor (RNaseOUT Recombinant Ribonuclease Inhibitor, Invitrogen, Cat. No. 10777019) was supplemented in all reaction mixtures to inhibit RNA degradation. The synthesized first-strand cDNAs were then used as templates in the RT-PCR or RT-qPCR reactions. RT-PCR and RT-qPCR reactions were performed using Phusion DNA polymerase (NEB, Cat. No. M0530S) and SYBRTM Green PCR Master Mix (Applied Biosystems, Cat. No. 4367659), respectively, following manufacturer's protocols. Quantitative analysis of relative expression of target genes normalized to reference genes using qPCR data was performed with the Pfaffl method as previously described²²⁷. Detailed information

including RT-(q)PCR protocols, primer sequences and quantification method (standard curve, efficiency) are provided in Appendix A.

2.4.6 Western blotting

HC11 cell pellets were resuspended in cold RIPA buffer supplemented with 1 mM dithiothreitol (DTT) and a protease inhibitor cocktail (one tablet per 10 mL, cComplete, Roche, Cat. No. 04693159001). The mixture was incubated at 4 °C for 30 minutes on a rotator, followed by centrifugation at maximum speed (14,000 rpm) at 4 °C for 30 min. The pellet containing cell debris and nuclei was discarded. The protein concentration in the supernatant fraction was measured by the BCA assay (Pierce™ BCA Protein Assay Kit, Thermo Scientific™, Cat. No. 23225). 15 µg of protein was mixed with 5x SDS-loading dye and denatured at 95 °C for 5 min (CSN2 immunoblot). The protein mixture was separated on 10 % (w/v) acrylamide gels for SDS-PAGE and then transferred to PVDF membranes at 80 V for 1 hr. The membrane was blocked in 5 % (w/v) non-fat milk in 1x TBS-T (1x TBS with 0.1 % (v/v) Tween20, pH 7.4) at room temperature for 1 hr. The membrane was incubated with the primary antibody in blocking buffer overnight at 4 °C. The next day, the membrane was washed with 1x TBS-T for 30 min (10 min x 3 washes) and incubated in secondary antibody in blocking buffer at room temperature for 1 hr. Membrane was washed with 1x TBS-T for 30 min (10 min x 3 washes) again. Blots were developed with the Amersham ECL Prime Western Blotting Detection Reagent (GE Healthcare Life Sciences, Cat. No. RNP2232) and imaged on an ImageQuant LAS4000 imaging system (GE Healthcare Life Sciences). The antibodies used in immunoblot were as follows: Beta-CSN2: the primary antibody was the goat anti-β-casein polyclonal antibody (Santa Cruz

Biotechnology, SC-17971), 1:4,000 dilution; secondary antibody was donkey anti-goat IgG (H+L) secondary antibody (HRP) (Novus Biologicals, Cat. No. NB7357), 1:40,000 dilution. ACTB: the primary antibody was mouse anti- β -actin antibody (Sigma, A2228), 1:10,000 dilution; secondary antibody was goat anti-mouse IgG (H+L) secondary antibody (HRP) (Novus Biologicals, Cat. No. NB7539), 1:20,000 dilution.

2.4.7 Immunofluorescence

For immunofluorescence detection of CSN2, HC11 cells were grown on glass coverslips and induced to differentiate. Samples were collected at the following time points: P day 2, R day 1, D 12 hr, 24 hr, day 3 and day 6. Cells were washed with phosphate-buffered saline (PBS) three times and then fixed in 4 % paraformaldehyde (PFA) in PBS for 45 min in the dark at room temperature. Cells were washed with PBS three times, followed by incubation with 20 mM NH_4Cl in PBS for 5 min at room temperature. Samples were stored in PBS at 4 °C until use. For permeabilization of the cell membrane, cells were incubated with 0.2 % Triton X-100 in PBS solution for 15 min at room temperature, followed by washing 3x with PBS and blocking in 5 % bovine serum albumin (BSA) for 45 min. Cells were washed with PBS three times and then incubated with primary antibody (goat anti- β -casein polyclonal antibody, Santa Cruz Biotechnology, SC-17971, 1:10 dilution) at room temperature for one hr. Cells were washed with PBS three times and then incubated with secondary antibody (donkey anti-goat IgG-FITC, Santa Cruz Biotechnology, SC-2024, 1:20 dilution) at room temperature for one hr. Cells were then washed with PBS three times. To stain nuclei, cells were incubated with 1 mg/mL Hoechst 33258 in H_2O for 30 seconds at room temperature and then washed with PBS three times prior to mounting on glass slides.

For immunofluorescence detection of ZIP14, HC11 cells were grown on glass coverslips and induced to differentiate. Samples were processed on D day 6 and R day 6. The fixation and permeabilization procedures were the same as above. Samples were incubated with primary antibody (rabbit anti-SLC39a14 antibody, Abcam, ab106568, 1:100 dilution) at 4°C overnight and on the following day, cells were incubated with secondary antibody (donkey anti-rabbit, 568/600nm, Invitrogen, A10042, 1:500 dilution) for one hr at room temperature.

CSN2 immunofluorescence images were acquired on a Nikon A1R laser scanning confocal microscope equipped with the Nikon Elements software platform, Ti-E Perfect Focus system with a Ti Z drive, using a 100x oil objective (NA 1.45) and the following channels: CSN2 (green) (488 nm laser line, PMT gain: 45 or 110, pinhole size: 1 or 4 AU, emission filter: 525/50 nm); Hoechst 33258 (blue) (405 nm laser line, PMT gain: 80 or 95, pinhole size: 1 AU, emission filter: 450/50 nm). ZIP14 immunofluorescence images were acquired on a Nikon Ti-E spinning disc confocal microscope fitted with a Yokogawa CSU-X1 spinning disc head, equipped with the Nikon Elements software platform and Ti-E Perfect Focus system. Cells were imaged using a 60x oil objective (NA 1.40) and the following channels: ZIP14 (red) (561 nm laser line, EM gain: 300, emission filter: 620/60 nm) and Hoechst 33258 (blue) (405 nm laser line, EM gain: 300, emission filter: 482/35 nm).

2.4.8 RNAseq

To prepare samples for RNAseq, three biological replicates of HC11 cells were trypsinized and harvested. Cell pellets were stored at -80 °C after flash freezing until use. RNA was extracted with the RNease Mini Kit (QIAGEN, Cat. No. 74106). DNA

was removed by DNaseI treatment (Thermo Scientific Cat. No. EN0525). RNA samples were then submitted to the Next-Gen Sequencing Core Facility at University of Colorado BioFrontiers Institute for library construction and sequencing. Specifically, libraries were prepared using the NEXTflex Rapid Illumina Directional RNA-Seq Library Prep Kit with polyA enrichment (Bioo Scientific). Sequencing was performed on the NextSeq platform using paired-end reads (High Output, 2 x 75). After sequencing, read quality was assessed using FastQC (version 0.11.2). Illumina adaptors were trimmed using Trimmomatic 0.32 in paired-end mode. Reads were then mapped to mm10 gtf file using Tophat²²⁸. Mapped reads were counted using HTSeq²²⁹ with the options {-f -r -s -m intersection-strict}. Differential expression of genes was analyzed using DESeq2²²⁶. The expression level of zinc homeostasis genes was represented as fragments per kilobase per million mapped reads (FPKM) using the following equation: $FPKM = \frac{\text{number of reads}}{\text{length of region in kilobase} \times \text{number of mapped reads in millions}}$.

2.4.9 Inductively coupled plasma mass spectrometry (ICP-MS)

All ICP-MS samples were spiked with known amounts of two internal standard elements, Yttrium (Y) and Gallium (Ga) to correct technical or human errors. The ion counts of zinc (Zn) in each sample measured by ICP-MS were corrected by the ratio of measured Y or Ga (ppb) to the known amount of Y or Ga (ppb). The Zn ion counts were then converted to parts per billion (ppb) using a Zn standard curve. The Zn ppb signal was normalized to total cell number to compare Zn in different samples. To prepare the HC11 cells for ICP-MS, 10×10^6 cells were trypsinized and harvested in 15

mL metal-free conical tubes (VWR, 89049-172) and then cell pellets were dried at 50 °C in a fume hood overnight. The next day, 200 µL of Trace-metal grade 65 % Nitric Acid (FLUKA, 02650) was added to cell pellets and the mixture was heated in boiling water for 30 minutes. After the samples cooled down to room temperature, the nitric acid concentration in samples was corrected to 2 % using chelex-treated Milli-Q water. 5 ppb of Y and 5 ppb of Ga were added to each sample as internal standard elements. Samples were submitted for ICP-MS analysis to the LEGS Lab at CU Boulder. Zn (ppb) was converted to the concentration ([Zn]) of Zn per cell. Detailed protocols and data analysis is in Appendix C.

2.4.10 Measurement of labile cytosolic Zn²⁺ using NES-ZapCV2

An HC11 cell line stably expressing the cytosolic Zn²⁺ sensor NES-ZapCV2²³⁰ was generated using the PiggyBac transposase system (System Biosciences) following the manufacturer's instruction. Fluorescence imaging was performed on a Nikon Ti-E wide-field fluorescence microscope equipped with Nikon elements software, an iXon3 EMCCD camera (Andor), mercury arc lamp, and YFP FRET (434/16 excitation, 458 dichroic, 535/20 emission), CFP (434/16 excitation, 458 dichroic, 470/24 emission), YFP (495/10 excitation, 515 dichroic, 535/20 emission) filter sets. The FRET ratio (R) of YFP FRET intensity / CFP intensity was recorded every 40 seconds over a time course. To perform a titration experiment, the FRET ratio of a randomly selected cytoplasmic region in single cell was recorded every 40 seconds for ~ 3 min in the resting state. All FRET ratios were then averaged to acquire the resting ratio (R). Cells were then treated with 150 µM TPA (Zn²⁺ chelator) for an extended time (~ 20 min) to ensure that FRET R decreased and stabilized. The minimum ratio, R_{min}, was acquired by

averaging ratios of the last 3 time points of TPA treatment. After cells were washed twice with phosphate-free HHBSS buffer, a mixture of pyrithione (a Zn^{2+} ionophore, final concentration 0.75 μM) and $ZnCl_2$ (final concentration 20 μM) was added to cells. FRET ratio increased and reached a plateau. The maximum ratio, R_{max} , was calculated by taking the mean of all ratios measured in the plateau phase. The labile Zn^{2+} concentration can be calculated using this equation: $[Zn^{2+}] = K_d \times [(R - R_{min}) / (R_{max} - R)]^{1/n}$. For the NES-ZapCV2 cytosolic sensor, the $K_d = 2.3$ nM and Hill Coefficient (n) = 0.532²³⁰. Alternatively, the labile Zn^{2+} concentration can be represented as the fractional saturation (FS) of sensors, which was defined as $FS = (R - R_{min}) / (R_{max} - R_{min})$. Cells with a dynamic range (R_{max} / R_{min}) in the range of 1.5 – 2.5 were selected for analysis.

2.4.11 Promoter reporter assay

The promoter reporter assay designed to test the promoter activity in response to hormone treatment was performed using the Secrete-Pair Dual Luminescence Assay Kit (GeneCopoeia) following the manufacturer's instructions. The CSN2, ZIP14 and MT2 promoters were amplified from the HC11 cell genome using the NucleoSpin BloodXL kit (MACHEREY-NAGEL, ref 740950.50). The MT1 promoter was synthesized by IDT. All promoters were inserted into the multiple cloning site 1 (MCS1) of the pEZX-LvGA01 vector (GeneCopoeiaTM, catalog No. ZX107) 5' upstream of the Gaussia Luciferase (GLuc) ORF. This vector also constitutively expresses an internal control reporter, SEAP (secreted alkaline phosphatase). Both GLuc and SEAP can be secreted into cell media upon being synthesized. The promoter activity is reported using the ratio of GLuc signal to the SEAP signal. Detailed information about promoter

sequences: for CSN2, the 983-bp promoter sequence includes a 900-bp fragment upstream of the transcription start site (TSS) and a 100-bp fragment downstream of the TSS; for ZIP14, the 1850-bp promoter sequence includes a 1349-bp fragment upstream of the TSS and a 500-bp fragment downstream of the TSS; for MT1, the 1209-bp promoter sequence includes a 956-bp fragment upstream of the TSS and a 122-bp fragment downstream of the TSS; for MT2, the 1301-bp promoter sequence includes a 1000-bp fragment upstream of the TSS and a 300-bp fragment downstream of the TSS. The TSS position was acquired from the Eukaryotic Promoter Database (EPD). HC11 cell lines stably expressing promoter constructs were generated using lentiviral transduction and selected for successful transduction by puromycin. To determine the promoter activity in response to lactogenic hormone treatment, 4×10^5 HC11 stable cells were plated in a 35 mm dish in the proliferation media (2 mL) for 3 days and then cultured in the resting media (2 mL) for one more day. Cells were then treated with the lactogenic hormones for 6 days with fresh media replaced every 2 days. For luciferase analysis, 200 μ L of media was collected at 4, 18, 24 hr, day2, 3, 4, 5 and 6 post hormone treatment. 200 μ L of fresh media was added back to cell culture to compensate for the volume change after media collection. All samples were frozen at -20 °C use. The GLuc and SEAP catalyzed luminescence reactions were performed using the Secrete-Pair™ Dual Luminescence Assay Kit (GeneCopoeia) following the manufacturer's instructions. Luminescence was recorded using a BioTek Synergy H1 hybrid plate reader (gain: 200; integration time: 3 s). 2 biological replicates were utilized at each time point and 3 technical replicates were measured for each biological replicate.

2.5 Results

2.5.1 Characterization of HC11 cell differentiation

The HC11 cell line was isolated from the COMMA-1D mammary epithelial cell line²³¹ which was established from the mammary tissue of BALB/c mice in the middle of pregnancy²³². The endogenous expression of several milk genes in HC11 cells can be rapidly induced by a combination of lactogenic hormones (prolactin and cortisol) without the requirement of any matrix protein^{231,233}. For this reason, the HC11 cell line has been widely used as a model system to investigate mammary cell differentiation^{234–236}. HC11 cells were induced to differentiation using a previously established protocol^{231,237} (Figure 2.1A). Samples were collected in the proliferation state (P day 2), resting state (R day 1) and upon treatment with prolactin and cortisol, representing the differentiation state (D 12 hr, 24 hr, day 3 and day 6). The progression of differentiation was characterized by examining the mRNA level of two lactation markers, casein (CSN2) and whey acid protein (WAP) in all samples using RT-PCR. As shown in Figure 2.1B, mRNA of CSN2 and WAP were not detected until 3 days after hormone treatment and the mRNA levels of both genes further increased at day 6 after treatment. Figure 2.1C shows that that CSN2 protein levels, as detected by Western blot appear at 3 days after treatment and increase further 6 days after treatment, paralleling the mRNA signature. CSN2 and WAP expression are induced by the JAK-STAT and glucocorticoid receptor (GR) signaling pathways^{231,238,239}. To examine differentiation markers at the single cell level, I performed immunofluorescence to examine CSN2 protein expression over the course of differentiation. The total number of cells and number of cells that stained

positively for CSN2 expression were counted and the percentage of cells with CSN2 expression was quantified. As shown in Figure 2.1D, CSN2 expression was essentially undetectable in P day 2 (0.00%) and R day 1 samples (0.08%). After hormone treatment, CSN2 was expressed in a heterogeneous manner with some cells exhibiting strong expression and others with undetectable levels D 12 hr (0.74 %), 24 hr (0.68 %) and day 3 (13.4 %) samples. By day 6 after hormone treatment, CSN2 expression was detected in almost each single cell (95.5%). Although it took 3 days of hormone treatment to detect the steady-state mRNA and protein level of lactation markers, using a luciferase promoter assay, I identified that gene transcription from the CSN2 promoter was initiated early at 18 hr and the transcriptional activity continued to increase at 24 hr, day 2, 3, 4, 5 6 post lactogenic hormone treatment (Figure 2.1E).

Figure 2.1

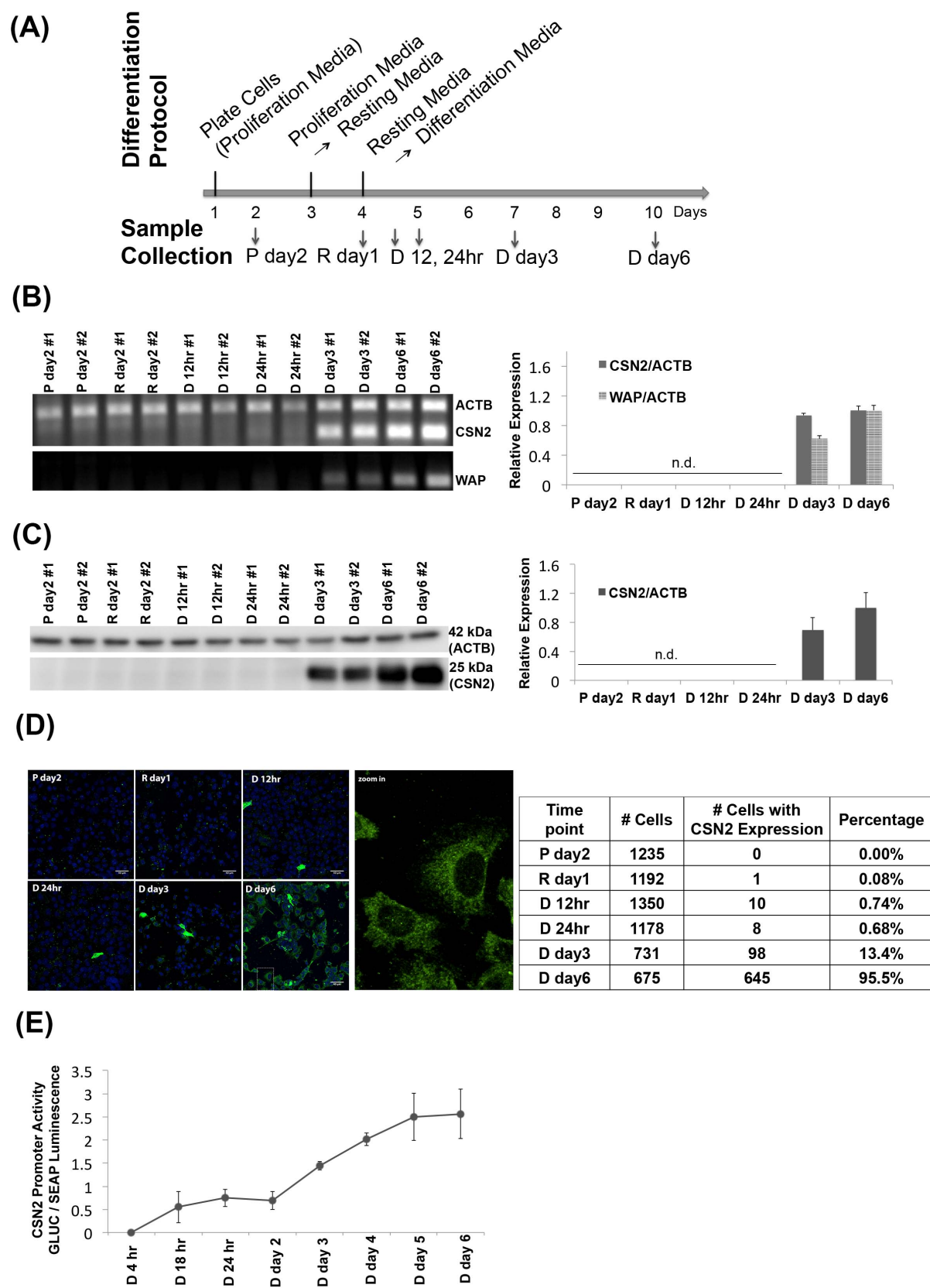


Figure 2.1: Characterization of HC11 cell differentiation upon hormone treatment. (A) Outline of the differentiation protocol (P, proliferation media; R, resting media; D, differentiation media. (B) RT-PCR of control ACTB, and differentiation markers CSN2 and WAP. Left: Agarose gel showing intensity of PCR signal over the course of differentiation; Right: quantification of relative expression of CSN2 and WAP normalized to ACTB. (C) Immunoblot of CSN2 and ACTB protein expression at different time points. Left: SDS-PAGE and Right: quantification of relative protein expression (CSN2 normalized to ACTB). (D) Immunofluorescence of casein protein expression at the single cell level. Left: representative fluorescence images. Scale bar, 40 μm . Right: Quantification of immunofluorescence (total # cells with CSN2 expression divided by the total cell number. Total number of cells are from 2 independent experiments). n.d., not detected. (E) Dual luciferase reporter assay of the transcriptional activity of the CSN2 promoter at different time points post hormone treatment. The Gaussia Luciferase (GLUC) signal was normalized to the signal of the constitutively expressed secreted alkaline phosphatase (SEAP). $n = 2$ biological replicates. Error bars represent standard deviation.

2.5.2 Changes in global gene expression at 24 hr and 6 days post hormone treatment.

To define how treatment with lactogenic hormones remodeled global gene expression of mammary epithelial cells, I performed next-generation RNA sequencing (RNAseq) of R day 1 (control), D 24 hr (early stage differentiation) and D day 6 (later stage differentiation) samples, with 3 biological replicates under each condition. The expression of genes in D 24 hr and D day 6 samples relative to R day 1 samples was analyzed using DESeq2, which uses the p-value, log₂ fold-change (y-axis in the MA plots) and mean counts (normalized to the sequencing depth of all samples) to identify genes as differentially expressed. As shown in the MA plots in Figure 2.2A, the red dots are differentially expressed genes at D 24 hr (1909 genes, $p < 0.001$) or D day 6 (8161 genes, $p < 0.001$) compared to R day 1, with each dot representing a gene. The volcano plots in Figure 2.2B depict differentially-expressed genes with $p < 0.001$ and fold change in expression (differentiated cells versus R day 1) > 2 , and allows direct

visualization of the fold change and statistical significance of the differentially expressed genes. The genes that were differentially expressed by more than 2-fold are highlighted in red, with 1132 genes at 24 hr and 2943 genes at day 6 post hormone treatment, which accounts for 4.5 % or 11.7 % of 25059 total mouse genes⁸, respectively.

To gain insight into the biological functions that were altered upon differentiation, the gene enrichment and functional annotation of the downregulated and upregulated genes at 24 hr and day 6 (fold change > 2, $p < 0.001$) post-hormone treatment were analyzed using DAVID 6.8 with GOTERM_BP_DIRECT (BP: biological processes). Enrichment of biological processes was ranked based on the p-value (EASE score) associated with each annotation term, with lower p-value indicating greater enrichment. The p-value of each term of each condition is included in the appendix B. The top GO terms were selected and clustered according to their biological functions. As shown in Figure 2.2C, cell proliferation and cell migration were significantly downregulated at 24 hr, and further downregulated at day 6 post-hormone treatment. The major biological processes that were upregulated in differentiated cells were immune response, transport, ER unfolded protein response, cellular zinc ion homeostasis, hormone response, cell signaling and metabolic processes. Among these processes, ion transport, response to glucocorticoid and activation of MAPK activity were enriched in both down- and up-regulated genes in D day 6 samples. Fatty acid biosynthetic processes were first downregulated at 24 hr and then upregulated at day 6 after hormone treatment. Overall, RNAseq revealed that lactogenic hormone treatment significantly altered the activities of numerous different biological processes in

mammary epithelial cells, including cellular zinc ion homeostasis, which was upregulated at 6 days of hormone treatment

Figure 2.2

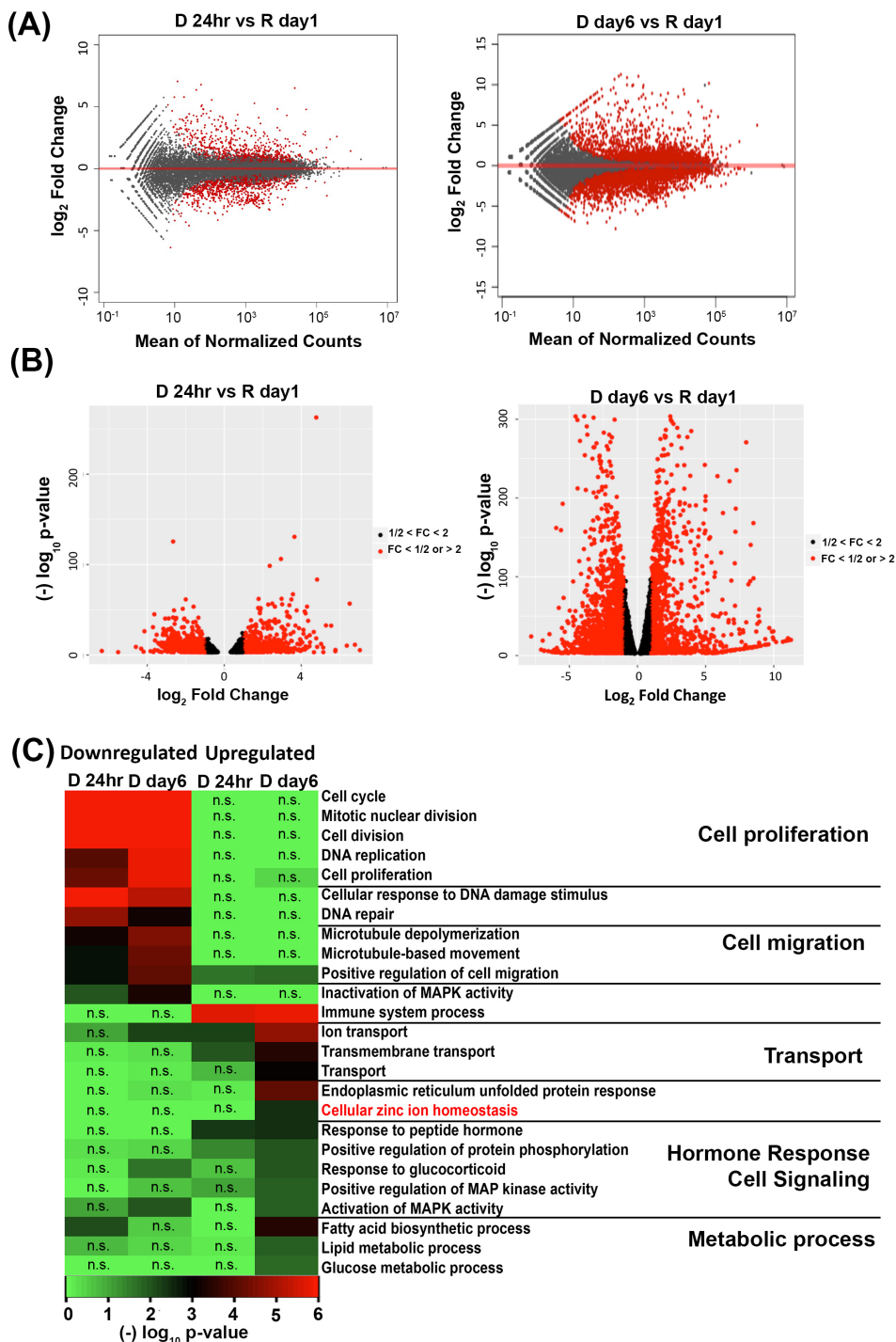


Figure 2.2: Global gene expression changes at 24 hr and 6 days post hormone treatment. (A) MA plots of \log_2 fold change of mRNA level in D 24 hr and D day 6 samples relative to that in R day1 versus mean normalized counts for each gene. Sequencing reads were processed using DEseq2 and each red dot represents a differentially expressed gene ($p < 0.001$). (B) Volcano plots of the $-\log_{10}$ (p-value) versus \log_2 (fold change in gene expression) for genes with $p < 0.001$. Dots highlighted in red indicate > 2 -fold change. FC: fold change. (C) Heat map of the top 11 downregulated (left) and top 14 upregulated (right) functional gene categories. Functional annotation was performed using the “Functional Annotation Chart” with GOTERM_BP_DIRECT ($P < 0.05$) in DAVID. The log p-value of each functional term under each condition was represented in the heatmap, with lower p-value indicating greater enrichment. n.s., not significant, $p \geq 0.05$.

2.5.3 Differential expression of zinc-dependent genes in differentiated cells

To explore how the expression of zinc-regulatory and zinc-dependent genes were modulated by lactogenic hormone treatment, the differentially expressed genes at 24 hr and day 6 post hormone treatment (fold change > 2 , $p < 0.001$) were annotated using DAVID 6.8 with UniProt (UP)_Keywords. According to the definition of “Ligand” keyword (KW9993) in the Uniprot database, the UP_Keyword “Zinc” (KW0862, which is in the “Ligand” category) was assigned to genes when the translated gene products (i.e. proteins) bind, are associated with, or whose activity is dependent on zinc. In D 24 hr samples, 62 out of 671 (9.2 %) downregulated genes and 24 out of 461 (5.2 %) upregulated genes were annotated as zinc genes, respectively. In D day 6 samples, 149 out of 1684 (8.8 %) downregulated genes and 91 out of 1259 (7.2 %) upregulated genes were annotated as zinc genes, respectively (Figure 2.3A). The 149 downregulated and 91 upregulated zinc genes were then sorted based on fold change or p-value. Interestingly, two zinc transporters, SLC39a8 (ZIP8) and SLC39a14 (ZIP14), were reported among the top 10 genes with highest fold change or lowest p-value respectively (Table 2.1).

Table 2.1 Top downregulated and upregulated zinc genes

Downregulated Zinc Genes		Upregulated Zinc Genes	
Gene Full Name (symbol)	log ₂ FC	Gene Full Name (symbol)	log ₂ FC
Histocompatibility (minor) HA-1 (Hmha1)	-4.66	Kallikrein 1-related peptidase b3 (Klk1b3)	7.93
Amidohydrolase domain containing 1 (Amdhd1)	-4.57	Tripartite motif-containing 55 (Trim55)	6.99
Snail family zinc finger 1 (Snai1)	-4.54	Kruppel-like factor 15 (Klf15)	5.65
ArfGAP with coiled-coil, ankyrin repeat and PH domains 1 (Acap1)	-4.54	Kallikrein 1-related peptidase b4 (Klk1b4)	5.51
Sp7 transcription factor 7 (Sp7)	-4.42	Melanophilin (Mlph)	5.43
Nitric oxide synthase 2, inducible (Nos2)	-4.21	Zinc finger protein 385B (Zfp385b)	5.41
Dystrophin related protein 2 (Drp2)	-4.01	Zinc finger, imprinted 1 (Zim1)	5.23
Neutralized E3 ubiquitin protein ligase 1A (Neurl1a)	-4.01	Dipeptidase 1 (Dpep1)	4.59
Activation-induced cytidine deaminase (Aicda)	-3.96	Angiotensin I converting enzyme peptidyl-dipeptidase A (Ace2)	4.23
Tripartite motif-containing 9 (Trim9)	-3.94	Solute carrier family 39 (zinc transporter), member 8 (SLC39a8)	4.21
	(-) log P-value		(-) log P-value
Snail family zinc finger 1 (Snai1)	303.6	Amyloid beta (A4) precursor protein (App)	274.9
Cysteine and glycine-rich protein 2 (Csrp2)	290.9	Carboxypeptidase Q (Cpq)	254.3
PDZ and LIM domain 7 (Pdlim7)	280.4	Collagen, type IX, alpha 1 (Col9a1)	229.7
PR domain containing 1, with ZNF domain (Prdm1)	264.5	Pleckstrin homology domain containing, family F member 1 (Plekhf1)	182.2
Zinc finger protein 703 (Zfp703)	201.5	Jade family PHD finger 2 (Jade2)	180.3
A disintegrin and metalloproteinase domain 12 (Adam12)	201.1	RAS protein activator like 1 (GAP1 like) (Rasal1)	160.3
Superoxide dismutase 3, extracellular (Sod3)	191.2	Ring finger protein 149 (Rnf149)	151.2
Zinc finger protein 385A (Zfp385a)	191.2	Solute carrier family 39 (zinc transporter), member 14 (SLC39a14)	149.8
Matrix metalloproteinase 11 (Mmp11)	163.5	Zinc finger protein 36 (Zfp36)	141.1
Kruppel-like factor 10 (Klf10)	163.3	Human immunodeficiency virus type 1 enhancer binding protein 3 (Hivep3)	134.7

To further examine functional categories of differentially expressed zinc-dependent genes, the gene enrichment and functional annotation of downregulated and upregulated genes in D 24 hr and D day 6 samples (fold change > 2, p < 0.001) were analyzed using DAVID 6.8 with GOTERM_MF_DIRECT (MF: Molecular Function), as described previously. The p-value of each term of each condition is included in the appendix. Top GO terms were selected based on the p-value. Because no GO term / molecular function was enriched from the analysis with the 24 upregulated zinc genes in D 24 hr samples, only top GO terms enriched in the differentially expressed zinc genes

in D day 6 samples were selected and represented in the heatmap with corresponding p-values (Figure 2.3B). Fourteen GO terms were enriched among these zinc-dependent genes, with 6 underlined terms enriched in both down- and upregulated zinc genes ($P < 0.05$). Ten out of fourteen terms were more enriched in the 149 downregulated zinc genes, such as nucleic acid binding, DNA binding and protein binding. Four terms were more enriched in the 91 upregulated zinc genes including hydrolase activity, nucleotide diphosphatase activity, phosphodiesterase I activity and zinc ion transmembrane transporter activity. In summary, enrichment analysis of functional categories of differentially expressed zinc-dependent genes revealed a shifted need for zinc during the switch of cell states (resting to differentiation), with a lower need for zinc for proteins involved in molecular binding and a higher need for zinc for a few enzyme classes. Combined with the fact that two zinc transporters (ZIP8 and ZIP14) were among the top differentially-regulated genes, our data suggest that zinc transport, distribution and zinc levels may also be altered upon hormone treatment.

Figure 2.3

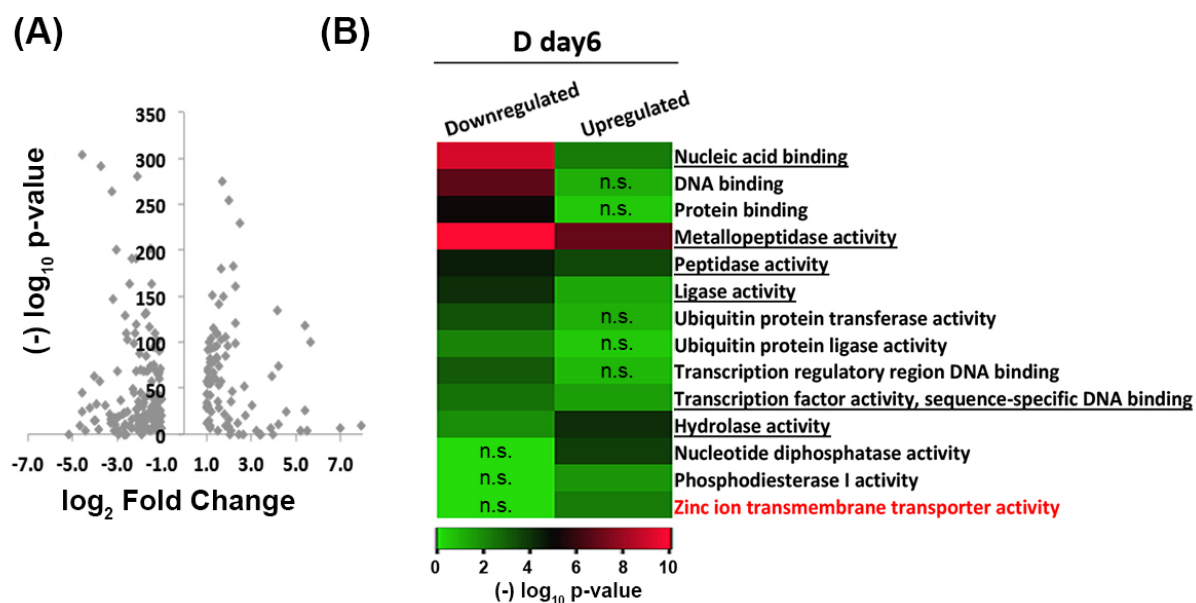


Figure 2.3: Differential expression of zinc-dependent genes at day 6 post hormone treatment compared to the resting state. (A) Comparison of $-\log_{10}(\text{p-value})$ and $\log_2(\text{fold change in gene expression})$ for genes with greater than 2-fold change (D day 6 versus R day 1). Fold change was determined using DESeq2 with $p < 0.001$ (B) Heat map of the 11 downregulated (left) and 4 upregulated (right) functional gene categories. Functional annotation was performed using the “Functional Annotation Chart” with GOTERM_MF_DIRECT ($P < 0.05$) in DAVID. The log p-value of each functional term under each condition was represented in the heatmap, with lower p-value indicating greater enrichment. The underlined terms were enriched in both down- and upregulated genes. n.s., not significant, $P \geq 0.05$.

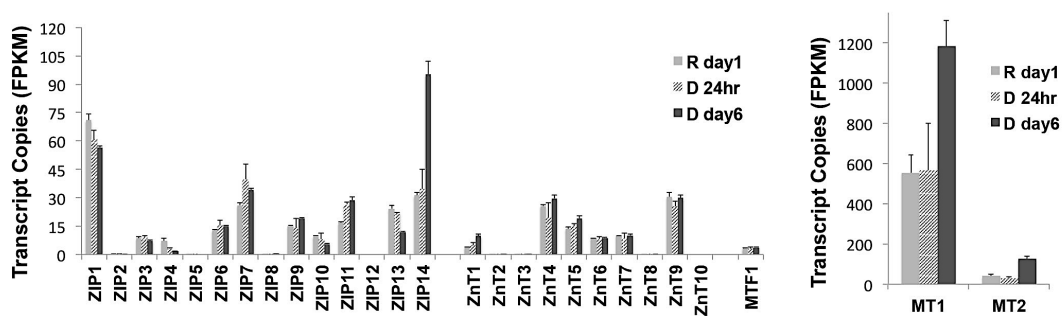
2.5.4 Differential expression of zinc homeostasis genes

Because cellular zinc ion homeostasis emerged as one of the major biological processes that was altered upon hormone treatment and two zinc transporters emerged as being differentially expressed upon analysis of zinc-dependent genes, I used our RNAseq data to specifically analyze how known zinc regulatory genes change upon differentiation. Because many zinc transporters are expressed at low levels, I first examined the average fragments per kilobase per million mapped reads (FPKM) for each zinc regulatory gene (Figure 2.4A). FPKM is a metric that provides a relative measure of mRNA expression level, as a greater number of fragments mapped corresponds to a greater amount of mRNA present in the sample. Genes with $\text{FPKM} < 1$ weren't included in differential expression analysis because the expression level was deemed too low to be reliable. 19 zinc homeostasis genes with $\text{FPKM} > 1$ were detected in all conditions and analyzed for differential expression using DESeq2. Figure 2.4B depicts the fold-change of differentially expressed genes with a $p < 0.001$ in D 24 hr and D day 6 samples relative to R day 1. Only 2 zinc homeostasis genes, ZIP4 and ZIP11, were differentially regulated at D 24. After 6 days of hormone treatment, 14 zinc homeostasis genes were differentially expressed. Among those, 3 genes were down-

regulated and all of them were ZIP genes, whereas 11 genes were up-regulated including 5 ZIPs, 3 ZnTs, 2 MTs and MTF1. These results demonstrate that expression of zinc homeostasis genes is significantly remodeled upon treatment with lactogenic hormones and reveal that zinc homeostasis is more significantly altered at a late stage of cell differentiation. For downstream analysis of how hormones affect mRNA expression, ZIP14, MT1 and MT2 were chosen as targets because of their relatively high expression level and fold change in D day6 samples compared to that in resting cells.

Figure 2.4

(A)



(B)

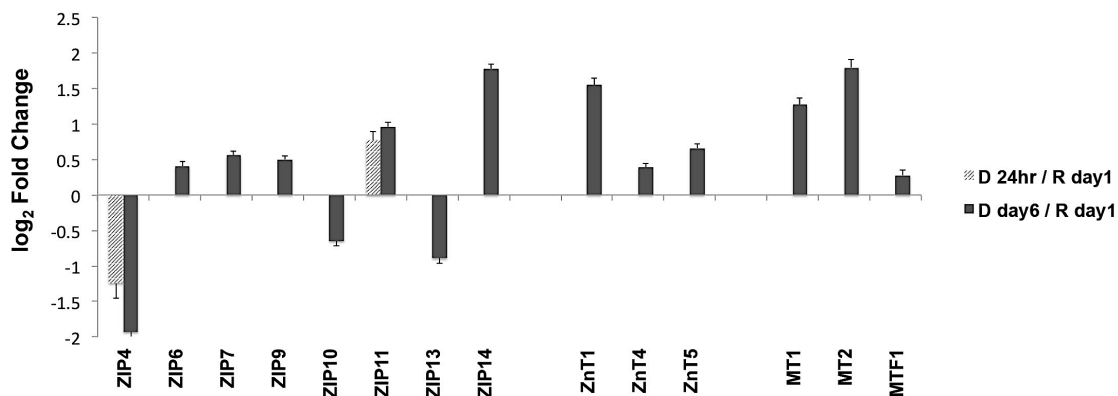


Figure 2.4: Differential expression of zinc homeostasis genes. (A) Mean FPKM values from 3 independent replicates for each zinc homeostasis gene under the resting and differentiated conditions. (B) Mean \log_2 (fold change) of differentially expressed zinc homeostasis genes upon hormone treatment normalized to expression under resting conditions. Only genes with mean FPKM > 1 were included. Differential expression was analyzed using DESeq2, $p < 0.001$. Error bars represent standard deviation.

2.5.5 Cortisol increases the steady-state level of ZIP14, MT1 and MT2 mRNAs.

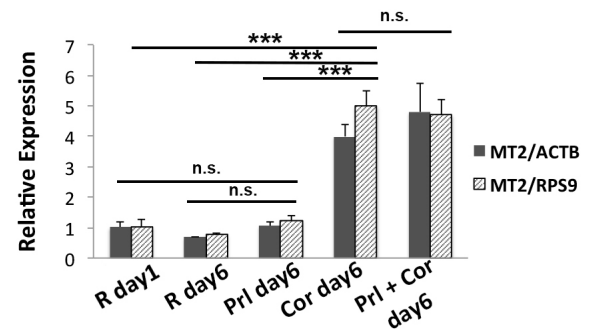
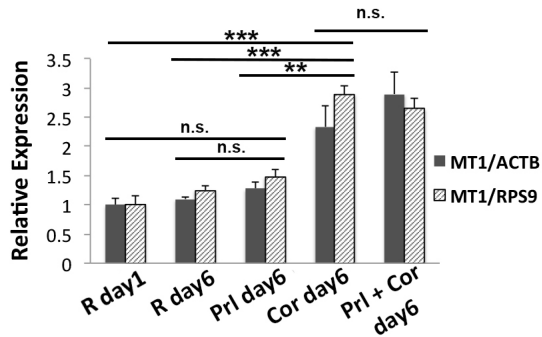
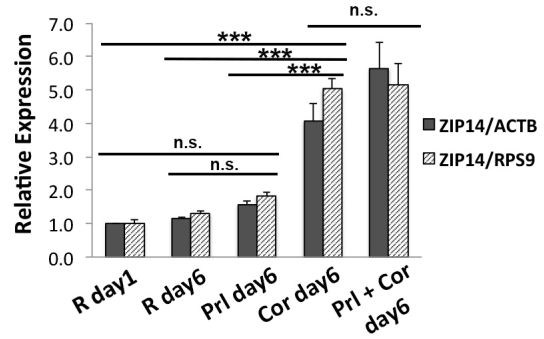
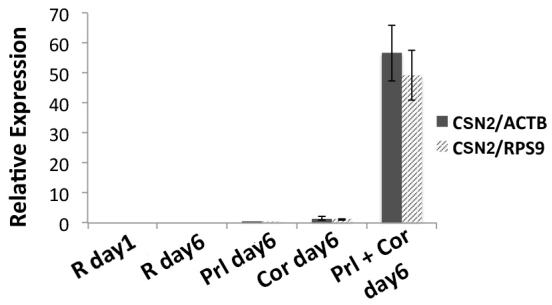
Two lactogenic hormones, prolactin and cortisol, were used to initiate HC11 cell differentiation. To distinguish the role of each hormone in regulating the mRNA levels of zinc homeostasis genes, HC11 cells were cultured in the proliferation media or resting media as in the differentiation protocol and then treated with prolactin (Prl), cortisol (Cor), or both hormones (Prl + Cor) for 6 days. Cells were collected at day 1 post treatment with the resting media (R day 1), and day 6 post treatment with hormone(s) (Prl day 6, Cor day 6 and Prl+Cor day 6). To eliminate the possibility that the higher levels of mRNA for zinc homeostasis genes resulted from extended culturing, I also collected cells that continued to grow in the resting media for another 6 days (R day 6) after one-day incubation in the resting media. Using RT-qPCR, the expression of ZIP14, MT1 and MT2 was analyzed and normalized to two reference genes ACTB and RPS9 (ribosomal protein S9). ZIP14, MT1 and MT2 were chosen as genes of interest because of their relatively high expression level compared to other zinc homeostasis genes. As shown in Figure 2.5A, cortisol was determined to be the primary factor that increased the steady-state level of ZIP14, MT1 and MT2 mRNAs. Prolactin treatment alone had no effect on the mRNA levels of ZIP14, MT1 and MT2 as the expression of Prl day 6 cells was not significantly different from that of R day 1 or R day 6. On the other hand, cortisol treatment alone (C day 6) significantly increased the expression of

ZIP14 (4.1 ± 0.5 fold normalized to ACTB, 5.0 ± 0.3 fold normalized to RPS9, $p < 0.0001$), MT1 (2.3 ± 0.3 fold normalized to ACTB, 2.9 ± 0.1 fold normalized to RPS9, $p < 0.0002$), and MT2 (4.0 ± 0.4 fold normalized to ACTB, 5.0 ± 0.5 fold normalized to RPS9, $p < 0.0001$) compared to their expression level in R day 1, R day 6 or P day6 samples. Finally, there was no significant difference in the mRNA levels of ZIP14, MT1 and MT2 between the cells treated with cortisol alone (Cor day 6) and the cells treated with both hormones (Prl+Cor day 6). CSN2 was used as a positive control because its mRNA expression was strongly activated by the treatment of prolactin and cortisol (Figure 2.5A).

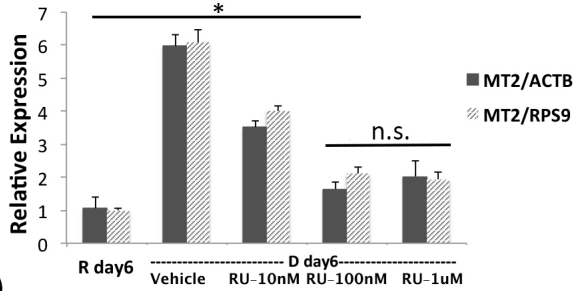
To examine whether cortisol affects the mRNA level of ZIP14, MT1 and MT2 *via* the canonical glucocorticoid receptor (GR) signaling pathway, HC11 cells were treated with a GR antagonist RU486 to competitively inhibit receptor binding with cortisol⁵⁸. To determine the optimal dosage of RU486, cells were treated with the differentiation media supplemented with 0 nM (DMSO, vehicle), 10 nM, 100 nM or 1 μ M of RU486 and the MT2 mRNA level was examined using RT-qPCR under each condition. MT2 was used as a positive control for cortisol dependence because previous work showed cortisol increased MT2 mRNA levels and RU486 abolished the effect⁵⁸. Statistical analysis of RT-qPCR data showed that treatment with 100 nM RU486 significantly lowered the MT2 mRNA level compared to vehicle and 10 nM RU486 treatment ($p < 0.0001$), while there was no difference between 100 nM and 1 μ M (Figure 2.5B). It was noteworthy that 100 nM RU486 did not reduce the mRNA level of MT2 (1.6 ± 0.2 fold normalized to ACTB, 2.1 ± 0.2 fold normalized to RPS9) to the basal level observed in the R day1 samples (1.0 ± 0.4 normalized to ACTB, 1.0 ± 0.0 normalized to RPS9) ($P <$

0.05). To assess the effect of RU486 on the mRNA level of MT1 and ZIP14, HC11 cells were treated with the differentiation media supplemented with 100 nM RU486 for 6 days and the relative expression of ZIP14 and MT1 was determined using RT-qPCR. The steady-state ZIP14 mRNA level was lowered by RU486 treatment (3.1 ± 0.6 fold normalized to ACTB, 2.4 ± 0.2 fold normalized to RPS9) compared to the vehicle group (5.6 ± 0.4 fold normalized to ACTB, 5.0 ± 0.5 fold normalized to RPS9) with a p-value < 0.01 , but it was still higher than that of basal level in the R day 1 samples (1.0 ± 0.2 normalized to ACTB, 1.0 ± 0.2 normalized to RPS9) with p-value < 0.01 (Figure 2.5C). The effect of RU486 on MT1 mRNA level was inconclusive due to the variance of the results (Figure 2.5C). When normalized to RPS9, MT1 mRNA level in the vehicle-treated and RU486-treated samples was significantly different (vehicle, 3.8 ± 0.1 ; RU486, 2.6 ± 0.2 , $p < 0.0001$). However, when normalized to ACTB, there was no difference in the MT1 mRNA level between the vehicle-treated and the RU486-treated groups. Overall, these data show that cortisol increased the steady-state mRNA levels of ZIP14 and MT1 partially *via* the nuclear GR signaling pathway.

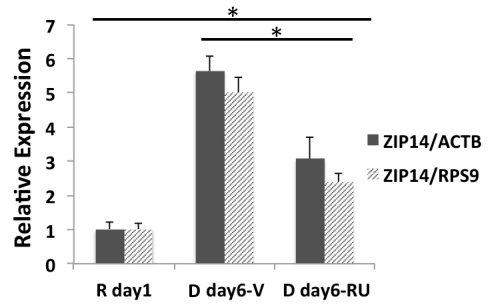
(A)



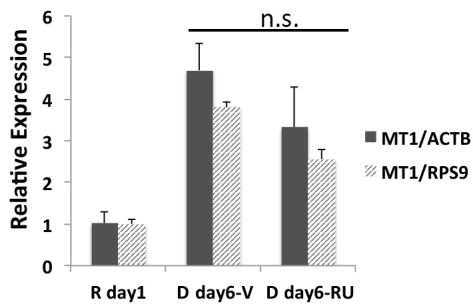
(B)



(C)



(D)



(E)

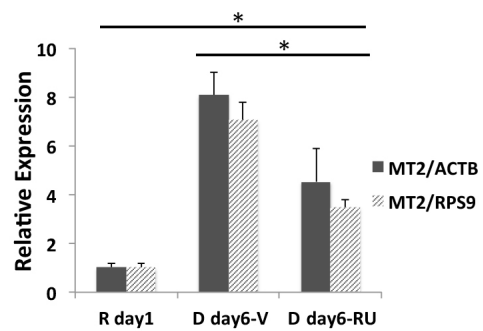


Figure 2.5: Hydrocortisone increases the steady-state level of ZIP14, MT1 and MT2 mRNAs. (A) RT-qPCR of CSN2, ZIP14, MT1 and MT2 normalized to either ACTB or RSP9 reference genes. ** $p < 0.0002$, *** $p < 0.0001$. (B) RT-qPCR of MT2 normalized to either ACTB or RSP9 in resting media and differentiation media in the presence and absence of different concentrations of the glucocorticoid receptor antagonist RU486 (RU). Statistical analysis showed that MT2 mRNA of R day 6 sample was significantly differently from that of RU-100 nM or RU-1000nM (1 mM) samples, *, $p < 0.01$, unpaired student's t-test, with no difference between the RU-100 nM and RU-1 mM group. A dose response indicated that 100 nM RU was the lowest concentration tested that yielded full inhibition of the cortisol response. (C-E) RT-qPCR of ZIP14 (C), MT1 (D) and (E) MT2 normalized to either ACTB or RSP9 in resting media and differentiation media with 100 nM RU or vehicle (V) control. $p < 0.01$, unpaired student's t-test. For MT1, RU treatment did not affect the mRNA level. Error bars represent standard deviation.

2.5.6 Measurement of total zinc and labile cytosolic Zn^{2+} over the progression of cell differentiation

I hypothesized that zinc levels (total zinc, labile Zn^{2+} or both) were regulated at a later stage of cell differentiation (day 6 after hormone treatment) because more zinc-dependent genes were differentially regulated at this time point suggesting altered zinc-binding capacity (Figure 2.3), and the differential expression of MTF1, Zn^{2+} -buffering MTs and zinc transporters implies a change in the cytosolic labile Zn^{2+} level (Figure 2.4). To determine the total cellular zinc level over the course of differentiation, HC11 cells were treated with lactogenic hormones and zinc was measured at different time points using ICP-MS, an elemental analysis technique that measures total metal in a bulk sample. As shown in Figure 2.6A, total zinc did not change over the progression of cell differentiation. Labile Zn^{2+} in the cytosol was measured using NES-ZapCV219, a genetically-encoded Zn^{2+} FRET ratiometric sensor fused with a nuclear export signal such that it localizes to the cytosol. To quantify cytosolic Zn^{2+} , an in situ calibration (Figure 2.6B) was performed to acquire the resting FRET ratio (R), the minimum ratio

(Rmin) after treatment with the Zn^{2+} chelator TPA, and the maximum ratio (Rmax) after treatment with the ionophore pyrithione and Zn^{2+} . The concentration of Zn^{2+} ($[Zn^{2+}]$) was calculated as described in section 2.4.10 and statistical analysis revealed that cytosolic Zn^{2+} did not change at 12 and 24 hr post hormone treatment, but an increase in $[Zn^{2+}]$ was detected in the D day 3 samples compared to the resting state R day 1 (R day1, 140.2 ± 29.8 pM; D day3, 166.6 ± 35.1 pM, $P < 0.0005$), with a further increase at day 6 post hormone treatment (D day 6, 211.9 ± 59.9 pM, $p < 0.0001$ compared to R day 1 or D day 3). Combined with the result that the mRNA and protein expression of 2 differentiation markers (CSN2 and WAP) increased on day 3 of hormone treatment (Figure 2.1), our data suggest that higher cytosolic Zn^{2+} is positively associated with the progression of cell differentiation.

Figure 2.6

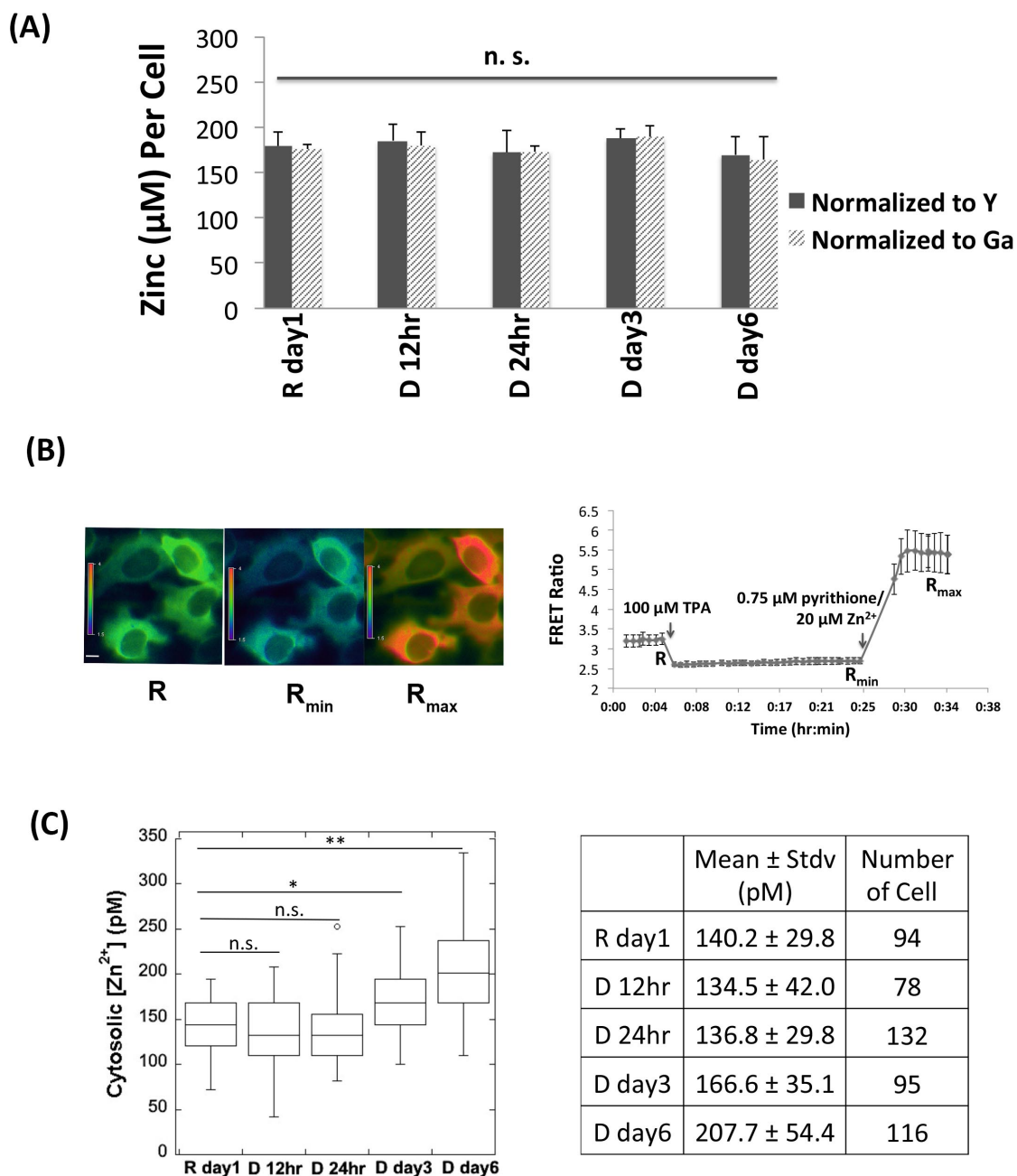


Figure 2.6. Measurement of total zinc and labile cytosolic Zn^{2+} over the progression of cell differentiation. (A) Quantification of total zinc by ICP-MS. The zinc ppb in each sample was normalized to the ppb of a spike in control Yttrium (Y) or Gallium (Ga) and then converted to concentration per cell. n.s. not significant, one-way ANOVA test. (B)

Pseudo-colored fluorescence ratio images (FRET / CFP) of HC11 cells expressing the ZapCV2 sensor (left) and FRET ratio in the cytosol as a function of *in situ* calibration (right). Images represent the resting state (R), post TPA treatment (R_{\min}) and post pyrithione/ Zn^{2+} treatment (R_{\max}). Scale bar, 10 μm . Data represent mean \pm stdv of 10 cells. (C) Quantification of cytosolic labile Zn^{2+} over the progression of differentiation reveals that Zn^{2+} increases at day 3 and day 6 post hormone treatment. The distribution of data is shown in the box plot with the ends of the box representing the upper and lower quartiles. * $p < 0.0005$; ** $p < 0.0001$. One-way ANOVA test.

2.5.7 ZIP14 is responsible for increased cytosolic Zn^{2+} at day 6 post hormone treatment and is important for the upregulation of WAP mRNA.

What defines the set-point of labile Zn^{2+} in a cell isn't well understood, but zinc transporters have been shown to alter the level of labile pools of Zn^{2+} in different cellular compartments^{43,47,58,106}. ZIP transporters transport Zn^{2+} into the cytosol, and would be predicted to increase cytosolic Zn^{2+} , while ZnT transporters transport Zn^{2+} out of the cytosol and would be predicted to decrease cytosolic Zn^{2+} . Because ZIP14 was significantly upregulated at later stages of differentiation and is the most highly expressed ZIP transporter in HC11 cells, I explored whether increased expression of ZIP14 was responsible for the increase in labile cytosolic Zn^{2+} . To accomplish this, ZIP14 expression was knocked down using two shRNAs targeting different regions of ZIP14 mRNA and the effect of knockdown (KD) on cytosolic Zn^{2+} in D day 6 cells was examined using the ZapCV2 FRET sensor. HC11 cells stably expressing ZIP14 shRNA-1, ZIP14 shRNA-2 or scrambled control (SC) shRNA were treated with lactogenic hormones for 6 days and ZIP14 mRNA expression was quantified by RT-qPCR (Figure 2.7A). ShRNA-1 and -2 lowered the ZIP14 mRNA expression by 27 % and 34 %, respectively (ZIP14/ACTB in SC cells: 1.00 ± 0.11 ; shRNA-1 cells: 0.73 ± 0.07 ; shRNA-2 cells: 0.66 ± 0.07). As shown in Figure 2.7B, the fractional saturation of

ZapCV2 was significantly lower in ZIP14 KD cells than in control cells (SC: 0.44 ± 0.07 ; ZIP14 shRNA-1: 0.32 ± 0.08 ; ZIP14 shRNA-2: 0.26 ± 0.03 ; $p < 0.0001$). The lower fractional saturation in shRNA-2 cells is consistent with the fact that shRNA-2 lowered ZIP14 mRNA level more than shRNA-1. This result demonstrates that ZIP14 transports Zn^{2+} into cytosol in differentiated mammary cells after 6 days of hormone treatment, and is a major regulator of the cytosolic labile Zn^{2+} pool.

To investigate the role of ZIP14 in mammary cell differentiation and lactation, the mRNA expression of differentiation markers CSN2 and WAP was measured in ZIP14-KD cells using RT-qPCR. HC11 cells stably expressing ZIP14 shRNA-1, ZIP14 shRNA-2 or scrambled control (SC) shRNA were treated with lactogenic hormones for 6 days. ZIP14-KD did not change the steady state CSN2 mRNA level (Figure 2.7C). However, WAP mRNA expression decreased significantly in ZIP14-KD cells, with a greater effect by shRNA-2 (Figure 2.7D). With WAP relative expression in SC cells normalized to 1.00, the WAP expression level was 0.41 ± 0.06 (WAP/ACTB) and 0.35 ± 0.07 (WAP/RPS9) in ZIP14 shRNA-1 KD cells, 0.13 ± 0.02 (WAP/ACTB) and 0.12 ± 0.02 (WAP/RPS9) in ZIP14 shRNA-4 KD cells. This result suggests that ZIP14 specifically, and zinc homeostasis in general, plays important role in the induction of WAP mRNA in differentiated mammary cells.

Using immunohistochemistry, Kelleher and coworkers showed that ZIP14 localized to an intracellular compartment in the mouse lactating mammary gland⁸⁰. However, the compartment in which ZIP14 resided was unclear. In this study, the intracellular localization of ZIP14 protein in non-differentiated and differentiated HC11 cells was examined using immunofluorescence (IF) (Figure 2.7E). HC11 cells were

grown in the proliferation media and resting media following the differentiation protocol, and were maintained in the resting media (R day 6) or differentiation media (D day 6) for another 6 days. IF revealed that in R day 6 cells, ZIP14 localized to punctae distributed throughout the cell, consistent with localization in vesicular compartments. After hormone treatment, some ZIP14 was still localized to vesicular compartments, but some ZIP14 enriched in a compact perinuclear region (Figure 2.7E). The identity of this perinuclear region remains unclear, but is consistent with Golgi localization. This result raises the possibility that ZIP14 transports Zn^{2+} into the cytosol from vesicles and this perinuclear organelle in order to regulate labile cytosolic Zn^{2+} levels.

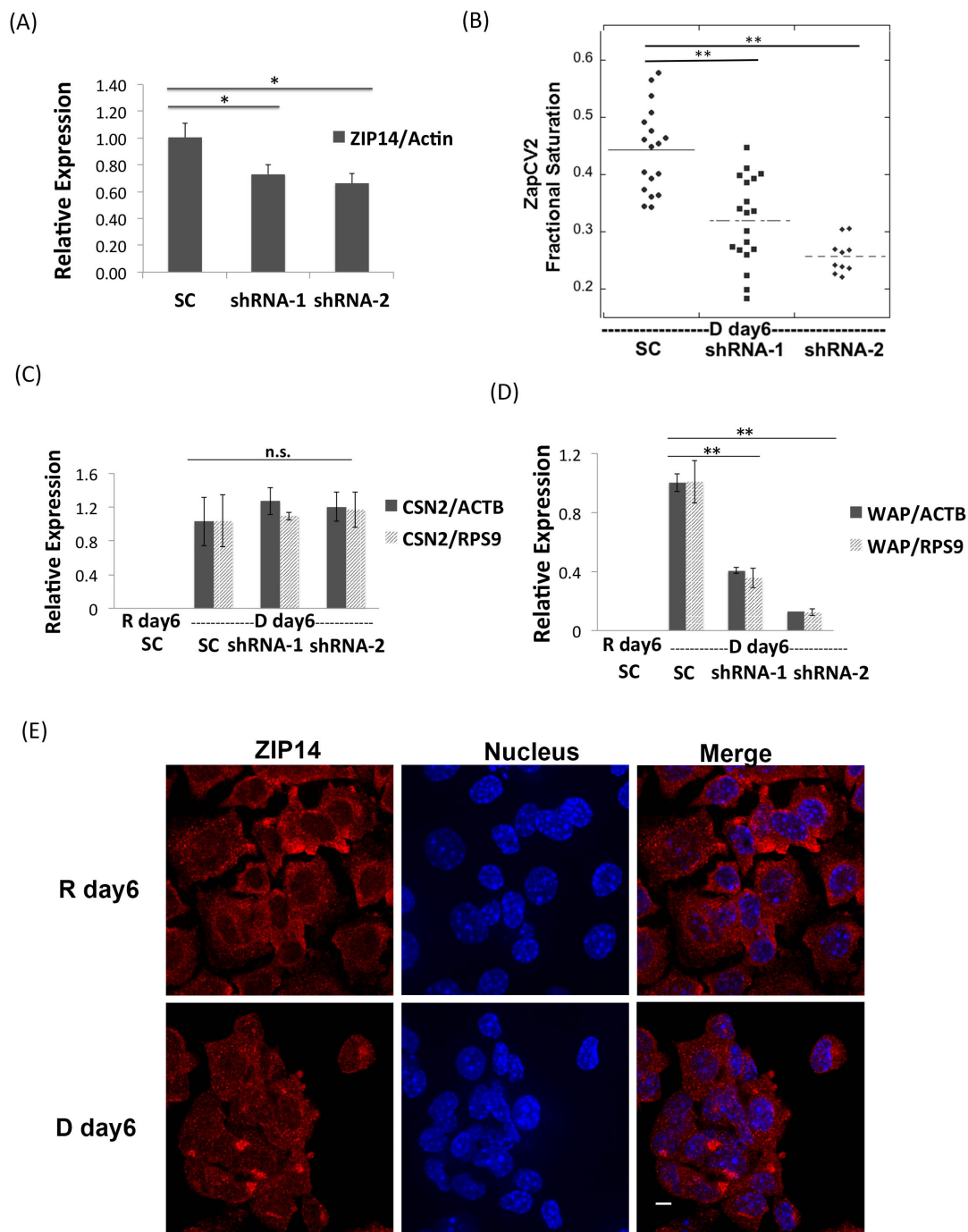


Figure 2.7. Functional studies of ZIP14. (A) The relative expression of ZIP14 was lowered in the ZIP14-KD cells expressing two different shRNAs compared to that in the cells expressing scrambled control shRNA, (B) Cytosolic Zn^{2+} level (represented as the fractional saturation of ZapCV2 sensor) decreased in the ZIP14-KD cells compared to the control cells at 6 days post hormone treatment. ZIP14 knockdown depressed the mRNA expression of WAP (D) but had no effect in the CSN2 mRNA level (C) in D day6

cells. Relative mRNA level in (A, C, D) was determined using qRT-PCR. *, $P < 0.05$; **, $p < 0.001$, unpaired student's t-test. (E) Immunofluorescence of ZIP14 in the resting cells (R day6) and differentiated cells with 6 days of hormone treatment (D day6). Scale bar, 5 μm .

2.6 Discussion

To date, most studies of cellular zinc homeostasis have focused on how the expression of a few key players in zinc homeostasis change to maintain or restore the balance of zinc in response to an external stimulus in normal cells, or the association of altered expression of those key players with human diseases. With the knowledge that about 10% of human proteins bind Zn^{2+} and potentially are Zn^{2+} dependent, profiling expression of all zinc-dependent genes would provide valuable information about how transient or long-term altered zinc homeostasis regulates cell biology in normal tissues/cells and human diseases. In this study, I utilized the differentiation of HC11 mouse MECs upon lactogenic hormone treatment to systematically study how zinc homeostasis and zinc-dependent processes are modulated in the switch of cell needs for zinc.

The transcriptomes of HC11 MECs changed globally upon hormone treatment. Functional annotation and enrichment analysis of genes that were differentially regulated more than 2-fold revealed that the major downregulated biological processes were classified into two groups: cell proliferation and cell migration (Figure 2.2C). Downregulation of proliferation genes was expected due to the switch from a proliferative to a differentiated cell state. Downregulation of microtubule-related migration genes may be explained by the fact that microtubules are essential for cell division^{240,241} and therefore there is a reduced need for microbutules due to repression

of cell division. The major upregulated biological processes include metabolic and transport processes, cell signaling activities, the ER unfolded protein response (UPR) and cellular zinc ion homeostasis. Upregulation of metabolic and transport process may be explained by the need to synthesize and secrete milk components (e.g. protein, lipids, ions, etc.) from MECs into milk. Cell signaling activities in response to peptide hormone and glucocorticoid were increased due to the addition of prolactin (a peptide hormone) and cortisol. The MAPK (mitogen activated protein kinase) signaling pathway activity was induced by prolactin *via* the interaction between JAK (Janus kinase) and MAPK pathways, where activated JAK phosphorylates Shc protein and then phosphorylated Shc activates Ras and the downstream MAPK signaling pathway¹⁷¹. Upregulation of the UPR is consistent with a recent study which found increased UPR in the lactating mammary gland and identified two transcription factors regulated by the UPR pathway that directly transcribe CSN2²⁴². Immune system processes were significantly upregulated in differentiated cells, possibly due to the stimulatory effect of glucocorticoid on the expression of innate immune-related genes²⁴³. Finally, cellular zinc ion homeostasis was upregulated in D day 6 cells suggesting a remodeling of zinc homeostasis in the late stage of differentiation to meet the requirements for different zinc needs in the differentiated cell.

Analysis of regulation of zinc-dependent processes revealed a shifted need for zinc from DNA, nucleotide and protein binding in non-differentiated cells, to activities of a few enzyme classes in differentiated cells (Figure 2.3B). In particular, zinc is needed for hydrolysis of nucleoside diphosphate by nucleotide diphosphatase and ribo- and deoxyribo-oligonucleotides by phosphodiesterase I. It is noteworthy that zinc-

dependent ubiquitin protein ligase and transferase activities are also downregulated in differentiated cells. The ubiquitin proteasome pathway (UPP) plays an important role in regulation of the cell cycle *via* dynamic degradation of key cell cycle regulators^{244,245}. Given that cell proliferation activities were significantly downregulated in differentiated cells (Figure 2.2C), it is possible that the repressed zinc-dependent ubiquitin proteasome pathway mediates the suppression of cell proliferation. Finally, zinc transporter activity was also upregulated in differentiated cells, consistent with the secretory phenotype of MECs that they actively uptake, redistribute and export zinc during differentiation.

Using RT-qPCR, previous studies have profiled the mRNA expression of zinc transporters in lactating mammary tissue and reported the fold change of each up- or downregulated zinc transporter in lactating tissue relative to non-lactating tissue^{80,225}. However, genes with low expression level (e.g. zinc transporters) are prone to have strong variance in the fold change²²⁶. Furthermore, without knowing the absolute expression level of genes, the actual biological effects of genes are questionable for genes with high fold change but low expression²²⁶. In this study, zinc homeostasis genes with very low expression level (FPKM < 1) were excluded from downstream analysis. Differential expression of zinc homeostasis genes was analyzed using DESeq2²²⁶. DESeq2 is a comprehensive method for differential expression analysis, which corrects fold change and p-value of gene expression based on the expression level (i.e. counts number) as well as variance of fold change across biological replicates (ref the DESeq2 paper). DESeq2 analysis revealed that the expression regulation is positively associated with the progression of cell differentiation as 2 zinc transporter

genes (ZIPs) were differentially regulated in D 24 hr samples and 14 zinc transporter genes were regulated in D day 6 samples compared to the R day 1 samples (Figure 2.4B). Zinc homeostasis genes were both up- and down-regulated, suggesting a complicated regulatory network of zinc homeostasis in the late stage of differentiation. However, a major discrepancy between our result and other's is ZnT2. ZnT2-null lactating mice had defects in mammary gland architecture and milk synthesis²⁴⁶. It has been shown that ZnT2 is transcriptionally activated by the STAT5-GR complex upon glucocorticoid hormone treatment in primary mouse pancreatic cells⁵⁸. Furthermore, prolactin-activated JAK-STAT signaling pathway directly induced ZnT2 transcription on its promoter in HC11 cells¹⁷³. Surprisingly, in our hands, ZnT2 expression was not detected at 24hr or day6 post glucocorticoid and prolactin treatment. Possibly, the ZnT2 transcription induction is induced by prolactin treatment alone but not by the combination of prolactin and glucocorticoid in HC11 cells.

To further investigate the underlying mechanism of expression regulation, ZIP14, MT1 and MT2 were chosen for their relatively high expression level and fold change in D day 6 samples. Numerous studies have shown that glucocorticoid enhances the mRNA expression of MT1 and MT2 in various organisms^{129,160,247}. Whether MTs expression is also regulated by prolactin remains unknown. Our research demonstrated that cortisol but not prolactin increased the mRNA levels of ZIP14, MT1 and MT2 (Figure 2.5A). Furthermore, the induction of ZIP14 and MT2 was only partially mediated by the classical nuclear glucocorticoid receptor (GR) signaling pathway as treatment with GR-specific antagonist RU486 did not completely abolished the mRNA increase of ZIP14 and MT2 in differentiated cells compared to resting cells (Figure 2.5C and E).

Additionally, ZIP14 and MT2 mRNA levels can be enhanced by the activation of membrane receptor by cortisol^{248–251} or the crosstalk of cortisol with other signaling pathways (e.g. JAK-STAT)^{58,252}.

The changes in expression of zinc homeostasis genes suggest that zinc homeostasis and zinc transport were actively regulated after 6 days of hormone treatment, suggesting that zinc levels may also change at this stage. To test this hypothesis, the total zinc level was quantified using ICP-MS, revealing no change in total zinc over the course of cell differentiation (Figure 2.6A). This is in contrast to a study by McCormick and colleagues in which the total zinc concentration in the lactating mouse mammary gland was determined to be higher than the non-lactating mammary gland²⁵³. One possible explanation is that total zinc concentration in lactating mammary gland is regulated in a temporal fashion. Kelleher showed that the total zinc level in lactating rat mammary gland increased throughout lactation (from day 1 to day 20) as measured by atomic absorption spectroscopy²²⁵. The differentiation of HC11 in our study may recapitulate a different stage of lactation than that in McCormick's study. Another possibility for the discrepancy is that the previous studies focused on the entire mammary gland, whereas we characterized MECs, and the mammary gland is comprised of MECs as well as surrounding tissues, which could have variable levels of zinc and / or influence zinc levels within MECs.

Using a genetically-encoded FRET sensor, ZapCV2, I found out that labile cytosolic Zn²⁺ increased by 19% at 24 hr and 48% at day 6 post hormone treatment above that in the resting cells (Figure 2.5C). Possible mechanisms for the higher cytosolic Zn²⁺ level at day 6 post hormone treatment compared to the resting cells

include (1) upregulated transport of Zn^{2+} from extracellular media or an intracellular organelle by ZIPs, (2) downregulated export of cytosolic Zn^{2+} by ZnTs, or (3) Zn^{2+} release from stably-bound proteins. Our analysis of the expression of zinc homeostasis genes revealed that ZIP14 was the most abundant zinc transporter in D day 6 cells and had a high relative fold change (Figure 2.8), leading us to examine whether ZIP14 was responsible for the elevation of cytosolic Zn^{2+} . Indeed, knock down of ZIP14 lowered the cytosolic Zn^{2+} level in D day 6 cells compared to control cells (Figure 2.7B). Immunofluorescence of ZIP14 demonstrated that there was an enrichment of ZIP14 in a peri-nuclear organelle in cells after 6 days of hormone treatment (Figure 2.7E), suggesting that ZIP14 possibly imported Zn^{2+} into cytosol from a peri-nuclear region in differentiated cells. The mechanism of how some ZIP14 localizes to this perinuclear region is still unknown at this point. Protein isoforms of ZnT2 and ZnT5 generated from alternative splicing have been reported in mouse mammary epithelial cells⁶⁰ and ZnT5 in Chinese hamster ovary cells¹¹⁵, respectively. The protein translated from those mRNA variants localized to different intracellular compartments^{60,115}, suggesting unique function of each variant. Possibly, a protein isoform of ZIP14 was synthesized upon hormone treatment and localizes to the peri-nuclear region.

Last but not least, we discovered that ZIP14 was crucial for the mRNA expression of the milk protein WAP (Figure 2.7D). However, this effect of ZIP14 was not seen in the CSN2 mRNA expression (Figure 2.7C). Although both genes are activated by the cooperation of prolactin and cortisol^{239,254}, the transcription of two genes operates differently: cortisol alone induced transcription of WAP but not CSN2¹⁶¹ whereas prolactin alone was sufficient to induce CSN2 but not WAP transcription²³⁸.

For now, whether or not the regulation of WAP mRNA expression by ZIP14 is mediated by the increase of cytosolic labile Zn^{2+} remains unknown and needs to be addressed with future studies.

2.7 Future direction

This study represents the first ever report that ZIP14 mRNA level is enhanced by glucocorticoid hormone treatment in differentiated mouse mammary epithelial cells. Moreover, ZIP14 actively transported Zn^{2+} into cytosol and ZIP14 expression is important for the production of a milk protein WAP. With many interesting questions remaining to be addressed, my future study will focus on the following topics:

2.7.1 The regulation of ZIP14, MT1 and MT2 mRNA expression by lactogenic hormones

In my study, I demonstrated a cortisol-induced increase of steady-state level of ZIP14, MT1 and MT2 mRNA at 6 days post-hormone treatment (Figure 2.4B and Figure 2.5). The steady-state level of mRNA is controlled by two factors: mRNA synthesis (transcription) and mRNA degradation. Using promoter reporter assay, I have made attempts to determine the transcriptional activity of promoters of 3 genes upon hormone treatment (Appendix D). However, the results from this assay are not interpretable because first, ZIP14_promoter HC11 cells did not express the internal control reporter SEAP and second, the MT1 and MT2 promoters need to be validated using their responses to zinc treatment. Troubleshooting is required to validate all promoter constructs and to determine why SEAP was not expressed in ZIP14 promoter construct.

2.7.2 Protein expression of ZIP14 at day6 post hormone treatment

To understand whether hormones regulate ZIP14 expression translationally, the change in protein level will be determined by western blotting in cells for up to 6 days of hormone treatment.

2.7.3 Zn²⁺ transport into cytosol by ZIP14 enriched in a peri-nuclear region in differentiated cells

I observed an enrichment of ZIP14 in a peri-nuclear region in the cells with 6 days of hormone treatment (Figure 2.7E). First, I will determine the identity of the peri-nuclear region by co-localizing ZIP14 with organellar markers (e.g. Golgi and ER) using co-immunofluorescence. Second, I will examine the hypothesis that ZIP14 actively transports Zn²⁺ from this intracellular organelle into cytosol. To test this, the labile Zn²⁺ level in the cytosol and the organelle will be measured in control cells and ZIP14-KD cells, using FRET sensors that can be specifically targeted to subcellular compartments. It is hypothesized that ZIP14-knockdown will lead to an accumulation of Zn²⁺ in the organelle and a decrease of cytosolic Zn²⁺. The latter has already been detected (Figure 2.7B). Also, I will measure and compare cytosolic Zn²⁺ level in ZIP14-KD cells with that in resting cells.

2.7.4 The regulation of WAP mRNA expression by ZIP14

ZIP14 expression is shown to be important for the proper production of WAP mRNA in differentiated cells (Figure 2.7D). I hypothesized that this effect of ZIP14 is mediated by the ZIP14-induced increase of cytosolic Zn²⁺. To test this hypothesis, WAP mRNA level will be determined using RT-qPCR in cells under zinc-deficient, normal and zinc-sufficient condition. Thereafter, I will explore whether this regulation

occurs at transcriptional or post-transcriptional level. Furthermore, the regulation of WAP protein production by ZIP14- Zn^{2+} pathway will be explored by western blotting.

Chapter 3

Superiority of SpiroZin2 Versus FluoZin-3 For Monitoring Vesicular Zn²⁺ Allows Identification of Lysosomal Zn²⁺ Accumulation In Lactating Mammary Cells

3.1 Abstract

Small-molecule fluorescent probes are powerful and ubiquitous tools for measuring the concentration and distribution of analytes in living cells. However, accurate characterization of these analytes requires rigorous evaluation of cell-to-cell heterogeneity in fluorescence intensities and intracellular distribution of probes. In this study, we perform a parallel and systematic comparison of two small-molecule fluorescent vesicular Zn²⁺ probes, FluoZin-3 AM and SpiroZin2, to evaluate each probe for measurement of vesicular Zn²⁺ pools. Our results reveal that SpiroZin2 is a specific lysosomal vesicular Zn²⁺ probe and affords uniform measurement of resting Zn²⁺ levels at the single cell level with proper calibration. In contrast, FluoZin-3 AM produces highly variable fluorescence intensities and non-specifically localizes in the cytosol and multiple vesicular compartments. We further applied SpiroZin2 to lactating mouse mammary epithelial cells and detected a transient increase of lysosomal free Zn²⁺ at 24 hour after lactation hormone treatment, which implies that lysosomes play a role in the regulation of Zn²⁺ homeostasis during lactation. This study demonstrates the need for critical characterization of small-molecule fluorescent probes to define the concentration and localization of analytes in different cell populations.

3.2 Publication status and author contributions

Han Y., Goldberg, J. M., Lippard, S. J., Palmer, A. E. Superiority of SpiroZin2 Versus FluoZin-3 for monitoring vesicular Zn^{2+} allows identification of lysosomal Zn^{2+} accumulation in lactating mammary cells. Scientific Reports. *Under revision*.

Y.H. and A.E.P. designed the research and analyzed the results. J.M.G. and S.J.L. contributed reagents and critical feedback. Y.H. carried out the research. Y.H., J.M.G. S.J.L. and A.E.P. wrote and edited the paper.

3.3 Introduction

Zinc is the second most abundant transition metal in mammals and an essential nutrient required for growth. Most intracellular Zn^{2+} , concentrations of which are typically hundreds of micromolar in mammalian cells², is tightly bound to proteins. As much as 10% of the human proteome has been predicted to bind Zn^{2+} ions²⁰³. In these Zn^{2+} -containing proteins, the ion serves as a structural component, stabilizing the three-dimensional fold or serving as a catalytic cofactor². The remaining intracellular Zn^{2+} is loosely bound to small-molecule/ion, peptide, and protein ligands and accumulates in pools that are readily exchangeable to maintain Zn^{2+} homeostasis²⁵⁵. Additionally, Zn^{2+} may be released from labile pools as a signaling agent²², although the mechanisms of Zn^{2+} utilization in sensing are less well understood.

Labile Zn^{2+} pools occur in the cytosol, discrete organelles, and within vesicles of secretory cells¹⁸³, and diverse patterns of dynamics have been observed for these pools. In some regions of the brain, for example, presynaptic glutamatergic vesicles co-release glutamate and Zn^{2+} into the synaptic cleft during neurotransmission, where it modulates the excitatory post-synaptic current by binding to ion channels ostensibly as

part of a gain control mechanism^{190,256}. Mitochondria in primary rat hippocampal neurons can transiently accumulate Zn^{2+} upon treatment with glutamate and Zn^{2+} , suggesting that mitochondria may serve as a temporary store of labile Zn^{2+} ²⁵⁷. Zn^{2+} accumulation in lysosomes has been suggested to play roles in oxidative neuronal death and progressive cell degeneration in neurodevelopmental diseases^{258,259}. During fertilization, mammalian egg cells release “ Zn^{2+} sparks” from intracellular vesicular stores that appear to play crucial roles in ovum activation¹⁹¹. Furthermore, in breast cancer cells, Zn^{2+} mobilized from intracellular stores increases the phosphorylation of tyrosine kinases¹⁹², implicating these pools in a distinct form of Zn^{2+} -dependent cell signaling.

Finally, mouse mammary epithelial cells form Zn^{2+} -rich vesicles in response to lactation hormone treatment²⁵³, although the mechanism(s) regulating these changes and the identity of the vesicular pools are not well understood. In order to understand the roles of labile Zn^{2+} and the factors that control its homeostasis in these and other cellular events, it is necessary to be able to record the dynamics and distribution of Zn^{2+} in subcellular compartments with high accuracy and precision.

Current tools to monitor labile Zn^{2+} include fluorescent protein (FP)-based sensors and small-molecule chemical probes. FP-based sensors are genetically encodable, and can be specifically targeted to organelles by incorporation of a signal sequence. They have been used to estimate the concentration of labile Zn^{2+} in the ER, Golgi, mitochondria and nucleus^{260–265}. However, measuring Zn^{2+} in vesicular compartments with FP-based probes has been more challenging as the currently available protein-based sensors suffer from low dynamic range in vesicles in response

to Zn^{2+} perturbation^{263,264}. A growing number of fluorescent small molecule probes have been developed to measure vesicular Zn^{2+} pools, including Zinquin¹⁸⁹, FluoZin-3¹⁶⁸, ZincBY-1¹⁹¹, SpiroZin1¹⁹⁷, and SpiroZin2¹⁹⁸. Many of these probes exhibit large dynamic ranges and they employ diverse mechanisms for detecting Zn^{2+} ions.

In this study, we performed a systematic evaluation of two small-molecule probes, FluoZin-3 AM and SpiroZin2, with an emphasis on comparing the variability of the fluorescence intensities and subcellular distributions of the two dyes in response to identical Zn^{2+} perturbations. FluoZin-3 AM has been widely used to measure vesicular Zn^{2+} in many different mammalian cells^{253,258,259,266}. Despite this broad application, FluoZin-3 AM has been reported to exhibit variable intracellular localization in both the cytosol and vesicles, as well as large variability in fluorescence intensity¹⁹⁹. SpiroZin2 is a red-shifted probe that is insensitive to changes in pH between pH 3 and 7 and has been used to image lysosomal Zn^{2+} in HeLa cells and acute hippocampal tissue slices¹⁹⁸. We find here that FluoZin-3 AM exhibits highly variable fluorescence intensities and non-specifically localizes in the cytosol and in multiple vesicular compartments. By comparison, SpiroZin2 produced consistent and uniform fluorescence intensities in different cells. In addition, we find that SpiroZin2 specifically localizes in late endosome/lysosome vesicles, making it an ideal probe to estimate lysosomal labile Zn^{2+} levels. We then used SpiroZin2 to detect changes in lysosomal Zn^{2+} pools upon manipulation of extracellular Zn^{2+} , dissipation of the lysosomal pH gradient, and differentiation of mouse mammary epithelial cells (HC11).

3.4 Methods

3.4.1 Chemicals

SpiroZin2 was synthesized as previously described and a 4 mM stock solution was prepared in DMSO¹⁹⁸. Tris(2-pyridylmethyl)amine (TPA) was purchased from Sigma-Aldrich (catalog number 723134) and diluted with DMSO to prepare 20 mM stock solutions. Pluronic F-127 (20% (w/v) solution in DMSO) was purchased from Thermo Fisher (catalog number P3000MP). FluoZin-3 AM (Thermo Fisher, catalog number F24195) was prepared as a 2 mM stock solution in DMSO. Stock solutions (5 mM) of 2-mercaptopyridine N-oxide (pyrithione, Sigma-Aldrich, catalog number 188549) were prepared in DMSO. Nuclear staining was achieved with NucBlue Live ReadyProbes Reagent (Thermo Fisher, catalog number R37605). An aqueous ZnCl₂ solution (1 mM) was diluted in phosphate-free HEPES-buffered Hanks' balanced salt (HHBSS) buffer (1.26 mM CaCl₂, 1.1 mM MgCl₂, 5.36 mM KCl, 137 mM NaCl, 16.65 mM D-glucose, and 30 mM HEPES, pH 7.4) to make a 200 μM ZnCl₂ stock solution. An insulin stock solution (4 mg/mL) was purchased from Life Technologies (catalog number 12585014). Human recombinant epidermal growth factor (EGF, VWR 47743-566) was prepared as a 10 μg/mL stock solution in water. Prolactin (Sigma-Aldrich L6520) was prepared as a 5 mg/mL stock solution in water. A stock solution (138 μM) of hydrocortisone (Sigma-Aldrich H0888) in absolute ethanol was also prepared. Bafilomycin A1 (Sigma-Aldrich B1793) was prepared as a 100 mM stock solution in DMSO.

3.4.2 Molecular cloning

The GalT-CFP plasmid encodes the first 60 amino acids of human galactosyltransferase (GalT) (NM_001497.3) followed by ECFP in the Clontech N1 vector. VAMP8-CFP was generated by replacing GalT with VAMP8 (NM_003761.4). LAMP1-EBFP was a gift from Michael Davidson (Addgene # 55246).

3.4.3 Cell culture

HC11 cells were grown in RPMI medium supplemented with 10% fetal bovine serum (FBS), 1% penicillin/streptomycin (pen/strep), 10 ng/mL EGF and 5 µg/mL insulin. To induce cell differentiation, 4×10^5 cells were plated in a 35-mm dish in the supplemented medium and reached confluency after 3 days. Cells were maintained in a resting medium containing RPMI, 2% FBS, 1% pen/strep, 5 µg/mL insulin for one additional day, then treated with a differentiation medium containing 2% FBS, 1% pen/strep, 5 µg/mL insulin, 5 µg/mL prolactin, and 1 µM hydrocortisone for up to 6 days. The medium was changed every 2 days.

3.4.4 Cell loading with zinc probes and calibration

FluoZin-3 AM and SpiroZin2 were loaded as previously described^{168,198}. Briefly, a 2 mM stock solution of FluoZin-3 AM DMSO stock solution was diluted to a final concentration of 3 µM in phosphate-free HHBSS buffer. Phosphate-free HHBSS buffer was used to avoid precipitation of Zn^{2+} by phosphate. HC11 cells were washed with phosphate-free HHBSS and then incubated with FluoZin-3 AM/phosphate-free HHBSS for 1 hr at 37 °C with 5% CO₂, followed by a 30 min wash in phosphate-free HHBSS buffer at 37 °C with 5% CO₂. Imaging was performed immediately after washing. For SpiroZin2, a 4 mM DMSO stock solution was diluted to a final concentration of 5 µM in

phosphate-free HHBSS buffer. HC11 cells were washed with phosphate-free HHBSS buffer and then incubated with 2 mL of SpiroZin2 solution for 1 h at 37 °C with 5% CO₂ prior to imaging. To apply pluronic during the staining procedure, the stock solution of zinc probe was mixed with an equal volume of Pluronic F-127 20% (w/v) solution and then the mixture was diluted in phosphate-free HHBSS buffer, making the final pluronic concentration about 0.025%. For Zn²⁺ calibrations, F_{min} measurements were acquired by treating cells with 150 μM TPA in phosphate-free HHBSS buffer. To obtain values for F_{max}, a solution containing 5 μM pyrithione/20 μM ZnCl₂ in phosphate-free HHBSS buffer was added to HC11 cells.

3.4.5 Live cell imaging

Fluorescence images in Figures 1-3 and 5 were acquired on a Nikon A1R laser scanning confocal microscope equipped with the Nikon Elements software platform, Ti-E Perfect Focus system with a Ti Z drive, using a 40x oil objective (NA 1.30) or a 100x oil objective (NA 1.45) and the following channels: SpiroZin2 (red) (514.5 nm laser line, photomultiplier tube (PMT) gain: 50 or 110, pinhole size: 1 or 4 airy unit (AU), emission filter: 600/50 nm); FluoZin-3 (green) (488 nm laser line, PMT gain: 45 or 110, pinhole size: 1 or 4 AU, emission filter: 525/50 nm); nucleus (blue) (405 nm laser line, PMT gain: 80 or 95, pinhole size: 1 AU, emission filter: 450/50 nm); LAMP1-EBFP (blue) (405 nm laser line, PMT gain: 95 or 110, pinhole size: 1 or 4 AU, emission filter: 450/50 nm); GalT-CFP (Cyan) (405 nm laser line, PMT gain: 90, pinhole size: 4 AU, emission filter: 482/35 nm).

Fluorescence images for colocalization of fluorescent probes with VAMP8-CFP in Figure 3 and all fluorescence images in Figure 4 were acquired on a Nikon Ti-E

spinning disc confocal microscope fitted with a Yokogawa CSU-X1 spinning disc head, equipped with the Nikon Elements software platform and Ti-E Perfect Focus system. Cells were imaged using a 60x oil objective (NA 1.40) or a 100x oil objective (NA 1.45) and the following channels: SpiroZin2 (red) (514 nm laser line, EM gain: 300, emission filter: 630/30 nm), FluoZin-3 (green) (488 nm laser line, EM gain: 300, emission filter: 525/50 nm), Vamp8-CFP (cyan) (445 nm laser line, EM gain: 300, emission filter: 482/35 nm).

Fluorescence imaging with a Zn^{2+} FRET sensor was performed on a Nikon Ti-E wide-field fluorescence microscope equipped with Nikon elements software, an iXon3 EMCCD camera (Andor), mercury arc lamp, and YFP FRET (434/16 excitation, 458 dichroic, 535/20 emission), CFP (434/16 excitation, 458 dichroic, 470/24 emission), YFP (495/10 excitation, 515 dichroic, 535/20 emission) filter sets.

3.4.6 Responses of probes to Zn^{2+} perturbation in HC11 cells

To test the responses of probes to Zn^{2+} perturbation, 8×10^5 HC11 cells were plated in a 35-mm glass bottom dish one day prior to imaging. Cells were stained with FluoZin-3 AM (with pluronic) or SpiroZin2 as described above. The nuclear dye was added to the cell culture medium 30 min prior to imaging. Cells were washed with phosphate-free HHBSS buffer and then imaged on a Nikon A1R laser scanning confocal microscope as described in the “Live Cell Imaging” section. Z-series images were recorded every 3 min throughout the experiment. After adding Zn^{2+} /pyrithione to cells, PMT gain was lowered from 50 to 15 for SpiroZin2 and from 45 to 25 for FluoZin-3 to avoid detector saturation. Image analysis was performed using ImageJ. Z-series images of each fluorescence channel per time point were flattened using the maximum

intensity Z-projection. To perform single cell analyses, 15 cells were randomly chosen and each cell was defined as an individual region of interest (ROI). Background fluorescence of each channel was calculated by averaging the signal intensities of an area (mean intensities) without cells. The fluorescence intensities of the FluoZin-3 or SpiroZin2 channel of each ROI were calculated by subtracting background fluorescence from the raw mean fluorescence intensities for each channel.

3.4.7 Variability of fluorescence Intensities of zinc probes

To test the variability of fluorescence intensities of FluoZin-3 and SpiroZin2, 8×10^5 HC11 cells were plated in a 35-mm glass bottom dish one day prior to imaging. Cells were stained with FluoZin-3 or SpiroZin2 with or without pluronic as described above. Nucleus dye was added to the cell culture medium 30 min prior to imaging. Cells were washed with phosphate-free HHBSS buffer and then imaged on a Nikon A1R laser scanning confocal microscope as described in the “Live Cell Imaging” section. Z-series images were recorded in the resting state (F) and 15 min post TPA treatment (Fmin). Image analysis was performed using ImageJ. Z-series images of each fluorescence channel per time point were flattened using the maximum intensity Z-projection. To perform single cell analyses, nucleus channel images were thresholded to identify the nuclear area. Touching objects were separated by a watershed algorithm. Next, segmented particles were identified by the “find maxima” command with “segmented particles” as the output type, and “light background” chosen when the background color was white. To create ROIs with each ROI corresponding to a single cell, segmented pictures were processed by the “analyze particles” command as follows: the range of the size of particles was adjusted so that each particle incorporated

a single cell and then the option “add to manager” was chosen to generate a list of ROIs. Applying the ROIs to the FluoZin-3 or Spirozin2 channel images allowed the quantification of the mean raw intensity of the sensor fluorescence at the single-cell level. The background fluorescence of each channel was calculated by averaging the signal intensities of an area (mean intensities) without cells. The fluorescence intensities of FluoZin-3 or SpiroZin2 channel of each cell were calculated by subtracting the background fluorescence from the raw mean fluorescence intensities.

3.4.8 Colocalization Assay of Zinc Probes with Vesicular Markers

To transiently express vesicular markers in HC11 cells, 500 ng of DNA encoding each fusion protein (LAMP1-EBFP, VAMP8-CFP or GalT-CFP) was electroporated into 1×10^6 cells with the Neon system (Life Technologies) 24-48 hr prior to imaging using the following parameters: pulse voltage: 1400 v; pulse width: 20 ms; pulse number: 2 pulses. Electroporated cells were plated in 35-mm glass-bottom imaging dishes. Before imaging, cells were stained with FluoZin-3 or SpiroZin2 with or without pluronic as described above. After staining, cells were washed with phosphate-free HHBSS buffer. To enhance the fluorescence intensities of zinc probe channels, 5 μ M pyrithione/20 μ M ZnCl_2 was added to cells. Fluorescence images were recorded 5-10 min after Zn^{2+} addition. Sensor co-localization experiments with LAMP1-EBFP and GalT-CFP were performed on a Nikon A1R laser scanning confocal microscope as described in the “Live Cell Imaging” section. Colocalization experiments with VAMP8-CFP were performed on a Nikon Ti-E spinning disc confocal microscope as described in the “Live Cell Imaging” section.

To perform the Pearson coefficient-based colocalization assay, cells with fluorescence signals in both the zinc sensor channel and the vesicular marker channel were selected for analysis with JACoP plugin for ImageJ (<https://imagej.nih.gov/ij/plugins/track/jacop.html>). An important criterion for choosing cells is that the fluorescence intensities of the two channels must be comparable. One to three regions of interest (ROI) were drawn within a cell and the Pearson coefficient was calculated by JACoP. Data were plotted with KaleidaGraph.

3.4.9 Cytosolic distribution of zinc probes

To determine the cytosolic distribution of FluoZin-3 and SpiroZin2, 8×10^5 HC11 cells were plated in a 35-mm glass bottom dish one day prior to imaging. Cells were stained with FluoZin-3 or SpiroZin2 with or without pluronic as described above. Nuclear dye was added to the cell culture medium 30 min prior to imaging. After staining, cells were washed with phosphate-free HBSS buffer. To enhance the fluorescence intensities of the zinc sensor channels, $5 \mu\text{M}$ pyridoxine/ $20 \mu\text{M}$ ZnCl_2 was added to the cells. Z-series fluorescence images were recorded 5-10 min after Zn^{2+} addition on a Nikon Ti-E spinning disc confocal microscope as described in the “Live Cell Imaging” section. Image analysis was performed using ImageJ. Z-series images of each fluorescence channel were flattened using the maximum intensity Z-projection. Cells with cytosolic distribution of dyes were counted by eye. The total number of cells was calculated with ImageJ. Nucleus channel images were thresholded to identify the nuclear area. Touching objects were separated with a watershed algorithm. The number of nuclei (i.e. cells) was determined with the command “analyze particles.” The

quantification of cytosolic distribution of dyes was determined by dividing the number of cells with cytosolic signal by the total number of cells per image.

3.4.10 Lysosomal pH measurement

HC11 cells were grown in a 96-well plate in growth media supplemented with 0.5 mg / mL of LysoSensor™ Yellow / Blue Dextran (ThermoFisher Scientific, L22460) overnight. The standard curve (A) was generated by incubating cells in 10 mM monensin and 10 mM nigericin in MES buffer (5 mM NaCl, 115 mM KCl, 1.3 mM MgSO₄, 25 mM MES), with the pH adjusted to within the range of 4.0–7.0 for 10 min. After the incubation, fluorescence was quantified with a fluorescence microplate reader (BioTek Synergy H1 hybrid) at emission wavelengths of 535 and 440 nm with excitation at 340 nm. To generate a standard curve, the ratio of emission 535nm / 440 nm was plotted against the pH value of MES buffer. The lysosomal pH post Bafilomycin A1 or DMSO treatment was calculated using the standard curve.

3.4.11 Monitoring cytosolic Zn²⁺ using a genetically-encoded Zn²⁺ FRET sensor

HC11 cells stably expressing a Zn²⁺ FRET Sensor (ZapCV2) were generated using the PiggyBac™ Transposon Vector System (System Biosciences). Fluorescence images were acquired in the YFP FRET and CFP channels. To perform data analysis, a cytoplasmic region (ROI) and a region without cells (background) were selected and the FRET ratio was calculated by dividing the background corrected YFP FRET intensity by the background corrected CFP FRET intensity.

3.4.12 Measurement of lysosomal Zn²⁺ level during lactation

HC11 cells were induced to differentiation as described above. To study the change in lysosomal Zn²⁺ over the progression of lactation, cells at different stages were stained with SpiroZin2 (without pluronic) and nuclear dye as described above, and then imaged on a Nikon A1R laser scanning confocal microscope as described in the “Live Cell Imaging” section. Z-series images were recorded in the resting state (F) and 15 min after TPA treatment (Fmin). Image analysis was performed with ImageJ. Z-series images of each fluorescence channel per time point were flattened using the maximum intensity Z-projection. To perform single cell analyses, the same workflow as described in the above section “Variability of Fluorescence Intensities of Zinc Probes” was used: nucleus channel images were analyzed to identify the nucleus area, segment cells, and create ROIs, with each ROI identifying a single cell. Applying the ROIs to the Spirozin2 channel allowed us to quantify the mean intensity of SpiroZin2 at the single-cell level in an entire field of view. Background fluorescence of each channel was calculated by averaging the signal intensities of an area (mean intensities) without cells. The fluorescence intensities of the SpiroZin2 channel of each cell were calculated by subtracting background fluorescence from the raw mean fluorescence intensities. Data plots and statistical analyses (ANOVA with Tukey’s HSD posthoc test) were generated with KaleidaGraph software.

3.5 Results

3.5.1 Titration of probes in HC11 cells

Because FluoZin-3 and SpiroZin2 employ different fluorescence sensing mechanisms, we performed a side-by-side comparison of their response to Zn^{2+} perturbations in HC11 cells. Figure 3.1 depicts the chemical structures of FluoZin-3 and SpiroZin2, along with representative fluorescence images and Zn^{2+} response curves. In these experiments, we used the cell-permeable acetoxymethyl (AM) ester derivative of FluoZin-3, FluoZin-3 AM, in which the negatively charged carboxylate groups are masked as neutral esters. After the functionalized dye crosses the cell membrane, intracellular esterases hydrolyze the esters, restoring the carboxylic acids and trapping the negatively charged probe inside the cell. In the absence of Zn^{2+} , FluoZin-3 fluorescence is quenched by photoinduced electron transfer (PET) from the chelating group. Upon Zn^{2+} binding, PET becomes unfavorable, which causes an increase in the fluorescence emission¹⁶⁸. In contrast, SpiroZin2 operates *via* a reaction-based turn-on mechanism that occurs when Zn^{2+} binding induces a ring-opening reaction that converts a non-fluorescent spirobenzopyran to a fluorescent cyanine dye¹⁹⁸. Figures 3.2c and 3.2d show representative fluorescence images of HC11 mouse mammary epithelial cells stained with SpiroZin2 and FluoZin-3, respectively. Cells treated with SpiroZin2 routinely exhibited fluorescence in a vesicular pattern. FluoZin-3 fluorescence signals were more variable, appearing to reside in vesicles, large puncta, and the cytosol.

In order to measure the response of each probe to Zn^{2+} perturbation, cells stained with either SpiroZin2 or FluoZin-3 were treated with reagents to determine the

minimum and maximum fluorescence signal of the apo and Zn^{2+} -bound states. To obtain the minimum fluorescence signal for the apo form of the sensor (F_{min}), the cell-permeable Zn^{2+} chelator tris (2-pyridylmethyl) amine (TPA) was added to cells. Subsequently, the maximal fluorescence signal for the bound form of the sensor (F_{max}) was obtained by addition of excess Zn^{2+} with the ionophore pyrithione. The titration curves in Figures 3.1c and 3.1d demonstrate that both SpiroZin2 and FluoZin-3 respond to Zn^{2+} chelating and saturating reagents within a few minutes in HC11 cells.

Single cell analysis of live cells treated with either FluoZin-3 or SpiroZin2 revealed significant heterogeneity in the fluorescence intensities and staining patterns of each dye. Although the fluorescence intensity of FluoZin-3 has been used widely to estimate intracellular resting labile Zn^{2+} levels under resting conditions^{113,267–270}, evidence suggests that the high fluorescence signal of FluoZin-3 in HeLa cells is at least partially due to accumulation of the dye in the Golgi complex rather than high concentrations of labile Zn^{2+} ¹⁹⁹. Moreover, variability in the amount of dye internalized by cells causes inconsistencies in resting fluorescence signals (F), and, therefore, estimated labile Zn^{2+} levels. We proposed that labile Zn^{2+} levels could be assessed more precisely by normalizing resting state fluorescence to apo state fluorescence after treatment with TPA (F/F_{min}). In this case, greater F/F_{min} ratios would indicate higher concentrations of labile Zn^{2+} .

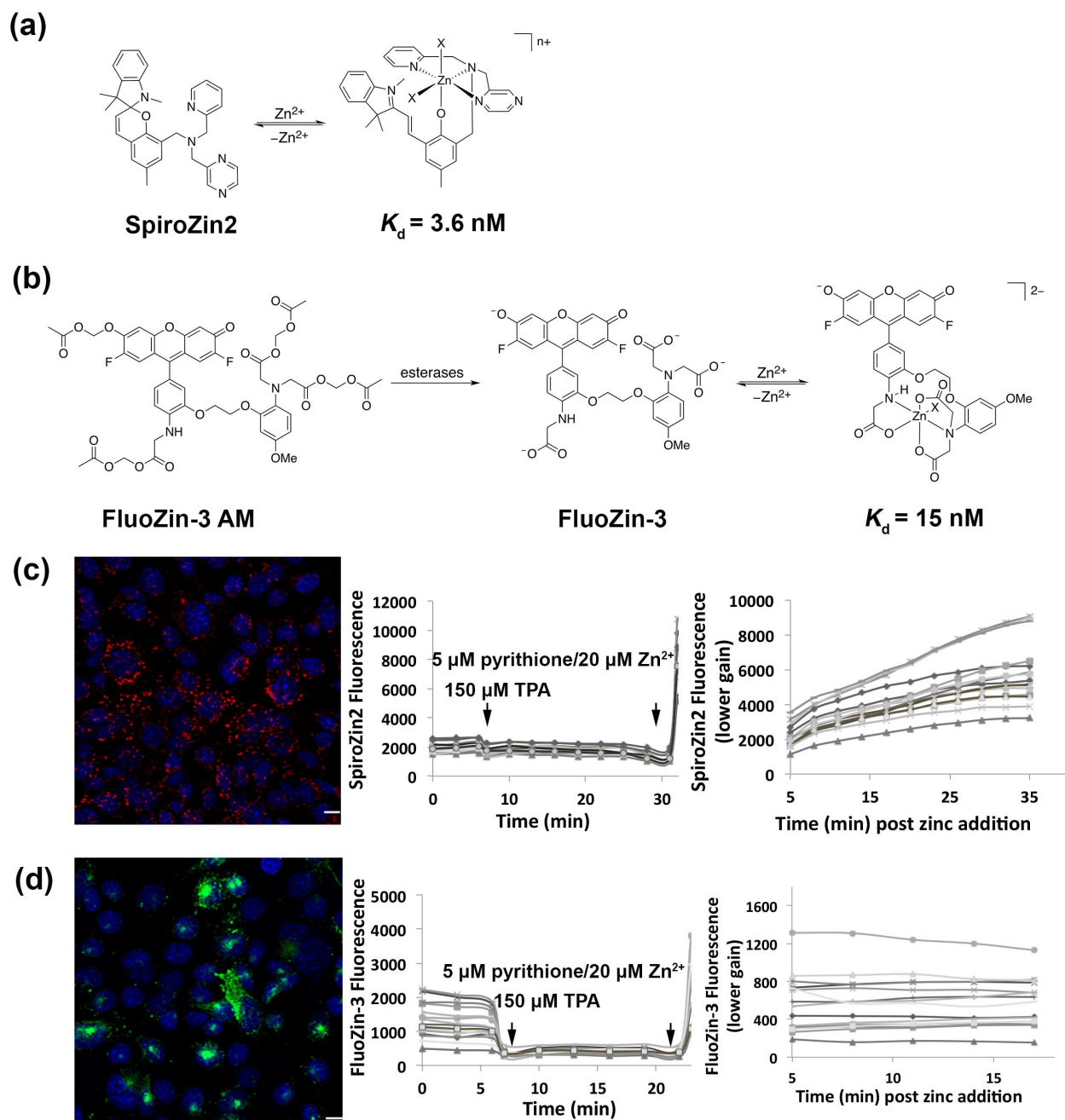


Figure 3.1. Titration of probes in HC11 cells. (a) Molecular structure of zinc-unbound and zinc-bound SpiroZin2 $\lambda_{\text{ex}} = 520 \text{ nm}$, $\lambda_{\text{em}} = 640 \text{ nm}$. (b) Molecular structure of FluoZin-3 AM, zinc-unbound and zinc-bound FluoZin-3, $\lambda_{\text{ex}} = 494 \text{ nm}$, $\lambda_{\text{em}} = 516 \text{ nm}$. (c) Representative image of SpiroZin2-stained HC11 cells and the titration curve of SpiroZin2 in HC11 cells. Red: SpiroZin2. Blue: nucleus. To avoid saturation of pixels, lower gain was applied to acquire images post zinc addition. (d) Representative image

of FluoZin-3-stained HC11 cells and the titration curve of FluoZin-3 in HC11 cells. Green: FluoZin-3. Blue: nucleus. To avoid saturation of pixels, lower gain was applied to acquire images post zinc addition. Scare bar, 10 mm.

3.5.2 SpiroZin2 staining yields consistent signals after normalization to TPA treatment while FluoZin3-stained cells have highly variable signals

To quantify the cellular heterogeneity of fluorescence signals of the two probes, we measured the fluorescence intensities of single HC11 cells stained with either SpiroZin2 or FluoZin-3 AM, with or without pluronic F-127, before (F) and after treatment with TPA (F_{min}). Pluronic F-127 is a non-ionic detergent that facilitates the dispersion of hydrophobic dyes in aqueous media and is often applied in standard FluoZin-3 staining protocols. Figures 3.2a and 3.2c show that both SpiroZin2 and FluoZin-3 staining resulted in highly variable resting fluorescence (F). In contrast, the normalized fluorescence (F/F_{min}) of SpiroZin2 gave consistent results across multiple trials. For example, in two independent experiments in the absence of pluronic, we found $F/F_{min} = 1.4 \pm 0.17$ and 1.3 ± 0.16 . In two separate experiments, we found that co-incubation with pluronic F-127 gave similar results: $F/F_{min} = 1.2 \pm 0.21$ and 1.2 ± 0.16 . These data suggest that the ratio F/F_{min} is a better indicator of resting Zn^{2+} levels than F. FluoZin-3 staining experiments gave a large range of F/F_{min} (ratios = 6.8 ± 4.5 and 6.1 ± 4.5 for two independent trials in the absence of pluronic; 8.4 ± 4.7 and 6.3 ± 4.4 in the presence of pluronic; Figures 3.2c and 3.2d). These results indicate that complete calibration measurements of F, F_{min}, and F_{max} are required to estimate relative Zn^{2+} levels using FluoZin-3. We also determined that the addition of pluronic had only minor effects on the ratio F/F_{min} for both SpiroZin2 (ratio = 1.3 ± 0.17 , - pluronic; 1.2 ± 0.17 , + pluronic, $p < 0.0001$, Student's t-test) and FluoZin-3 (ratio = $6.5 \pm$

4.6, - pluronic; 7.2 ± 4.6 , + pluronic, $p < 0.05$, Student's t-test). These data suggest that, although pluronic F-127 may affect the absolute amount of sensor taken up by a given cell, it does not affect sensor performance inside the cell.

When estimating relative labile Zn^{2+} concentrations in different cell populations, our experiments demonstrate the need for using normalized signals (F/F_{min}), which give uniform and consistent results from cell to cell, rather than resting fluorescence intensities (F), which we found to be highly variable. A quantitative measure of variability is the coefficient of variation (CV). The CV of F for SpiroZin2 was 20.3% - 36.8%, whereas the CV of F/F_{min} was 12.4% - 17.4%. On the other hand, FluoZin-3 produced highly variable F (CV = 58.8% - 86.3%) and F/F_{min} (CV = 55.9% - 74.6%) results. Thus, when FluoZin-3 is used to estimate or compare intracellular labile Zn^{2+} levels under different conditions or in different samples, a large number of cells must be investigated to compensate for the signal variability at the single cell level.

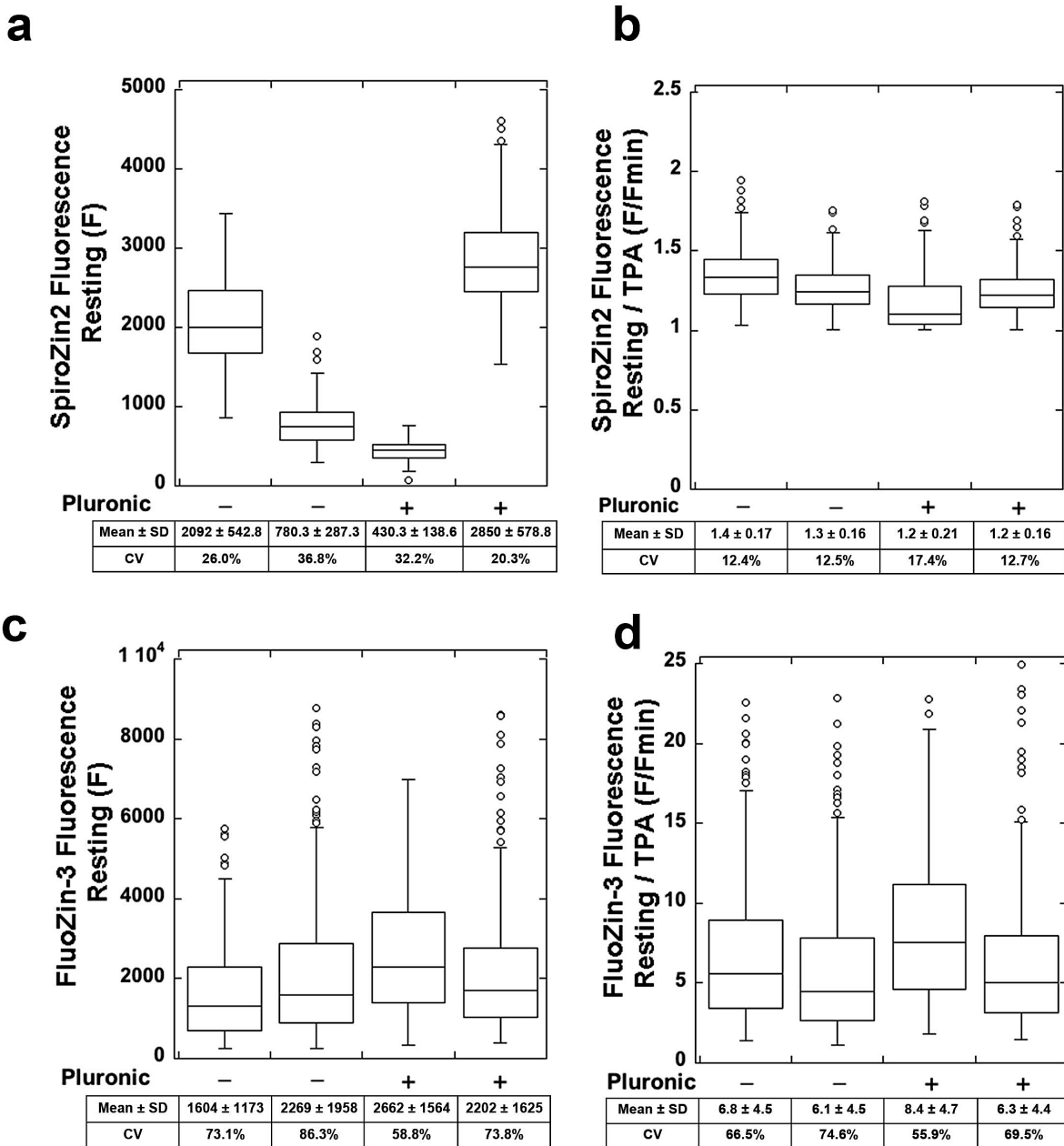


Figure 3.2. SpiroZin2 staining yields consistent signals after normalization to TPA treatment while FluoZin3-stained cells have highly variable signals. (a) SpiroZin2 fluorescence at resting state with and without the addition of pluronic. (b) SpiroZin2 signal at resting state normalized to TPA treatment with and without the addition of pluronic. (c) FluoZin-3 fluorescence at resting state with and without the addition of pluronic. (d) FluoZin-3 signal at resting state normalized to TPA treatment with and without the addition of pluronic. Normalization to TPA treatment was accomplished by dividing the respective probe fluorescent intensity by the fluorescence intensity upon

TPA treatment for each cell. Each point is an individual cell, $n > 62$ for each sample. Two biological replicates per condition. SD, standard deviation. CV, coefficient of variation.

3.5.3 Colocalization assay of zinc probes with vesicular markers

Both SpiroZin2 and FluoZin-3 co-localize with lysosomal markers in a variety of eukaryotic cells including HeLa cells, cultured hippocampal neurons, breast cancer cells, and *C. elegans* intestinal cells^{193,198,258,271}. FluoZin-3 was also reported to accumulate in the Golgi apparatus of HeLa cells and DT40 chicken B cells^{199,272}. The mechanism by which dyes are sequestered in acidic vesicular compartments is not yet fully understood, and it is possible that a given dye can be distributed unequally across different types of vesicles (e.g. lysosomal, secretory, and Golgi apparatus vesicles). To study the distribution of SpiroZin2 and FluoZin-3 in different vesicular compartments, we performed a colocalization analysis of each dye with three vesicular markers, LAMP1-EBFP, GalT-CFP and VAMP8-CFP. Lysosome associated membrane protein 1 (LAMP1) is a highly glycosylated integral membrane protein that is found in late endosomes and lysosomes, and is frequently used as a marker for these organelles²⁷³. GalT-CFP is comprised of the first sixty amino acids of human galactosyltransferase (GalT), a trans-Golgi targeting sequence, fused to CFP. Vesicle-associated membrane protein 8 (VAMP8) is a marker for secretory vesicles that is associated with exocytosis in different types of mammalian cells including pancreatic acinar cells²⁷⁴, mast cells²⁷⁵, cytotoxic T lymphocytes²⁷⁶, platelets²⁷⁷, and kidney collecting duct epithelia²⁷⁸.

To perform the co-localization assay, HC11 cells transiently expressing FP-tagged vesicular markers were stained with SpiroZin2 or FluoZin-3 and imaged by fluorescence microscopy. Dual color images were analyzed with an intensity correlation

assay based on the Pearson correlation coefficient (PC), which ranges from -1 to 1 , with -1 indicating negative correlation, 0 no correlation, and 1 complete positive correlation. PC analysis requires the intensities of the two channels to be comparable because uneven intensities of two channels can lead to artificially diminished PC values²⁷⁹. Under resting conditions in HC11 cells, we found that the fluorescence intensities of the sensors were too low compared to those of the FP-tagged marker proteins, presumably due to the low levels of intracellular Zn^{2+} . In order to achieve comparable intensities in the dye and marker-FP channels, we added a Zn^{2+} /pyrithione solution to dye-stained cells, which increased the sensor fluorescence intensities after a few minutes. PC-based co-localization analysis revealed that SpiroZin2 was strongly co-localized with LAMP1 (PC = 0.68 ± 0.11), but poorly co-localized with GalT (PC = -0.07 ± 0.10) and VAMP8 (PC = 0.08 ± 0.13), indicating that it preferentially resides in late endosomes and lysosomes (Figure 3.3). Because FluoZin-3 is commonly delivered to cells with pluronic, we tested whether this procedure affects subcellular localization. Figure 3.4 shows that FluoZin-3 co-localizes with LAMP1 reasonably well (PC = 0.54 ± 0.12 without pluronic, 0.64 ± 0.1 with pluronic). However, we observed that some portion of FluoZin-3 also populates the Golgi (PC = 0.22 ± 0.22 without pluronic, 0.23 ± 0.21 with pluronic) and secretory vesicles (PC = 0.41 ± 0.25 with pluronic). Because vesicular compartments may have different amounts of labile Zn^{2+} , the non-specific localization of FluoZin-3 may contribute to the highly variable fluorescence intensities of FluoZin-3 staining in Figure 3.2.

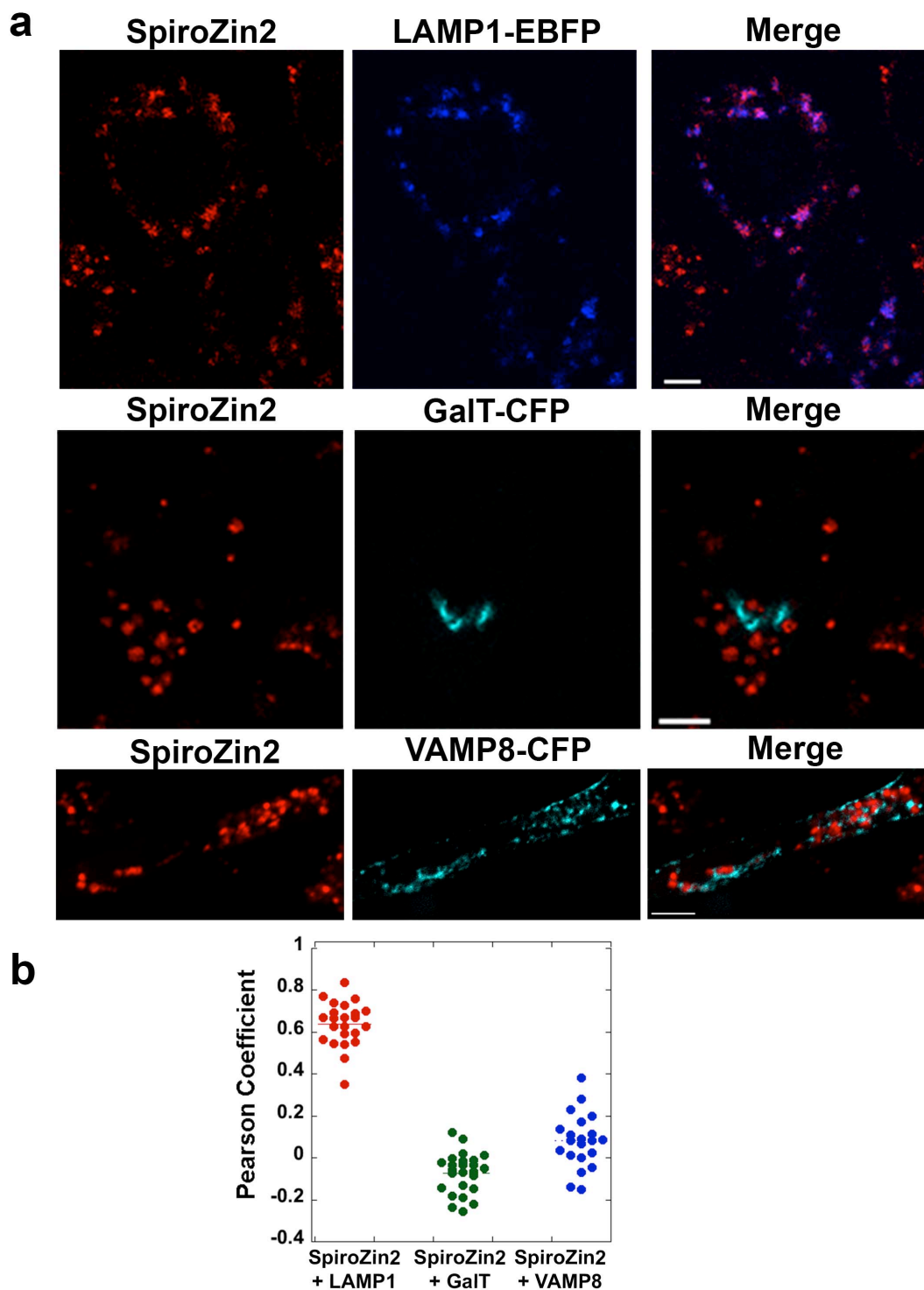


Figure 3.3. Co-localization analysis of SpiroZin2 and three vesicular markers demonstrates that SpiroZin2 resides in lysosomal vesicles. (a) Representative images of SpiroZin2-stained cells, vesicular markers- FP, and merged channel. (b) Pearson coefficient plot of co-localization analysis. Each dot represents an intracellular ROI. Pearson analysis included a minimum of 11 cells per condition. Scale bar, 5 μ m.

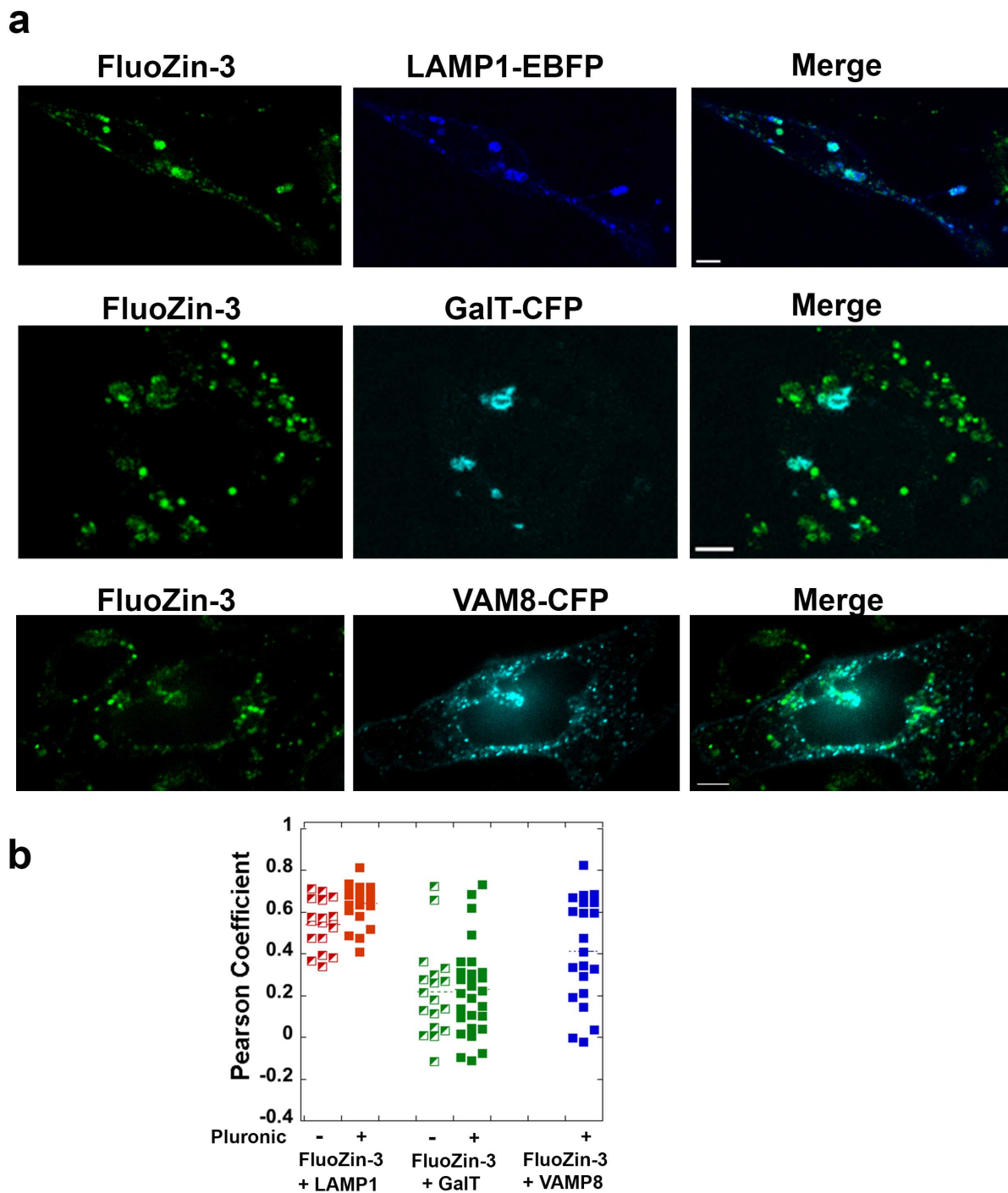
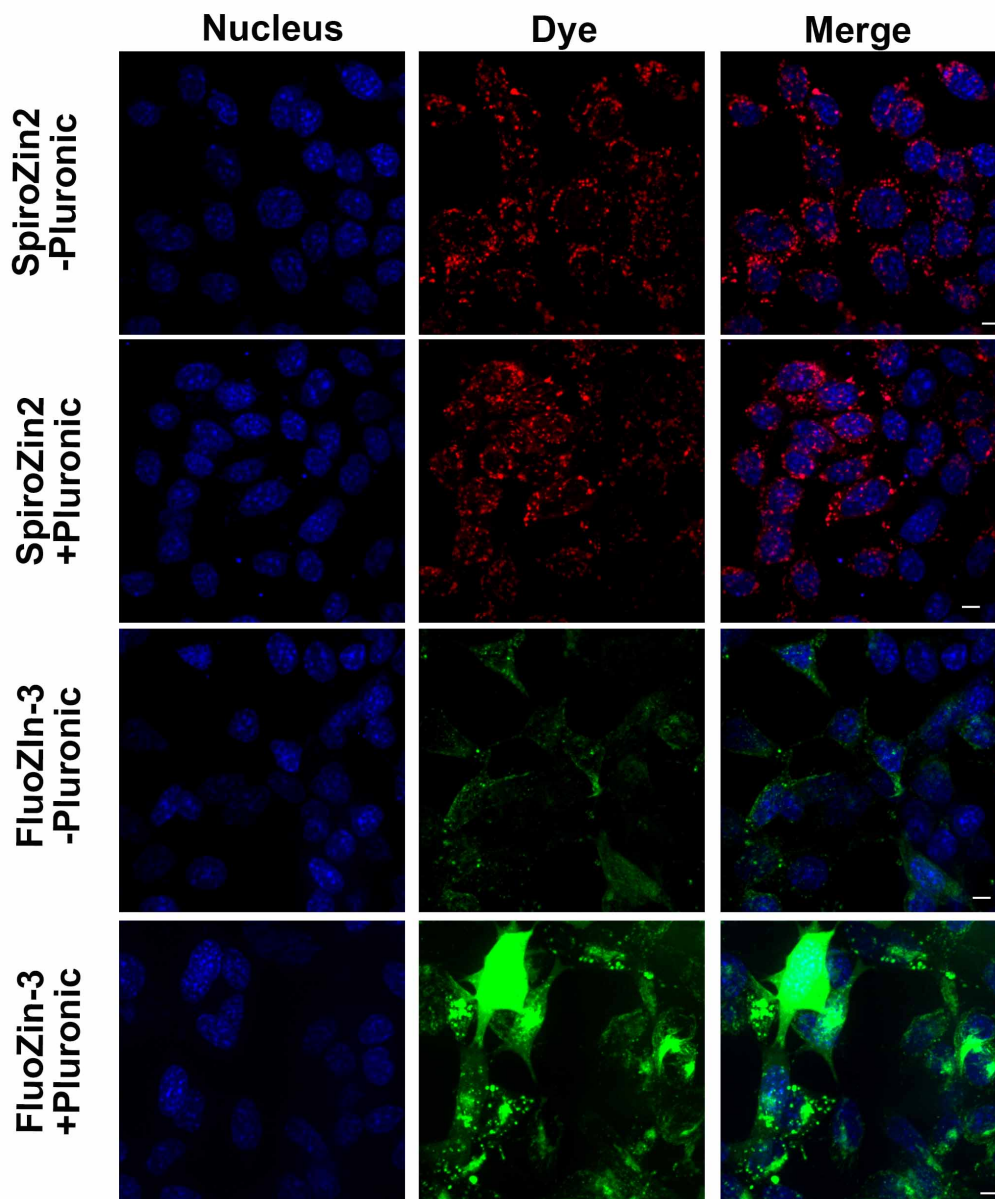


Figure 3.4. Co-localization analysis of FluoZin-3 and three vesicular markers demonstrates that FluoZin-3 non-specifically localizes to lysosomal, Golgi, and secretory vesicles. (a) Representative fluorescence images of Spirozin2-stained cells, vesicular markers- FP, and the merged channel. (b) Pearson coefficient plot of co-localization analysis. Each dot represents an intracellular ROI. A minimum of 18 cells were analyzed for each condition. Scale bar, 5 μ m.

3.5.4 A population of FluoZin-3 localizes to the cytosol

Similar to reports from other researchers^{199,258}, we observed cytosolic signals in some cells treated with FluoZin-3 (Figure 3.1d). To rigorously quantify the cytosolic distribution of SpiroZin2 and FluoZin-3, we stained HC11 cells with each dye in the presence and absence of pluronic and then determined the percentage of cells exhibiting cytosolic signals. As shown in Figure 3.5, none of the SpiroZin2-stained cells showed cytosolic signals under any condition, whereas 0.38% and 13.7% of FluoZin-3-treated cells exhibited cytosolic staining in the absence and presence of pluronic, respectively. In the presence of pluronic, the increase in cytosolic FluoZin-3 signals may be attributable to the increased aqueous solubility of FluoZin-3 AM. Alternatively, it is possible that pluronic facilitates the general uptake of FluoZin-3 into cells and the dye accumulates in cytosol after saturating vesicular organelles. Therefore, when using pluronic it is advisable to optimize the concentration of the FluoZin-3 to avoid accumulation of dye in the cytoplasm. In contrast, SpiroZin2 exhibited unambiguous and consistent vesicular localization.



Quantification of Cytosolic Distribution of Dyes

	Number of cells with cytosolic signal / Total number of cells	
	- Pluronic	+Pluronic
SpiroZin2	0/927	0/1044
FluoZin-3	3/780 (0.38%)	103/751 (13.7%)

Figure 3.5. A population of FluoZin-3 localizes to the cytosol. HC11 cells were stained with SpiroZin2 or FluoZin-3 with and without pluronic. Fluorescence images in each channel were acquired 5 min post treatment with 5 μ M pyrithione/20 μ M ZnCl₂. Quantification reveals that SpiroZin2 does not localize to the cytosol but the cytosolic localization of FluoZin-3 depends on the presence of pluronic. Scale bar, 5 μ m.

3.5.5 SpiroZin2 reveals changes in lysosomal Zn²⁺ upon perturbation

To further characterize the ability of SpiroZin2 to detect lysosomal Zn²⁺, we investigated the dynamic range of the sensor in lysosomes and monitored the lysosomal Zn²⁺ pool as a function of a series of perturbations. To define the full dynamic range, we carried out *in situ* calibrations using TPA to determine F_{min}, and Zn²⁺ with pyrithione to determine F_{max}. As shown in Figure 3.6A, the dynamic range of SpiroZin2 in lysosomes is 5.3 ± 1.2 . An important feature of a lysosomal probe is insensitivity to pH. Whereas SpiroZin2 is insensitive to pH changes between 4.0 and 6.0 *in vitro*, this property was not previously tested in cells. To assess the pH dependence of SpiroZin2 in cells, we first validated that LysoSensor™ Yellow / Blue Dextran, a lysosomal pH indicator, could detect changes in pH from 4 to 6 (Appendix E 1A). We demonstrated that treatment of cells with NH₄⁺ lead to a lysosomal pH shift within 2.5 min (Appendix E 1B) and showed that this shift in pH did not alter SpiroZin2 fluorescence intensity (Appendix E 1C), confirming that SpiroZin2 fluorescence is not affected by changes in pH within this range in cells.

We also examined how lysosomal Zn²⁺ pools respond to an increase in extracellular Zn²⁺. Previously we demonstrated that elevation of extracellular Zn²⁺ leads to a slow increase in cytosolic Zn²⁺ in HeLa cells followed by sequestration into intracellular organelles such as the ER and mitochondria²⁶⁰. Here, we show that HC11 cells also exhibit a steady increase in cytosolic Zn²⁺ detected *via* the genetically encoded fluorescent Zn²⁺ sensor, ZapCV2²³⁰, when treated with 40 mM extracellular Zn²⁺ (Figure 3.6A). Surprisingly, lysosomal Zn²⁺ increased more quickly than cytosolic Zn²⁺, reaching a peak within 5 min, while cytosolic Zn²⁺ continued to rise after 45 min of

treatment. This result suggests that the extracellular Zn^{2+} is rapidly internalized into lysosomes *via* endocytosis, which operates on a time scale of seconds to minutes²⁸⁰. Our data also revealed that this increase in lysosomal Zn^{2+} was transient; the Zn^{2+} level dropped quickly and stabilized within 20 min. The possible routes of lysosomal Zn^{2+} export could be Zn^{2+} leak through lysosomal ion channel transient receptor potential mucolipin 1 (TRPML1)⁶⁵, and/or export to the extracellular environment by lysosomal exocytosis¹⁹⁴.

Finally, we used Bafilomycin A1, a vacuolar H^+ ATPase inhibitor²⁸¹ to dissipate the H^+ gradient across the lysosomal membrane (Figure 3.6B), and show that this procedure decreases the lysosomal Zn^{2+} pool, as detected by a decrease in SpiroZin2 fluorescence intensity (Figure 3.6C – E). These results suggest that lysosomal Zn^{2+} accumulation is facilitated by the proton gradient *via* Zn^{2+}/H^+ exchange. The Cation Diffusion Facilitator (CDF) protein family transports divalent cations and is present in diverse organisms from bacteria to humans²⁸². It is well established that the *E.coli* CDF protein, YiiP, acts as a Zn^{2+}/H^+ antiporter^{283,284}. YiiP is a homologue of mammalian ZnT transporters, and Zn^{2+} transport by ZnT1 and ZnT5 has been suggested to be facilitated by proton gradients^{285,286}. Given that ZnT2 and ZnT4 transport Zn^{2+} into lysosome^{55,56,65}, it is possible that ZnT2 and ZnT4 act as Zn^{2+}/H^+ antiporters, whereby dissipation of the proton gradient disrupts lysosomal Zn^{2+} accumulation.

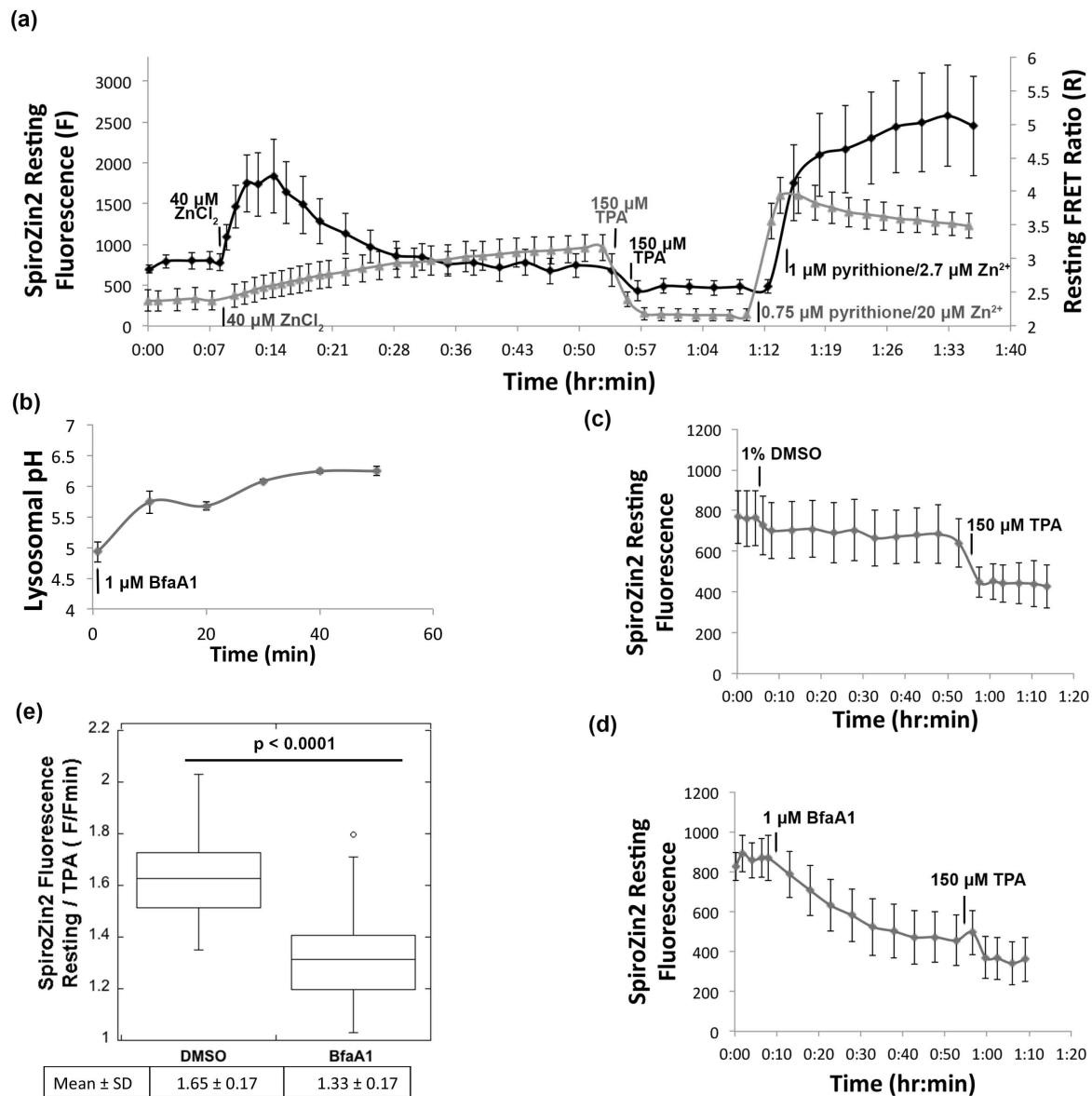


Figure 3.6. SpiroZin2 reveals changes in lysosomal Zn^{2+} upon perturbation. (a) The resting fluorescence of SpiroZin2 (left y axis) and resting FRET ratio (right y axis) of ZapCV2 were recorded over a timecourse upon treatment with 40 μM $ZnCl_2$, 150 μM TPA and 1 μM pyrithione / 2.7 μM Zn^{2+} (SpiroZin2), 0.75 μM pyrithione / 20 μM Zn^{2+} (ZapCV2). (b) lysosomal pH increased upon treatment with 1 μM Bafilomycin A1. SpiroZin2 resting fluorescence was recorded every 5 min for 45 min post treatment with vehicle (1% DMSO) (c) or 1 μM Bafilomycin A1 (d), followed by treatment with 150 μM TPA. (e) The lysosomal Zn^{2+} level (F/F_{min}) in Bafilomycin A1-treated cells is lower than that in DMSO-treated cells. F, the mean of the fluorescence intensities at 40 min and 45 min post treatment with DMSO or Bafilomycin A1; F_{min} , the mean of the fluorescence intensities of the last three time points post TPA treatment. $n > 24$, $p < 0.0001$, unpaired student's t-test.

3.6.6 A substantial increase in lysosomal Zn²⁺ was detected in SpiroZin2-stained mammary epithelial cells at 24 hr post hormone treatment

Given its superior performance, we used SpiroZin2 to track vesicular Zn²⁺ concentrations in mouse mammary epithelial cells (HC11), which differentiate in response to lactation hormones. Because accumulation of Zn²⁺ in intracellular vesicles in secreting HC11 cells has been hypothesized to be a hormone-dependent process²⁵³, we chose to study this phenomenon. Previous reports indicate that lysosome-related organelles in *C. elegans* intestinal cells serve as major Zn²⁺ storage sites that play important roles in maintaining Zn²⁺ homeostasis¹⁹³. To examine whether late endosomes/lysosomes serve a similar function in secreting HC11 cells, we induced differentiation of HC11 cells with lactation hormones according to established protocols^{231,237} and analyzed the relative Zn²⁺ concentrations by SpiroZin2 as a function of time. Single-cell analyses were performed as illustrated in Figure 3.7a. Cells were stained simultaneously with a nuclear dye and SpiroZin2. Nuclear channel images were analyzed with ImageJ to identify the nuclear area, segment cells, and define regions of interest (ROIs), with each ROI corresponding to a single cell. The mean fluorescence intensity in the corresponding SpiroZin2 channel was quantified for each cell in the entire field of view. Normalized fluorescence intensities were measured by treating the cells with TPA and calculating F/F_{min}, as described above. As shown in Figure 3.7b, we detected a substantial increase in labile Zn²⁺ concentrations 24 hours after hormone treatment relative to proliferating resting cells ($p < 0.0001$), an observation that suggests late endosomes or lysosomes may serve as temporary storage sites for Zn²⁺ during HC11 cell differentiation.

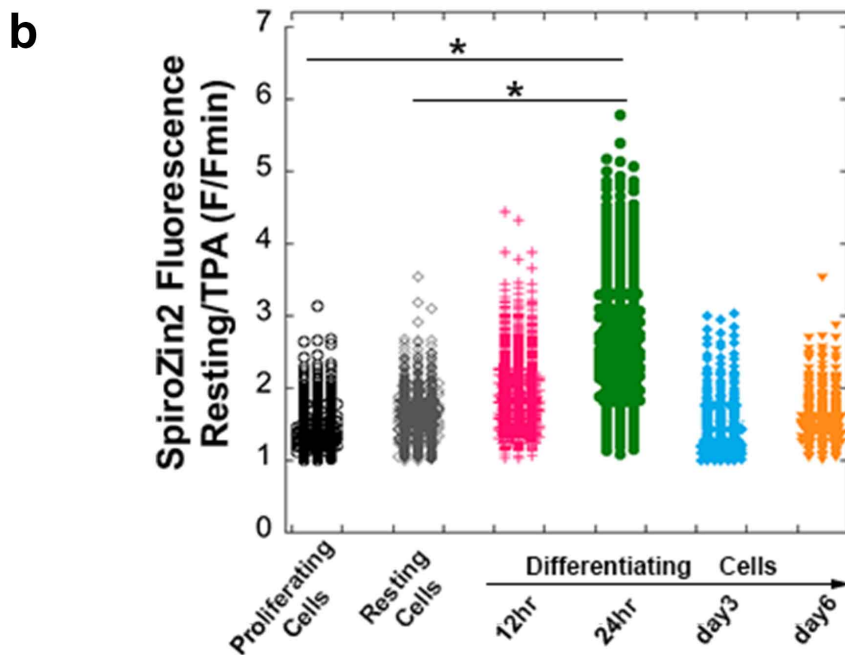
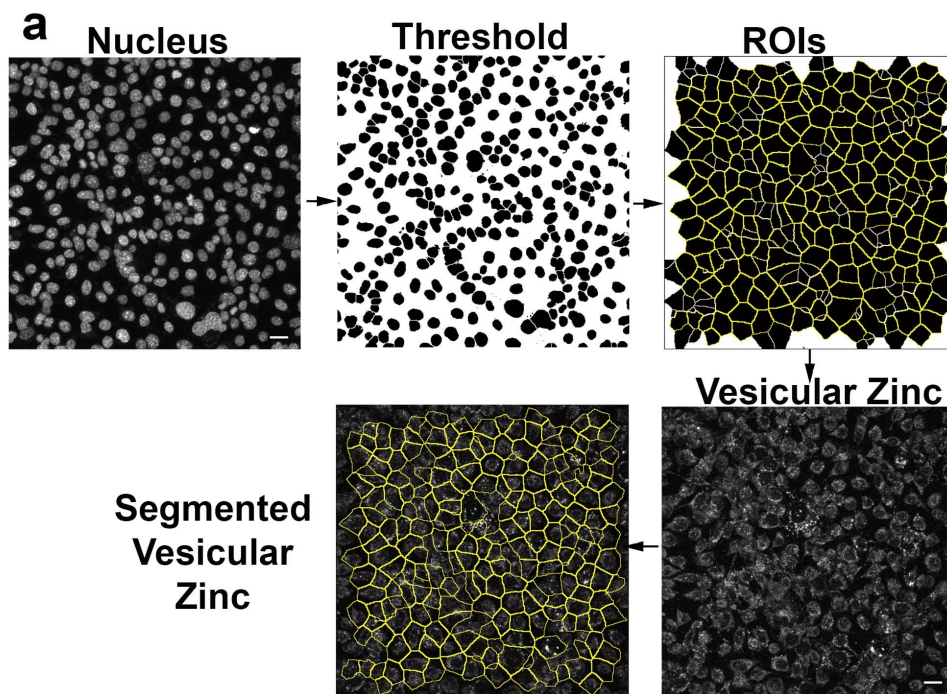


Figure 3.7. A substantial increase in lysosomal Zn^{2+} was detected in SpiroZin2-stained mammary epithelial cells at 24 hr post hormone treatment (5 $\mu\text{g}/\text{mL}$ insulin, 5 $\mu\text{g}/\text{mL}$ prolactin, and 1 μM hydrocortisone). (a) Cell segmentation method for single-cell analysis. scale bar, 40 μm . (b) SpiroZin2 fluorescence signal at resting state normalized to its signal after 30 min of TPA treatment. Each point is an individual cell, $n > 297$ for each sample. Two biological replicates per condition. *, $p < 0.0001$, one-way ANOVA test.

3.7 Discussion

Live-cell imaging of individual cells using small-molecule fluorescent probes is a powerful and widely used approach for estimating the concentration and distribution of analytes in cells. However, few studies rigorously evaluate the heterogeneity in fluorescence signal and localization from cell to cell and explicitly compare the functionality of different probes. In this study, we performed a parallel and systematic comparison of two small-molecule vesicular Zn^{2+} probes, FluoZin-3 AM and SpiroZin2, to evaluate each probe for measurement of vesicular Zn^{2+} pools. Our work reveals that SpiroZin2 specifically reports on lysosomal Zn^{2+} pools and can be used to monitor changes in lysosomal Zn^{2+} in a variety of perturbations (changes in extracellular Zn^{2+} , dissipation of the lysosomal H^+ gradient, and cell differentiation).

One of the primary applications of small molecule fluorescent Zn^{2+} sensors is to compare relative amounts of Zn^{2+} in different biological samples, for example between different cell types or between cells in different physiological states, such as differentiated versus undifferentiated. As evident in published studies^{113,267–270}, it is common practice to use resting fluorescence intensities of FluoZin-3 to estimate relative Zn^{2+} levels in different cell populations. Our results indicate that the resting FluoZin-3 or SpiroZin2 fluorescence intensities (F) are highly variable among cells (Figure 3.2), with an average coefficient of variation (CV) of 28% for SpiroZin2 and 73% for FluoZin-3, and should not be used to represent relative Zn^{2+} levels. In contrast, for SpiroZin2 the ratio of fluorescence intensity of the resting state to that after TPA treatment (F/F_{min}) was uniform and consistent, with a substantially decreased average CV (13.7%, Figure 3.2). Therefore, instead of F , F/F_{min} is a more appropriate and precise parameter to

assess relative labile Zn^{2+} levels in cells when using SpiroZin2. Unfortunately for FluoZin-3, fluorescence signals normalized to F_{min} (F/F_{min}) remained highly variable (average CV 66%). One possible explanation for this high variability in fluorescence signal under resting conditions is that individual cells internalize different amounts of dye. In this case, normalization of F to the F_{min} signal in each individual cell provides an internal control for that cell and mitigates the variability. For FluoZin-3, the large degree of signal heterogeneity, even after normalization, most likely results from the widespread heterogeneity in dye localization in addition to affects from differential dye accumulation.

Unlike targeted genetically-encoded sensors that can be localized to a specific organelle by a tagging sequence, small molecule fluorescent probes tend to accumulate adventitiously in different compartments³⁹. Because previous reports suggest that FluoZin-3 AM accumulates in multiple organelles in mammalian cells¹⁹⁹, we rigorously determined the intracellular distribution of the dyes. Our data reveal that SpiroZin2 exclusively localizes in lysosomal vesicles (Figure 3.3). Whereas previous work¹⁹⁸ showed SpiroZin2 accumulated in lysosomes, it did not establish that SpiroZin2 was exclusively in lysosomes, as we do here. FluoZin-3 AM non-specifically accumulates in the cytosol, as well as across three populations of vesicles: lysosomal vesicles, trans-Golgi vesicles and secretory vesicles. Owing to possible different labile Zn^{2+} levels in different vesicular compartments, the heterogeneous intracellular localization of FluoZin-3 may contribute to the variable fluorescence intensities of FluoZin-3 staining observed in Figure 3.2, even after normalization to F_{min} . This high degree of variation confounds interpretation of Zn^{2+} measurements made by FluoZin-3 in different biological

samples or under different conditions. In order to compare relative Zn^{2+} levels in a particular subcellular compartment across samples or conditions using FluoZin-3, researchers should simultaneously measure FluoZin-3 signals and organelle markers, carry out full probe calibrations by recording F , F_{min} , and F_{max} in individual cells, and restrict analysis to those cells in which FluoZin-3 co-localizes with a genetically-encoded marker for the compartment of interest.

In the present study we used F/F_{min} to provide a relative measure of the labile Zn^{2+} pool in lysosomes. It should be noted that, although sensors can be used to quantify Zn^{2+} , doing so requires a full sensor calibration, estimation of the dissociation constant (K_d) for Zn^{2+} ideally in the compartment of interest, and demonstration that the probe is in equilibrium with the labile pool within a particular compartment. Small compartments, such as lysosomes, pose an additional challenge because of their extremely small volumes.

Our results reveal that SpiroZin2 is a specific lysosomal Zn^{2+} probe that provides reliable measurements of resting lysosomal Zn^{2+} pools in single cell analyses, when properly normalized, and how these pools change with different cellular perturbations. We demonstrate that lysosomal Zn^{2+} pools respond rapidly to perturbation of extracellular Zn^{2+} and that the lysosomal Zn^{2+} pool relies on activity of the V-ATPase of lysosomes. We also applied SpiroZin2 to lactating mouse mammary epithelial cells and detected a transient increase of lysosomal free Zn^{2+} 24 hr after treatment with a lactation hormone. This finding is significant because a growing number of studies suggest that lysosomes play a key role in Zn^{2+} homeostasis. Zn^{2+} can be delivered into lysosomes from the cytosol by two Zn^{2+} transporters, Slc30a2 and Slc30a4^{55,56,65}, or

through other cellular processes such as autophagy^{94,287}. Lysosomes serve as Zn^{2+} storage reserves and protect cells from Zn^{2+} overload in *C. elegans* intestinal cells and HeLa cells^{193,194}. Even so, lysosomal accumulation of Zn^{2+} can also be toxic, inducing lysosomal membrane permeabilization (LMP) and cell death under certain pathological conditions^{258,266,288,289}. Lysosomal Zn^{2+} can be transported into the cytosol by the lysosomal ion channel transient receptor potential mucolipin 1 (TRPML1)⁶⁵, and/or exported to the extracellular environment by lysosomal exocytosis¹⁹⁴. Although the mechanism of the transient increase of lysosomal Zn^{2+} lactating mouse mammary epithelial cells is unknown, we propose that lysosomes serve as temporary Zn^{2+} storage sites and play key roles in the regulation of Zn^{2+} homeostasis during lactation. Previous work has implicated lysosomes as playing an important role in redistribution of Zn^{2+} pools during involution of mammary tissue upon weaning^{195,196,290}. Here, we show they also play a role during differentiation to a lactation phenotype, suggesting that lysosomes may be a major player during remodeling of Zn^{2+} homeostasis and redistribution of labile Zn^{2+} pools.

3.8 Future Directions

Future work of this study will focus on elucidating (1) the broader application of SpiroZin2 and (2) the sources of the transient increase of lysosomal Zn^{2+} in differentiated HC11 cells.

First, lysosome have been suggested as a Zn^{2+} storage site to protect cells from Zn^{2+} toxicity^{193,194}. On the other hand, lysosomal accumulation of Zn^{2+} and following cell death has been associated with a variety of health problems^{258,266,288,289}. However, the accumulation of lysosomal Zn^{2+} detected in the above studies was quantified using

FluoZin-3, which has non-specific subcellular localization and highly variable signals. The biological roles of lysosome in zinc homeostasis and whether or not the accumulation of lysosomal Zn^{2+} is a hallmark in some human diseases cannot be addressed without accurately quantifying lysosomal Zn^{2+} . The application of SpiroZin2 in the future study of lysosomal Zn^{2+} will profoundly aid in addressing the above questions.

Second, I am interested in determining the source of the transient accumulation of Zn^{2+} in lysosome. It has been shown that lysosomal Zn^{2+} accumulation was caused by Zn^{2+} transport by lysosomal ZnT2 or ZnT4(ref). However, ZnT2 mRNA expression was undetected whereas ZnT4 mRNA expression did not change at 24 hr post hormone treatment (Figure 2.4B). Using western blot, protein expression of ZnT2 and ZnT4 was quantified relative to ACTB expression but protein expression level of both genes did not increase at 24 hr post hormone treatment (data not shown). A remaining possibility is ZnT4 translocates to lysosome membrane transiently at 24 hr post hormone treatment, leading to the increase of lysosomal Zn^{2+} . I will test this possibility by co-localizing ZnT4 with a lysosomal membrane marker Lamp1 using co-immunofluorescence.

Chapter 4

Implications in Zinc Homeostasis and Cell Signaling

In this chapter, I will discuss the major implications from this study for hormone-regulated zinc homeostasis and cell signaling.

Using the differentiation of HC11 cells upon lactogenic hormone treatment, I found out that 11 zinc transporters were differentially regulated at day6 post treatment with lactogenic hormones (prolactin and cortisol). ZIP14 was selected for downstream analysis due to its relatively high expression level and fold change, however, the broad effect of lactogenic hormone(s) on the expression of zinc transporters remains to be profiled. To address this, the expression of the other 10 transporters needs to be examined with treatment with prolactin alone, cortisol alone and the combination of both hormones. This experiment will deepen our understanding in the different roles of cortisol and prolactin in regulating zinc homeostasis. While prolactin majorly regulates mammary gland differentiation and lactation, cortisol is detected in many types of tissues and controls gene expression in response to stress. Knowing the expression of what zinc homeostasis genes are under the control of cortisol will help us to elucidate how zinc homeostasis is modulated in different biological processes (e.g. stress).

A ~50% increase of cytosolic Zn^{2+} was also detected at day6 post hormone treatment. It has been shown that Zn^{2+} treatment controls the mRNA expression of ZnT1, ZnT2 and ZIP10 via the Zn^{2+} - MTF1 axis. To study whether or not the 50% increase of cytosolic Zn^{2+} plays roles in the expression of transporters, the mRNA levels of 11 transporters need to be profiled in proliferating HC11 cells treated with Zn^{2+} . This experiment can also discover any novel transporter regulated by Zn^{2+} treatment. I also

showed that cortisol stimulated the mRNA expression of ZIP14 and ZIP14 directly transported Zn^{2+} into cytosol. It will be interesting to develop a hierarchy in zinc homeostasis regulated by cortisol where ZIP14 increases cytosolic Zn^{2+} and the latter further controls the expression of other zinc transporters. This experiment will extend our knowledge of how cells systematically regulate zinc homeostasis in a temporal fashion in response to hormone treatment.

My data also showed that ZIP14 is important for the mRNA expression of the whey acid protein (WAP) but not beta-casein (CSN2). It remains to be addressed that whether or not ZIP14 regulates WAP mRNA level at the transcriptional level or post-transcriptional level (mRNA degradation). Once the target(s) of ZIP14 regulation is identified, a potential broader effect of ZIP14 KD in the expression of genes can be predicted and examined. For example, if ZIP14 KD represses the WAP transcription via lowering the activity or expression level of a transcription factor, it is plausible that ZIP14 KD also affects the expression of all downstream genes that are regulated by this transcription factor.

The association between cortisol-induced ZIP14 expression, cytosolic Zn^{2+} increase and WAP expression suggests that the increase of cytosolic Zn^{2+} mediates the cortisol signaling cascade. However, ZIP14 is probably not essential for the glucocorticoid-receptor (GR) signaling pathway, as casein mRNA expression was unaffected in ZIP14-KD cells and it is well known that casein expression is regulated synergistically by STAT5 (prolactin-induced signal transducer) and GR. Although both genes are activated by the cooperation of prolactin and cortisol^{239,254}, the transcription of CSN2 and WAP operates differently: cortisol alone induces transcription of WAP with

GR present on WAP promoter but not CSN2¹⁶¹, whereas prolactin alone was sufficient to induce CSN2 but not WAP transcription²³⁸. GR regulates the transcription of target genes via recruiting other transcription factors or mediators to the promoter region. I hypothesize that ZIP14-regulated cytosolic Zn²⁺ level modulates the expression level or activity of transcription factor(s) or mediator(s) that are recruited by GR to specifically control the transcription of a subset of genes including WAP. Verifying this hypothesis can elucidate how zinc signal (i.e. changes in cytosolic Zn²⁺ level) to regulate gene expression in cell signaling cascade.

A complete list of target genes that are regulated by ZIP14 can be acquired by comparing the mRNA expression level of transcriptome in differentiated cells and ZIP14-KD differentiated cells. Knowing the identities of these target genes will aid me to reveal the mechanism of ZIP14 regulation. For example, enrichment of known elements that specifically bind certain transcription factors in promoter regions of these target genes can be analyzed by bioinformatic tools to find out what transcription factor(s) are regulated by ZIP14. Moreover, bioinformatic analysis can also suggest the cellular pathways that are regulated by ZIP14 in differentiated cells.

Overall, the findings in this study suggest a remodeled zinc homeostasis upon lactogenic hormones treatment, which regulates gene expression in differentiated mammary epithelial cells.

Bibliography

- (1) Lin, H.-Y.; Cheng, P.-Y.; Wan, C.-F.; Wu, A.-T. A Turn-on and Reversible Fluorescence Sensor for Zinc Ion. *Analyst* **2012**, *137* (19), 4415–4417.
- (2) Kambe, T.; Tsuji, T.; Hashimoto, A.; Itsumura, N. The Physiological, Biochemical, and Molecular Roles of Zinc Transporters in Zinc Homeostasis and Metabolism. *Physiological Reviews* **2015**, *95* (3), 749–784.
- (3) Laity, J. H.; Lee, B. M.; Wright, P. E. Zinc Finger Proteins: New Insights into Structural and Functional Diversity. *Curr. Opin. Struct. Biol.* **2001**, *11* (1), 39–46.
- (4) Vallee, B. L.; Auld, D. S. Zinc Coordination, Function, and Structure of Zinc Enzymes and Other Proteins. *Biochemistry* **1990**, *29* (24), 5647–5659.
- (5) Andreini, C.; Bertini, I. A Bioinformatics View of Zinc Enzymes. *J. Inorg. Biochem.* **2012**, *111*, 150–156.
- (6) Vallee, B. L.; Falchuk, K. H. The Biochemical Basis of Zinc Physiology. *Physiological Reviews* **1993**, *73* (1), 79–118.
- (7) Hucho, F.; Buchner, K. Signal Transduction and Protein Kinases: The Long Way from the Plasma Membrane into the Nucleus. *Naturwissenschaften* **1997**, *84* (7), 281–290.
- (8) González-Espinosa, C.; Guzmán-Mejía, F. 8 - Basic Elements of Signal Transduction Pathways Involved in Chemical Neurotransmission. In *Identification of Neural Markers Accompanying Memory*; Meneses, A., Ed.; Elsevier: San Diego, 2014; pp 121–133.
- (9) Berridge, M. J.; Lipp, P.; Bootman, M. D. The Versatility and Universality of Calcium Signalling. *Nature Reviews Molecular Cell Biology* **2000**, *1* (1), 11–21.
- (10) Clapham, D. E. Calcium Signaling. *Cell* **2007**, *131* (6), 1047–1058.
- (11) Gsponer, J.; Christodoulou, J.; Cavalli, A.; Bui, J. M.; Richter, B.; Dobson, C. M.; Vendruscolo, M. A Coupled Equilibrium Shift Mechanism in Calmodulin-Mediated Signal Transduction. *Structure* **2008**, *16* (5), 736–746.
- (12) Frederickson, C. J.; Koh, J.-Y.; Bush, A. I. The Neurobiology of Zinc in Health and Disease. *Nat. Rev. Neurosci.* **2005**, *6* (6), 449–462.
- (13) Yamasaki, S.; Sakata-Sogawa, K.; Hasegawa, A.; Suzuki, T.; Kabu, K.; Sato, E.; Kurosaki, T.; Yamashita, S.; Tokunaga, M.; Nishida, K.; et al. Zinc Is a Novel

- Intracellular Second Messenger. *The Journal of Cell Biology* **2007**, *177* (4), 637–645.
- (14) Haase, H.; Hebel, S.; Engelhardt, G.; Rink, L. Flow Cytometric Measurement of Labile Zinc in Peripheral Blood Mononuclear Cells. *Anal. Biochem.* **2006**, *352* (2), 222–230.
- (15) Haase, H.; Ober-Blöbaum, J. L.; Engelhardt, G.; Hebel, S.; Heit, A.; Heine, H.; Rink, L. Zinc Signals Are Essential for Lipopolysaccharide-Induced Signal Transduction in Monocytes. *J. Immunol.* **2008**, *181* (9), 6491–6502.
- (16) Dubben, S.; Hönscheid, A.; Winkler, K.; Rink, L.; Haase, H. Cellular Zinc Homeostasis Is a Regulator in Monocyte Differentiation of HL-60 Cells by 1 α ,25-Dihydroxyvitamin D3. *Journal of Leukocyte Biology* *87* (5), 833–844.
- (17) Percival, M. D.; Yeh, B.; Falgueyret, J. P. Zinc Dependent Activation of CAMP-Specific Phosphodiesterase (PDE4A). *Biochem. Biophys. Res. Commun.* **1997**, *241* (1), 175–180.
- (18) Londesborough, J.; Suoranta, K. Zinc-Containing Cyclic Nucleotide Phosphodiesterases from Bakers' Yeast. *Meth. Enzymol.* **1988**, *159*, 777–785.
- (19) Plum, L. M.; Brieger, A.; Engelhardt, G.; Hebel, S.; Nessel, A.; Arlt, M.; Kaltenberg, J.; Schwaneberg, U.; Huber, M.; Rink, L.; et al. PTEN-Inhibition by Zinc Ions Augments Interleukin-2-Mediated Akt Phosphorylation. *Metallomics* **2014**, *6* (7), 1277–1287.
- (20) Wilson, M.; Hogstrand, C.; Maret, W. Picomolar Concentrations of Free Zinc(II) Ions Regulate Receptor Protein-Tyrosine Phosphatase β Activity. *J. Biol. Chem.* **2012**, *287* (12), 9322–9326.
- (21) Wessels, I.; Maywald, M.; Rink, L. Zinc as a Gatekeeper of Immune Function. *Nutrients* **2017**, *9* (12).
- (22) Maret, W. Zinc in Cellular Regulation: The Nature and Significance of “Zinc Signals.” *Int J Mol Sci* **2017**, *18* (11).
- (23) Ho, Y.; Samarasinghe, R.; Knoch, M. E.; Lewis, M.; Aizenman, E.; DeFranco, D. B. Selective Inhibition of MAPK Phosphatases by Zinc Accounts for ERK1/2-Dependent Oxidative Neuronal Cell Death. *Mol Pharmacol* **2008**, *74* (4), 1141–1151.
- (24) Takeda, A. Zinc Homeostasis and Functions of Zinc in the Brain. *Biometals* **2001**, *14* (3–4), 343–351.

- (25) Kelleher, S. L.; McCormick, N. H.; Velasquez, V.; Lopez, V. Zinc in Specialized Secretory Tissues: Roles in the Pancreas, Prostate, and Mammary Gland. *Adv Nutr* **2011**, *2* (2), 101–111.
- (26) Kenny, D. A.; Jurata, L. W.; Saga, Y.; Gill, G. N. Identification and Characterization of LMO4, an LMO Gene with a Novel Pattern of Expression during Embryogenesis. *Proc Natl Acad Sci U S A* **1998**, *95* (19), 11257–11262.
- (27) Sum, E. Y. M.; Shackleton, M.; Hahm, K.; Thomas, R. M.; O'Reilly, L. A.; Wagner, K.-U.; Lindeman, G. J.; Visvader, J. E. Loss of the LIM Domain Protein Lmo4 in the Mammary Gland during Pregnancy Impedes Lobuloalveolar Development. *Oncogene* **2005**, *24* (30), 4820–4828.
- (28) Asselin-Labat, M.-L.; Sutherland, K. D.; Barker, H.; Thomas, R.; Shackleton, M.; Forrest, N. C.; Hartley, L.; Robb, L.; Grosveld, F. G.; van der Wees, J.; et al. Gata-3 Is an Essential Regulator of Mammary-Gland Morphogenesis and Luminal-Cell Differentiation. *Nat. Cell Biol.* **2007**, *9* (2), 201–209.
- (29) Kouros-Mehr, H.; Storch, E. M.; Sternlicht, M. D.; Werb, Z. GATA-3 Maintains the Differentiation of the Luminal Cell Fate in the Mammary Gland. *Cell* **2006**, *127* (5), 1041–1055.
- (30) Wiseman, B. S.; Sternlicht, M. D.; Lund, L. R.; Alexander, C. M.; Mott, J.; Bissell, M. J.; Soloway, P.; Itohara, S.; Werb, Z. Site-Specific Inductive and Inhibitory Activities of MMP-2 and MMP-3 Orchestrate Mammary Gland Branching Morphogenesis. *J. Cell Biol.* **2003**, *162* (6), 1123–1133.
- (31) Rudolph-Owen, L. A.; Cannon, P.; Matrisian, L. M. Overexpression of the Matrix Metalloproteinase Matrilysin Results in Premature Mammary Gland Differentiation and Male Infertility. *Mol. Biol. Cell* **1998**, *9* (2), 421–435.
- (32) Aggett, P. J.; Atherton, D. J.; More, J.; Davey, J.; Delves, H. T.; Harries, J. T. Symptomatic Zinc Deficiency in a Breast-Fed Preterm Infant. *Arch Dis Child* **1980**, *55* (7), 547–550.
- (33) Murthy, S. C.; Udagani, M. M.; Badakali, A. V.; Yelameli, B. C. Symptomatic Zinc Deficiency in a Full-Term Breast-Fed Infant. *Dermatol. Online J.* **2010**, *16* (6), 3.
- (34) Chohanadisai, W.; Lönnnerdal, B.; Kelleher, S. L. Identification of a Mutation in SLC30A2 (ZnT-2) in Women with Low Milk Zinc Concentration That Results in Transient Neonatal Zinc Deficiency. *J. Biol. Chem.* **2006**, *281* (51), 39699–39707.
- (35) Itsumura, N.; Inamo, Y.; Okazaki, F.; Teranishi, F.; Narita, H.; Kambe, T.; Kodama, H. Compound Heterozygous Mutations in SLC30A2/ZnT2 Results in Low Milk Zinc Concentrations: A Novel Mechanism for Zinc Deficiency in a Breast-Fed Infant. *PLoS ONE* **2013**, *8* (5), e64045.

- (36) Isumura, N.; Kibihara, Y.; Fukue, K.; Miyata, A.; Fukushima, K.; Tamagawa-Mineoka, R.; Katoh, N.; Nishito, Y.; Ishida, R.; Narita, H.; et al. Novel Mutations in SLC30A2 Involved in the Pathogenesis of Transient Neonatal Zinc Deficiency. *Pediatr. Res.* **2016**, *80* (4), 586–594.
- (37) Ackland, M. L.; Michalczyk, A. Zinc Deficiency and Its Inherited Disorders -a Review. *Genes Nutr* **2006**, *1* (1), 41–49.
- (38) Huang, L.; Gitschier, J. A Novel Gene Involved in Zinc Transport Is Deficient in the Lethal Milk Mouse. *Nat. Genet.* **1997**, *17* (3), 292–297.
- (39) Carter, K. P.; Young, A. M.; Palmer, A. E. Fluorescent Sensors for Measuring Metal Ions in Living Systems. *Chem. Rev.* **2014**, *114* (8), 4564–4601.
- (40) Dufner-Beattie, J.; Langmade, S. J.; Wang, F.; Eide, D.; Andrews, G. K. Structure, Function, and Regulation of a Subfamily of Mouse Zinc Transporter Genes. *J. Biol. Chem.* **2003**, *278* (50), 50142–50150.
- (41) Gaither, L. A.; Eide, D. J. The Human ZIP1 Transporter Mediates Zinc Uptake in Human K562 Erythroleukemia Cells. *J. Biol. Chem.* **2001**, *276* (25), 22258–22264.
- (42) Bin, B.-H.; Fukada, T.; Hosaka, T.; Yamasaki, S.; Ohashi, W.; Hojyo, S.; Miyai, T.; Nishida, K.; Yokoyama, S.; Hirano, T. Biochemical Characterization of Human ZIP13 Protein A homo-dimerized zinc transporter involved in the spondylocheiro dysplastic Ehlers-danlos syndrome. *J. Biol. Chem.* **2011**, *286* (46), 40255–40265.
- (43) Jeong, J.; Walker, J. M.; Wang, F.; Park, J. G.; Palmer, A. E.; Giunta, C.; Rohrbach, M.; Steinmann, B.; Eide, D. J. Promotion of Vesicular Zinc Efflux by ZIP13 and Its Implications for Spondylocheiro Dysplastic Ehlers–Danlos Syndrome. *Proc Natl Acad Sci U S A* **2012**, *109* (51), E3530–E3538.
- (44) Gaither, L. A.; Eide, D. J. Functional Expression of the Human HZIP2 Zinc Transporter. *J. Biol. Chem.* **2000**, *275* (8), 5560–5564.
- (45) Girijashanker, K.; He, L.; Soleimani, M.; Reed, J. M.; Li, H.; Liu, Z.; Wang, B.; Dalton, T. P.; Nebert, D. W. Slc39a14 Gene Encodes ZIP14, a Metal/Bicarbonate Symporter: Similarities to the ZIP8 Transporter. *Mol. Pharmacol.* **2008**, *73* (5), 1413–1423.
- (46) Hojyo, S.; Fukada, T.; Shimoda, S.; Ohashi, W.; Bin, B.-H.; Koseki, H.; Hirano, T. The Zinc Transporter SLC39A14/ZIP14 Controls G-Protein Coupled Receptor-Mediated Signaling Required for Systemic Growth. *PLOS ONE* **2011**, *6* (3), e18059.

- (47) Liuzzi, J. P.; Lichten, L. A.; Rivera, S.; Blanchard, R. K.; Aydemir, T. B.; Knutson, M. D.; Ganz, T.; Cousins, R. J. Interleukin-6 Regulates the Zinc Transporter Zip14 in Liver and Contributes to the Hypozincemia of the Acute-Phase Response. *PNAS* **2005**, *102* (19), 6843–6848.
- (48) Kelleher, S. L.; Lopez, V.; Lönnnerdal, B.; Dufner-Beattie, J.; Andrews, G. K. Zip3 (Slc39a3) Functions in Zinc Reuptake from the Alveolar Lumen in Lactating Mammary Gland. *Am. J. Physiol. Regul. Integr. Comp. Physiol.* **2009**, *297* (1), R194-201.
- (49) Kelleher, S. L.; Lönnnerdal, B. Zip3 Plays a Major Role in Zinc Uptake into Mammary Epithelial Cells and Is Regulated by Prolactin. *American Journal of Physiology - Cell Physiology* **2005**, *288* (5), C1042–C1047.
- (50) Palmiter, R. D.; Findley, S. D. Cloning and Functional Characterization of a Mammalian Zinc Transporter That Confers Resistance to Zinc. *EMBO J* **1995**, *14* (4), 639–649.
- (51) McMahon, R. J.; Cousins, R. J. Mammalian Zinc Transporters. *J. Nutr.* **1998**, *128* (4), 667–670.
- (52) Dutta, A.; Sankavaram, K.; Chong, L.; Palermo, A.; Michel, R. G.; Freake, H. C. Rapid Homeostatic Response of H4IIE Cells to Diethylenetriaminepentaacetic Acid Is Not Due to Changes in the Amount or Localization of ZnT-1 Protein. *Nutr Res* **2011**, *31* (5), 404–411.
- (53) Fujimoto, S.; Itsumura, N.; Tsuji, T.; Anan, Y.; Tsuji, N.; Ogra, Y.; Kimura, T.; Miyamae, Y.; Masuda, S.; Nagao, M.; et al. Cooperative Functions of ZnT1, Metallothionein and ZnT4 in the Cytoplasm Are Required for Full Activation of TNAP in the Early Secretory Pathway. *PLoS ONE* **2013**, *8* (10), e77445.
- (54) Wang, F.; Kim, B.-E.; Dufner-Beattie, J.; Petris, M. J.; Andrews, G.; Eide, D. J. Acrodermatitis Enteropathica Mutations Affect Transport Activity, Localization and Zinc-Responsive Trafficking of the Mouse ZIP4 Zinc Transporter. *Hum. Mol. Genet.* **2004**, *13* (5), 563–571.
- (55) Falcón-Pérez, J. M.; Dell'Angelica, E. C. Zinc Transporter 2 (SLC30A2) Can Suppress the Vesicular Zinc Defect of Adaptor Protein 3-Depleted Fibroblasts by Promoting Zinc Accumulation in Lysosomes. *Exp. Cell Res.* **2007**, *313* (7), 1473–1483.
- (56) Palmiter, R. D.; Cole, T. B.; Findley, S. D. ZnT-2, a Mammalian Protein That Confers Resistance to Zinc by Facilitating Vesicular Sequestration. *EMBO J* **1996**, *15* (8), 1784–1791.

- (57) Bostanci, Z.; Alam, S.; Soybel, D. I.; Kelleher, S. L. Prolactin Receptor Attenuation Induces Zinc Pool Redistribution through ZnT2 and Decreases Invasion in MDA-MB-453 Breast Cancer Cells. *Exp. Cell Res.* **2014**, *321* (2), 190–200.
- (58) Guo, L.; Lichten, L. A.; Ryu, M.-S.; Liuzzi, J. P.; Wang, F.; Cousins, R. J. STAT5-Glucocorticoid Receptor Interaction and MTF-1 Regulate the Expression of ZnT2 (Slc30a2) in Pancreatic Acinar Cells. *Proc. Natl. Acad. Sci. U.S.A.* **2010**, *107* (7), 2818–2823.
- (59) Guo, L.; Cousins, R. J. Zinc-Regulated ZnT1 (SLC30A1) and Glucocorticoid-Regulated ZnT2 (SLC30A2) Influence Zinc Efflux from Pancreatic Acinar Cells. *The FASEB Journal* **2009**, *23* (1_supplement), 216.5-216.5.
- (60) Lopez, V.; Kelleher, S. L. Zinc Transporter-2 (ZnT2) Variants Are Localized to Distinct Subcellular Compartments and Functionally Transport Zinc. *Biochemical Journal* **2009**, *422* (1), 43–52.
- (61) Dufner-Beattie, J.; Kuo, Y.-M.; Gitschier, J.; Andrews, G. K. The Adaptive Response to Dietary Zinc in Mice Involves the Differential Cellular Localization and Zinc Regulation of the Zinc Transporters ZIP4 and ZIP5. *J. Biol. Chem.* **2004**, *279* (47), 49082–49090.
- (62) Wenzel, H. J.; Cole, T. B.; Born, D. E.; Schwartzkroin, P. A.; Palmiter, R. D. Ultrastructural Localization of Zinc Transporter-3 (ZnT-3) to Synaptic Vesicle Membranes within Mossy Fiber Boutons in the Hippocampus of Mouse and Monkey. *PNAS* **1997**, *94* (23), 12676–12681.
- (63) Cole, T. B.; Wenzel, H. J.; Kafer, K. E.; Schwartzkroin, P. A.; Palmiter, R. D. Elimination of Zinc from Synaptic Vesicles in the Intact Mouse Brain by Disruption of the ZnT3 Gene. *Proc. Natl. Acad. Sci. U.S.A.* **1999**, *96* (4), 1716–1721.
- (64) Hogstrand, C.; Kille, P.; Ackland, M. L.; Hiscox, S.; Taylor, K. M. A Mechanism for Epithelial-Mesenchymal Transition and Anoikis Resistance in Breast Cancer Triggered by Zinc Channel ZIP6 and STAT3 (Signal Transducer and Activator of Transcription 3). *Biochem. J.* **2013**, *455* (2), 229–237.
- (65) Kukic, I.; Lee, J. K.; Coblentz, J.; Kelleher, S. L.; Kiselyov, K. Zinc-Dependent Lysosomal Enlargement in TRPML1-Deficient Cells Involves MTF-1 Transcription Factor and ZnT4 (Slc30a4) Transporter. *Biochem. J.* **2013**, *451* (2), 155–163.
- (66) McCormick, N. H.; Kelleher, S. L. ZnT4 Provides Zinc to Zinc-Dependent Proteins in the Trans-Golgi Network Critical for Cell Function and Zn Export in Mammary Epithelial Cells. *Am J Physiol Cell Physiol* **2012**, *303* (3), C291–C297.

- (67) Taylor, K. M.; Morgan, H. E.; Johnson, A.; Nicholson, R. I. Structure-Function Analysis of HKE4, a Member of the New LIV-1 Subfamily of Zinc Transporters. *Biochem. J.* **2004**, 377 (Pt 1), 131–139.
- (68) Huang, L.; Kirschke, C. P.; Zhang, Y.; Yu, Y. Y. The ZIP7 Gene (Slc39a7) Encodes a Zinc Transporter Involved in Zinc Homeostasis of the Golgi Apparatus. *J. Biol. Chem.* **2005**, 280 (15), 15456–15463.
- (69) Kambe, T.; Narita, H.; Yamaguchi-Iwai, Y.; Hirose, J.; Amano, T.; Sugiura, N.; Sasaki, R.; Mori, K.; Iwanaga, T.; Nagao, M. Cloning and Characterization of a Novel Mammalian Zinc Transporter, Zinc Transporter 5, Abundantly Expressed in Pancreatic Beta Cells. *J. Biol. Chem.* **2002**, 277 (21), 19049–19055.
- (70) Suzuki, T.; Ishihara, K.; Migaki, H.; Matsuura, W.; Kohda, A.; Okumura, K.; Nagao, M.; Yamaguchi-Iwai, Y.; Kambe, T. Zinc Transporters, ZnT5 and ZnT7, Are Required for the Activation of Alkaline Phosphatases, Zinc-Requiring Enzymes That Are Glycosylphosphatidylinositol-Anchored to the Cytoplasmic Membrane. *J. Biol. Chem.* **2005**, 280 (1), 637–643.
- (71) He, L.; Girijashanker, K.; Dalton, T. P.; Reed, J.; Li, H.; Soleimani, M.; Nebert, D. W. ZIP8, Member of the Solute-Carrier-39 (SLC39) Metal-Transporter Family: Characterization of Transporter Properties. *Mol. Pharmacol.* **2006**, 70 (1), 171–180.
- (72) Aydemir, T. B.; Liuzzi, J. P.; McClellan, S.; Cousins, R. J. Zinc Transporter ZIP8 (SLC39A8) and Zinc Influence IFN-Gamma Expression in Activated Human T Cells. *J. Leukoc. Biol.* **2009**, 86 (2), 337–348.
- (73) Begum, N. A.; Kobayashi, M.; Moriwaki, Y.; Matsumoto, M.; Toyoshima, K.; Seya, T. Mycobacterium Bovis BCG Cell Wall and Lipopolysaccharide Induce a Novel Gene, BIGM103, Encoding a 7-TM Protein: Identification of a New Protein Family Having Zn-Transporter and Zn-Metalloprotease Signatures. *Genomics* **2002**, 80 (6), 630–645.
- (74) Huang, L.; Kirschke, C. P.; Gitschier, J. Functional Characterization of a Novel Mammalian Zinc Transporter, ZnT6. *J. Biol. Chem.* **2002**, 277 (29), 26389–26395.
- (75) Matsuura, W.; Yamazaki, T.; Yamaguchi-Iwai, Y.; Masuda, S.; Nagao, M.; Andrews, G. K.; Kambe, T. SLC39A9 (ZIP9) Regulates Zinc Homeostasis in the Secretory Pathway: Characterization of the ZIP Subfamily I Protein in Vertebrate Cells. *Biosci. Biotechnol. Biochem.* **2009**, 73 (5), 1142–1148.
- (76) Berg, A. H.; Rice, C. D.; Rahman, M. S.; Dong, J.; Thomas, P. Identification and Characterization of Membrane Androgen Receptors in the ZIP9 Zinc Transporter

- Subfamily: I. Discovery in Female Atlantic Croaker and Evidence ZIP9 Mediates Testosterone-Induced Apoptosis of Ovarian Follicle Cells. *Endocrinology* **2014**, *155* (11), 4237–4249.
- (77) Kirschke, C. P.; Huang, L. ZnT7, a Novel Mammalian Zinc Transporter, Accumulates Zinc in the Golgi Apparatus. *J. Biol. Chem.* **2003**, *278* (6), 4096–4102.
- (78) Lichten, L. A.; Ryu, M.-S.; Guo, L.; Embury, J.; Cousins, R. J. MTF-1-Mediated Repression of the Zinc Transporter Zip10 Is Alleviated by Zinc Restriction. *PLOS ONE* **2011**, *6* (6), e21526.
- (79) Chimienti, F.; Devergnas, S.; Favier, A.; Seve, M. Identification and Cloning of a β -Cell-Specific Zinc Transporter, ZnT-8, Localized Into Insulin Secretory Granules. *Diabetes* **2004**, *53* (9), 2330–2337.
- (80) Kelleher, S. L.; Velasquez, V.; Croxford, T. P.; McCormick, N. H.; Lopez, V.; MacDavid, J. Mapping the Zinc-Transporting System in Mammary Cells: Molecular Analysis Reveals a Phenotype-Dependent Zinc-Transporting Network during Lactation. *J. Cell. Physiol.* **2012**, *227* (4), 1761–1770.
- (81) Martin, A. B.; Aydemir, T. B.; Guthrie, G. J.; Samuelson, D. A.; Chang, S.-M.; Cousins, R. J. Gastric and Colonic Zinc Transporter ZIP11 (Slc39a11) in Mice Responds to Dietary Zinc and Exhibits Nuclear Localization. *J. Nutr.* **2013**, *143* (12), 1882–1888.
- (82) Bosomworth, H. J.; Thornton, J. K.; Coneyworth, L. J.; Ford, D.; Valentine, R. A. Efflux Function, Tissue-Specific Expression and Intracellular Trafficking of the Zn Transporter ZnT10 Indicate Roles in Adult Zn Homeostasis. *Metallomics* **2012**, *4* (8), 771–779.
- (83) Patrushev, N.; Seidel-Rogol, B.; Salazar, G. Angiotensin II Requires Zinc and Downregulation of the Zinc Transporters ZnT3 and ZnT10 to Induce Senescence of Vascular Smooth Muscle Cells. *PLoS ONE* **2012**, *7* (3), e33211.
- (84) Chowanadisai, W.; Graham, D. M.; Keen, C. L.; Rucker, R. B.; Messerli, M. A. Neurulation and Neurite Extension Require the Zinc Transporter ZIP12 (Slc39a12). *Proc. Natl. Acad. Sci. U.S.A.* **2013**, *110* (24), 9903–9908.
- (85) A. Colvin, R.; R. Holmes, W.; P. Fontaine, C.; Maret, W. Cytosolic Zinc Buffering and Muffling: Their Role in Intracellular Zinc Homeostasis. *Metallomics* **2010**, *2* (5), 306–317.
- (86) Kang, Y. J. Metallothionein Redox Cycle and Function. *Exp Biol Med (Maywood)* **2006**, *231* (9), 1459–1467.

- (87) Jiang, L.-J.; Maret, W.; Vallee, B. L. The Glutathione Redox Couple Modulates Zinc Transfer from Metallothionein to Zinc-Depleted Sorbitol Dehydrogenase. *PNAS* **1998**, *95* (7), 3483–3488.
- (88) Kelly, E. J.; Quaife, C. J.; Froelick, G. J.; Palmiter, R. D. Metallothionein I and II Protect against Zinc Deficiency and Zinc Toxicity in Mice. *J Nutr* **1996**, *126* (7), 1782–1790.
- (89) Krężel, A.; Maret, W. Zinc-Buffering Capacity of a Eukaryotic Cell at Physiological PZn. *J Biol Inorg Chem* **2006**, *11* (8), 1049–1062.
- (90) Maret, W. The Function of Zinc Metallothionein: A Link between Cellular Zinc and Redox State. *J Nutr* **2000**, *130* (5), 1455S–1458S.
- (91) Maret, W. Oxidative Metal Release from Metallothionein via Zinc-Thiol/Disulfide Interchange. *PNAS* **1994**, *91* (1), 237–241.
- (92) Malaiyandi, L. M.; Dineley, K. E.; Reynolds, I. J. Divergent Consequences Arise from Metallothionein Overexpression in Astrocytes: Zinc Buffering and Oxidant-Induced Zinc Release. *Glia* **45** (4), 346–353.
- (93) Aizenman, E.; Stout, A. K.; Hartnett, K. A.; Dineley, K. E.; McLaughlin, B.; Reynolds, I. J. Induction of Neuronal Apoptosis by Thiol Oxidation: Putative Role of Intracellular Zinc Release. *J. Neurochem.* **2000**, *75* (5), 1878–1888.
- (94) Lee, S.-J.; Koh, J.-Y. Roles of Zinc and Metallothionein-3 in Oxidative Stress-Induced Lysosomal Dysfunction, Cell Death, and Autophagy in Neurons and Astrocytes. *Mol Brain* **2010**, *3* (1), 30.
- (95) Maret, W. Metallothionein/Disulfide Interactions, Oxidative Stress, and the Mobilization of Cellular Zinc. *Neurochemistry International* **1995**, *27* (1), 111–117.
- (96) Jacob, C.; Maret, W.; Vallee, B. L. Selenium Redox Biochemistry of Zinc-Sulfur Coordination Sites in Proteins and Enzymes. *Proc. Natl. Acad. Sci. U.S.A.* **1999**, *96* (5), 1910–1914.
- (97) Maret, W.; Vallee, B. L. Thiolate Ligands in Metallothionein Confer Redox Activity on Zinc Clusters. *Proc. Natl. Acad. Sci. U.S.A.* **1998**, *95* (7), 3478–3482.
- (98) Cortese-Krott, M. M.; Münchow, M.; Pirev, E.; Heßner, F.; Bozkurt, A.; Uciechowski, P.; Pallua, N.; Kröncke, K.-D.; Suschek, C. V. Silver Ions Induce Oxidative Stress and Intracellular Zinc Release in Human Skin Fibroblasts. *Free Radical Biology and Medicine* **2009**, *47* (11), 1570–1577.

- (99) Kroncke, K. D.; Fehsel, K.; Schmidt, T.; Zenke, F. T.; Dasting, I.; Wesener, J. R.; Bettermann, H.; Breunig, K. D.; Kolbbachofen, V. Nitric Oxide Destroys Zinc-Sulfur Clusters Inducing Zinc Release from Metallothionein and Inhibition of the Zinc Finger-Type Yeast Transcription Activator LAC9. *Biochemical and Biophysical Research Communications* **1994**, *200* (2), 1105–1110.
- (100) Pearce, L. L.; Gandley, R. E.; Han, W.; Wasserloos, K.; Stitt, M.; Kanai, A. J.; McLaughlin, M. K.; Pitt, B. R.; Levitan, E. S. Role of Metallothionein in Nitric Oxide Signaling as Revealed by a Green Fluorescent Fusion Protein. *Proc. Natl. Acad. Sci. U.S.A.* **2000**, *97* (1), 477–482.
- (101) Günther, V.; Lindert, U.; Schaffner, W. The Taste of Heavy Metals: Gene Regulation by MTF-1. *Biochimica et Biophysica Acta (BBA) - Molecular Cell Research* **2012**, *1823* (9), 1416–1425.
- (102) Günes, Ç.; Heuchel, R.; Georgiev, O.; Müller, K.-H.; Lichtlen, P.; Blüthmann, H.; Marino, S.; Aguzzi, A.; Schaffner, W. Embryonic Lethality and Liver Degeneration in Mice Lacking the Metal-responsive Transcriptional Activator MTF-1. *The EMBO Journal* **1998**, *17* (10), 2846–2854.
- (103) Wang, Y.; Wimmer, U.; Lichtlen, P.; Inderbitzin, D.; Stieger, B.; Meier, P. J.; Hunziker, L.; Stallmach, T.; Forrer, R.; Rülcke, T.; et al. Metal-Responsive Transcription Factor-1 (MTF-1) Is Essential for Embryonic Liver Development and Heavy Metal Detoxification in the Adult Liver. *The FASEB Journal* **2004**, *18* (10), 1071–1079.
- (104) Langmade, S. J.; Ravindra, R.; Daniels, P. J.; Andrews, G. K. The Transcription Factor MTF-1 Mediates Metal Regulation of the Mouse ZnT1 Gene. *J. Biol. Chem.* **2000**, *275* (44), 34803–34809.
- (105) J. Hardyman, J. E.; Tyson, J.; A. Jackson, K.; Aldridge, C.; J. Cockell, S.; A. Wakeling, L.; A. Valentine, R.; Ford, D. Zinc Sensing by Metal-Responsive Transcription Factor 1 (MTF1) Controls Metallothionein and ZnT1 Expression to Buffer the Sensitivity of the Transcriptome Response to Zinc. *Metallomics* **2016**, *8* (3), 337–343.
- (106) Kim, J.-H.; Jeon, J.; Shin, M.; Won, Y.; Lee, M.; Kwak, J.-S.; Lee, G.; Rhee, J.; Ryu, J.-H.; Chun, C.-H.; et al. Regulation of the Catabolic Cascade in Osteoarthritis by the Zinc-ZIP8-MTF1 Axis. *Cell* **2014**, *156* (4), 730–743.
- (107) Kitamura, H.; Morikawa, H.; Kamon, H.; Iguchi, M.; Hojyo, S.; Fukada, T.; Yamashita, S.; Kaisho, T.; Akira, S.; Murakami, M.; et al. Toll-like Receptor-Mediated Regulation of Zinc Homeostasis Influences Dendritic Cell Function. *Nat. Immunol.* **2006**, *7* (9), 971–977.

- (108) Kong, B. Y.; Duncan, F. E.; Que, E. L.; Kim, A. M.; O'Halloran, T. V.; Woodruff, T. K. Maternally-Derived Zinc Transporters ZIP6 and ZIP10 Drive the Mammalian Oocyte-to-Egg Transition. *Mol. Hum. Reprod.* **2014**, *20* (11), 1077–1089.
- (109) Miyai, T.; Hojyo, S.; Ikawa, T.; Kawamura, M.; Irié, T.; Ogura, H.; Hijikata, A.; Bin, B.-H.; Yasuda, T.; Kitamura, H.; et al. Zinc Transporter SLC39A10/ZIP10 Facilitates Antiapoptotic Signaling during Early B-Cell Development. *Proc. Natl. Acad. Sci. U.S.A.* **2014**, *111* (32), 11780–11785.
- (110) Ryu, M.-S.; Lichten, L. A.; Liuzzi, J. P.; Cousins, R. J. Zinc Transporters ZnT1 (Slc30a1), Zip8 (Slc39a8), and Zip10 (Slc39a10) in Mouse Red Blood Cells Are Differentially Regulated during Erythroid Development and by Dietary Zinc Deficiency. *J. Nutr.* **2008**, *138* (11), 2076–2083.
- (111) Homma, K.; Fujisawa, T.; Tsuburaya, N.; Yamaguchi, N.; Kadowaki, H.; Takeda, K.; Nishitoh, H.; Matsuzawa, A.; Naguro, I.; Ichijo, H. SOD1 as a Molecular Switch for Initiating the Homeostatic ER Stress Response under Zinc Deficiency. *Mol. Cell* **2013**, *52* (1), 75–86.
- (112) Ishihara, K.; Yamazaki, T.; Ishida, Y.; Suzuki, T.; Oda, K.; Nagao, M.; Yamaguchi-Iwai, Y.; Kambe, T. Zinc Transport Complexes Contribute to the Homeostatic Maintenance of Secretory Pathway Function in Vertebrate Cells. *J. Biol. Chem.* **2006**, *281* (26), 17743–17750.
- (113) Liu, M.; Bao, S.; Gálvez-Peralta, M.; Pyle, C. J.; Rudawsky, A. C.; Pavlovicz, R. E.; Killilea, D. W.; Li, C.; Nebert, D. W.; Wewers, M. D.; et al. ZIP8 Regulates Host Defense through Zinc-Mediated Inhibition of NF- κ B. *Cell Reports* **2013**, *3* (2), 386–400.
- (114) Zhao, L.; Oliver, E.; Maratou, K.; Atanur, S. S.; Dubois, O. D.; Cotroneo, E.; Chen, C.-N.; Wang, L.; Arce, C.; Chabosseau, P. L.; et al. The Zinc Transporter ZIP12 Regulates the Pulmonary Vascular Response to Chronic Hypoxia. *Nature* **2015**, *524* (7565), 356–360.
- (115) Jackson, K. A.; Helston, R. M.; McKay, J. A.; O'Neill, E. D.; Mathers, J. C.; Ford, D. Splice Variants of the Human Zinc Transporter ZnT5 (SLC30A5) Are Differentially Localized and Regulated by Zinc through Transcription and mRNA Stability. *J. Biol. Chem.* **2007**, *282* (14), 10423–10431.
- (116) Weaver, B. P.; Andrews, G. K. Regulation of Zinc-Responsive Slc39a5 (Zip5) Translation Is Mediated by Conserved Elements in the 3'-Untranslated Region. *Biometals* **2012**, *25* (2), 319–335.

- (117) Song, J.; Kim, D.; Lee, C. H.; Lee, M. S.; Chun, C.-H.; Jin, E.-J. MicroRNA-488 Regulates Zinc Transporter SLC39A8/ZIP8 during Pathogenesis of Osteoarthritis. *J. Biomed. Sci.* **2013**, *20*, 31.
- (118) Mao, X.; Kim, B.-E.; Wang, F.; Eide, D. J.; Petris, M. J. A Histidine-Rich Cluster Mediates the Ubiquitination and Degradation of the Human Zinc Transporter, HZIP4, and Protects against Zinc Cytotoxicity. *J. Biol. Chem.* **2007**, *282* (10), 6992–7000.
- (119) Kambe, T.; Andrews, G. K. Novel Proteolytic Processing of the Ectodomain of the Zinc Transporter ZIP4 (SLC39A4) during Zinc Deficiency Is Inhibited by Acrodermatitis Enteropathica Mutations. *Mol. Cell. Biol.* **2009**, *29* (1), 129–139.
- (120) Wang, C.-Y.; Jenkitkasemwong, S.; Duarte, S.; Sparkman, B. K.; Shawki, A.; Mackenzie, B.; Knutson, M. D. ZIP8 Is an Iron and Zinc Transporter Whose Cell-Surface Expression Is Up-Regulated by Cellular Iron Loading. *J. Biol. Chem.* **2012**, *287* (41), 34032–34043.
- (121) Hogstrand, C.; Kille, P.; Nicholson, R. I.; Taylor, K. M. Zinc Transporters and Cancer: A Potential Role for ZIP7 as a Hub for Tyrosine Kinase Activation. *Trends in Molecular Medicine* **2009**, *15* (3), 101–111.
- (122) Nimmanon, T.; Ziliotto, S.; Morris, S.; Flanagan, L.; Taylor, K. Phosphorylation of Zinc Channel ZIP7 Drives MAPK, PI3K and MTOR Growth and Proliferation Signalling. *Metallomics* **2017**, *9* (5), 471–481.
- (123) Hessels, A. M.; Taylor, K. M.; Merks, M. Monitoring Cytosolic and ER Zn²⁺ in Stimulated Breast Cancer Cells Using Genetically Encoded FRET Sensors. *Metallomics* **2016**, *8* (2), 211–217.
- (124) Gitan, R. S.; Eide, D. J. Zinc-Regulated Ubiquitin Conjugation Signals Endocytosis of the Yeast ZRT1 Zinc Transporter. *Biochemical Journal* **2000**, *346* (2), 329–336.
- (125) Bin, B.-H.; Hojyo, S.; Hosaka, T.; Bhin, J.; Kano, H.; Miyai, T.; Ikeda, M.; Kimura-Someya, T.; Shirouzu, M.; Cho, E.-G.; et al. Molecular Pathogenesis of Spondylocheiroidysplastic Ehlers-Danlos Syndrome Caused by Mutant ZIP13 Proteins. *EMBO Mol Med* **2014**, *6* (8), 1028–1042.
- (126) Kimura, T.; Kambe, T. The Functions of Metallothionein and ZIP and ZnT Transporters: An Overview and Perspective. *International Journal of Molecular Sciences* **2016**, *17* (3), 336.
- (127) Thirumoorthy, N.; Shyam Sunder, A.; Manisenthil Kumar, K.; Senthil kumar, M.; Ganesh, G.; Chatterjee, M. A Review of Metallothionein Isoforms and Their Role in Pathophysiology. *World Journal of Surgical Oncology* **2011**, *9* (1), 54.

- (128) Cherian, M. G.; Jayasurya, A.; Bay, B.-H. Metallothioneins in Human Tumors and Potential Roles in Carcinogenesis. *Mutat. Res.* **2003**, *533* (1–2), 201–209.
- (129) Bury, N. R.; Chung, M. J.; Sturm, A.; Walker, P. A.; Hogstrand, C. Cortisol Stimulates the Zinc Signaling Pathway and Expression of Metallothioneins and ZnT1 in Rainbow Trout Gill Epithelial Cells. *Am. J. Physiol. Regul. Integr. Comp. Physiol.* **2008**, *294* (2), R623–629.
- (130) Majumder, S.; Ghoshal, K.; Li, Z.; Bo, Y.; Jacob, S. T. Silencing of Metallothionein-I Gene in Mouse Lymphosarcoma Cells by Methylation. *Oncogene* **1999**, *18* (46), 6287–6295.
- (131) Ghoshal, K.; Majumder, S.; Li, Z.; Dong, X.; Jacob, S. T. Suppression of Metallothionein Gene Expression in a Rat Hepatoma Because of Promoter-Specific DNA Methylation. *J. Biol. Chem.* **2000**, *275* (1), 539–547.
- (132) Ghoshal, K.; Datta, J.; Majumder, S.; Bai, S.; Dong, X.; Parthun, M.; Jacob, S. T. Inhibitors of Histone Deacetylase and DNA Methyltransferase Synergistically Activate the Methylated Metallothionein I Promoter by Activating the Transcription Factor MTF-1 and Forming an Open Chromatin Structure. *Mol. Cell. Biol.* **2002**, *22* (23), 8302–8319.
- (133) Li, Y.; Kimura, T.; Huyck, R. W.; Laity, J. H.; Andrews, G. K. Zinc-Induced Formation of a Coactivator Complex Containing the Zinc-Sensing Transcription Factor MTF-1, P300/CBP, and Sp1. *Mol. Cell. Biol.* **2008**, *28* (13), 4275–4284.
- (134) Okumura, F.; Li, Y.; Itoh, N.; Nakanishi, T.; Isobe, M.; Andrews, G. K.; Kimura, T. The Zinc-Sensing Transcription Factor MTF-1 Mediates Zinc-Induced Epigenetic Changes in Chromatin of the Mouse Metallothionein-I Promoter. *Biochim. Biophys. Acta* **2011**, *1809* (1), 56–62.
- (135) Chung, M. J.; Hogstrand, C.; Lee, S.-J. Cytotoxicity of Nitric Oxide Is Alleviated by Zinc-Mediated Expression of Antioxidant Genes. *Exp Biol Med (Maywood)* **2006**, *231* (9), 1555–1563.
- (136) Hasumi, M.; Suzuki, K.; Matsui, H.; Koike, H.; Ito, K.; Yamanaka, H. Regulation of Metallothionein and Zinc Transporter Expression in Human Prostate Cancer Cells and Tissues. *Cancer Letters* **2003**, *200* (2), 187–195.
- (137) Ostrakhovitch, E. A.; Olsson, P.-E.; Hofsten, J. von; Cherian, M. G. P53 Mediated Regulation of Metallothionein Transcription in Breast Cancer Cells. *Journal of Cellular Biochemistry* *102* (6), 1571–1583.
- (138) Bahadorani, S.; Mukai, S.; Egli, D.; Hilliker, A. J. Overexpression of Metal-Responsive Transcription Factor (MTF-1) in *Drosophila Melanogaster*

- Ameliorates Life-Span Reductions Associated with Oxidative Stress and Metal Toxicity. *Neurobiology of Aging* **2010**, *31* (7), 1215–1226.
- (139) Dalton, T. P.; Li, Q.; Bittel, D.; Liang, L.; Andrews, G. K. Oxidative Stress Activates Metal-Responsive Transcription Factor-1 Binding Activity OCCUPANCY IN VIVO OF METAL RESPONSE ELEMENTS IN THE METALLOTHIONEIN-I GENE PROMOTER. *J. Biol. Chem.* **1996**, *271* (42), 26233–26241.
- (140) Green, C. J.; Lichtlen, P.; Huynh, N. T.; Yanovsky, M.; Laderoute, K. R.; Schaffner, W.; Murphy, B. J. Placenta Growth Factor Gene Expression Is Induced by Hypoxia in Fibroblasts: A Central Role for Metal Transcription Factor-1. *Cancer Res.* **2001**, *61* (6), 2696–2703.
- (141) Murphy, B. J.; Andrews, G. K.; Bittel, D.; Discher, D. J.; McCue, J.; Green, C. J.; Yanovsky, M.; Giaccia, A.; Sutherland, R. M.; Laderoute, K. R.; et al. Activation of Metallothionein Gene Expression by Hypoxia Involves Metal Response Elements and Metal Transcription Factor-1. *Cancer Res* **1999**, *59* (6), 1315–1322.
- (142) der Maur, A. A.; Belser, T.; Wang, Y.; Günes, C.; Lichtlen, P.; Georgiev, O.; Schaffner, W. Characterization of the Mouse Gene for the Heavy Metal-Responsive Transcription Factor MTF-1. *Cell Stress Chaperones* **2000**, *5* (3), 196–206.
- (143) Smirnova, I. V.; Bittel, D. C.; Ravindra, R.; Jiang, H.; Andrews, G. K. Zinc and Cadmium Can Promote Rapid Nuclear Translocation of Metal Response Element-Binding Transcription Factor-1. *J. Biol. Chem.* **2000**, *275* (13), 9377–9384.
- (144) Saydam, N.; Georgiev, O.; Nakano, M. Y.; Greber, U. F.; Schaffner, W. Nucleocytoplasmic Trafficking of Metal-regulatory Transcription Factor 1 Is Regulated by Diverse Stress Signals <http://www.jbc.org> (accessed Jul 19, 2018).
- (145) Grzywacz, A.; Gdula-Argasińska, J.; Muszyńska, B.; Tyszka-Czochara, M.; Librowski, T.; Opoka, W. Metal Responsive Transcription Factor 1 (MTF-1) Regulates Zinc Dependent Cellular Processes at the Molecular Level. *Acta Biochim. Pol.* **2015**, *62* (3), 491–498.
- (146) Bittel, D. C.; Smirnova, I. V.; Andrews, G. K. Functional Heterogeneity in the Zinc Fingers of Metalloregulatory Protein Metal Response Element-Binding Transcription Factor-1. *J. Biol. Chem.* **2000**, *275* (47), 37194–37201.
- (147) Oakley, R. H.; Cidlowski, J. A. The Biology of the Glucocorticoid Receptor: New Signaling Mechanisms in Health and Disease. *J Allergy Clin Immunol* **2013**, *132* (5), 1033–1044.

- (148) Barnes, P. J. Anti-Inflammatory Actions of Glucocorticoids: Molecular Mechanisms. *Clin. Sci.* **1998**, *94* (6), 557–572.
- (149) Sapolsky, R. M.; Romero, L. M.; Munck, A. U. How Do Glucocorticoids Influence Stress Responses? Integrating Permissive, Suppressive, Stimulatory, and Preparative Actions. *Endocr. Rev.* **2000**, *21* (1), 55–89.
- (150) Baxter, J. D. Glucocorticoid Hormone Action. *Pharmacology & Therapeutics. Part B: General and Systematic Pharmacology* **1976**, *2* (3), 605–659.
- (151) Dostert, A.; Heinzl, T. Negative Glucocorticoid Receptor Response Elements and Their Role in Glucocorticoid Action. *Curr Pharm Des* **2004**, *10* (23), 2807–2816.
- (152) Orchinik, M.; Murray, T. F.; Moore, F. L. A Corticosteroid Receptor in Neuronal Membranes. *Science* **1991**, *252* (5014), 1848–1851.
- (153) Orchinik, M.; Murray, T. F.; Franklin, P. H.; Moore, F. L. Guanyl Nucleotides Modulate Binding to Steroid Receptors in Neuronal Membranes. *Proc. Natl. Acad. Sci. U.S.A.* **1992**, *89* (9), 3830–3834.
- (154) French-Mullen, J. M. Cortisol Inhibition of Calcium Currents in Guinea Pig Hippocampal CA1 Neurons via G-Protein-Coupled Activation of Protein Kinase C. *J. Neurosci.* **1995**, *15* (1), 903–911.
- (155) He, L.-M.; Zhang, C.-G.; Zhou, Z.; Xu, T. Rapid Inhibitory Effects of Corticosterone on Calcium Influx in Rat Dorsal Root Ganglion Neurons. *Neuroscience* **2003**, *116* (2), 325–333.
- (156) Iwasaki, Y.; Aoki, Y.; Katahira, M.; Oiso, Y.; Saito, H. Non-Genomic Mechanisms of Glucocorticoid Inhibition of Adrenocorticotropin Secretion: Possible Involvement of GTP-Binding Protein. *Biochemical and Biophysical Research Communications* **1997**, *235* (2), 295–299.
- (157) Di, S.; Malcher-Lopes, R.; Halmos, K. C.; Tasker, J. G. Nongenomic Glucocorticoid Inhibition via Endocannabinoid Release in the Hypothalamus: A Fast Feedback Mechanism. *J. Neurosci.* **2003**, *23* (12), 4850–4857.
- (158) Malcher-Lopes, R.; Di, S.; Marcheselli, V. S.; Weng, F.-J.; Stuart, C. T.; Bazan, N. G.; Tasker, J. G. Opposing Crosstalk between Leptin and Glucocorticoids Rapidly Modulates Synaptic Excitation via Endocannabinoid Release. *J. Neurosci.* **2006**, *26* (24), 6643–6650.
- (159) Han, J.-Z.; Lin, W.; Chen, Y.-Z. Inhibition of ATP-Induced Calcium Influx in HT4 Cells by Glucocorticoids: Involvement of Protein Kinase A. *Acta Pharmacol. Sin.* **2005**, *26* (2), 199–204.

- (160) Beltramini, M.; Zambenedetti, P.; Wittkowski, W.; Zatta, P. Effects of Steroid Hormones on the Zn, Cu and MTI/II Levels in the Mouse Brain. *Brain Res.* **2004**, *1013* (1), 134–141.
- (161) Puissant, C.; Houdebine, L. M. Cortisol Induces Rapid Accumulation of Whey Acid Protein mRNA but Not of AsI and B-Casein mRNA in Rabbit Mammary Explants. *Cell Biol. Int. Rep.* **1991**, *15* (2), 121–129.
- (162) Cox, R. P.; Ruckenstein, A. Studies on the Mechanism of Hormonal Stimulation of Zinc Uptake in Human Cell Cultures: Hormone-Cell Interactions and Characteristics of Zinc Accumulation. *J. Cell. Physiol.* **1971**, *77* (1), 71–81.
- (163) Cousins, R. J.; Coppen, D. E. Regulation of Liver Zinc Metabolism and Metallothionein by CAMP, Glucagon and Glucocorticoids and Suppression of Free Radicals by Zinc. *Experientia Suppl.* **1987**, *52*, 545–553.
- (164) Oliver, P. D.; Tate, D. J.; Newsome, D. A. Metallothionein in Human Retinal Pigment Epithelial Cells: Expression, Induction and Zinc Uptake. *Curr. Eye Res.* **1992**, *11* (2), 183–188.
- (165) Zheng, Y.; Huang, J.; Tao, L.; Shen, Z.; Li, H.; Mo, F.; Wang, X.; Wang, S.; Shen, H. Corticosterone Increases Intracellular Zn(2+) Release in Hippocampal HT-22 Cells. *Neurosci. Lett.* **2015**, *588*, 172–177.
- (166) Hager, L. J.; Palmiter, R. D. Transcriptional Regulation of Mouse Liver Metallothionein-I Gene by Glucocorticoids. *Nature* **1981**, *291* (5813), 340–342.
- (167) Kelly, E. J.; Sandgren, E. P.; Brinster, R. L.; Palmiter, R. D. A Pair of Adjacent Glucocorticoid Response Elements Regulate Expression of Two Mouse Metallothionein Genes. *PNAS* **1997**, *94* (19), 10045–10050.
- (168) Gee, K. R.; Zhou, Z.-L.; Ton-That, D.; Sensi, S. L.; Weiss, J. H. Measuring Zinc in Living Cells.: A New Generation of Sensitive and Selective Fluorescent Probes. *Cell Calcium* **2002**, *31* (5), 245–251.
- (169) FluoZinTM-3, AM, Cell Permeant, Catalog Number F24195, Thermo Fisher Scientific.
- (170) Bole-Feysot, C.; Goffin, V.; Edery, M.; Binart, N.; Kelly, P. A. Prolactin (PRL) and Its Receptor: Actions, Signal Transduction Pathways and Phenotypes Observed in PRL Receptor Knockout Mice. *Endocr Rev* **1998**, *19* (3), 225–268.
- (171) Watson, C. J.; Burdon, T. G. Prolactin Signal Transduction Mechanisms in the Mammary Gland: The Role of the Jak/Stat Pathway. *Rev. Reprod.* **1996**, *1* (1), 1–5.

- (172) Hynes, N. E.; Cella, N.; Wartmann, M. Prolactin Mediated Intracellular Signaling in Mammary Epithelial Cells. *J Mammary Gland Biol Neoplasia* **1997**, 2 (1), 19–27.
- (173) Qian, L.; Lopez, V.; Seo, Y. A.; Kelleher, S. L. Prolactin Regulates ZNT2 Expression through the JAK2/STAT5 Signaling Pathway in Mammary Cells. *Am J Physiol Cell Physiol* **2009**, 297 (2), C369–C377.
- (174) Seo, Y. A.; Lee, S.; Hennigar, S. R.; Kelleher, S. L. Prolactin (PRL)-Stimulated Ubiquitination of ZnT2 Mediates a Transient Increase in Zinc Secretion Followed by ZnT2 Degradation in Mammary Epithelial Cells. *J. Biol. Chem.* **2014**, 289 (34), 23653–23661.
- (175) Butrimovitz, G. P.; Purdy, W. C. The Determination of Zinc in Blood Plasma by Atomic Absorption Spectrometry. *Analytica Chimica Acta* **1977**, 94 (1), 63–73.
- (176) Hohnadel, D. C.; Sunderman, F. W.; Nechay, M. W.; McNeely, M. D. Atomic Absorption Spectrometry of Nickel, Copper, Zinc, and Lead in Sweat Collected from Healthy Subjects during Sauna Bathing. *Clinical Chemistry* **1973**, 19 (11), 1288–1292.
- (177) Siraj, K.; Kitte, S. A. Analysis of Copper, Zinc and Lead Using Atomic Absorption Spectrophotometer in Ground Water of Jimma Town of Southwestern Ethiopia. *International Journal of Chemical and Analytical Science* **2013**, 4 (4), 201–204.
- (178) Hill, S. J.; Fisher, A. S. Atomic Absorption, Methods and Instrumentation*. In *Encyclopedia of Spectroscopy and Spectrometry (Second Edition)*; Lindon, J. C., Ed.; Academic Press: Oxford, 1999; pp 46–53.
- (179) Dasgupta, A.; Wahed, A. Chapter 1 - Instrumentation and Analytical Methods. In *Clinical Chemistry, Immunology and Laboratory Quality Control*; Dasgupta, A., Wahed, A., Eds.; Elsevier: San Diego, 2014; pp 1–18.
- (180) Fuwa, K.; Pulido, P.; McKay, R.; Vallee, B. L. Determination of Zinc in Biological Materials by Atomic Absorption Spectrometry. *Anal. Chem.* **1964**, 36 (13), 2407–2411.
- (181) Beauchemin, D. Inductively Coupled Plasma Mass Spectrometry. *Anal. Chem.* **2010**, 82 (12), 4786–4810.
- (182) Houk, R. S.; Thompson, J. J. Inductively Coupled Plasma Mass Spectrometry. *Mass Spectrometry Reviews* 7 (4), 425–461.
- (183) Carpenter, M. C.; Lo, M. N.; Palmer, A. E. Techniques for Measuring Cellular Zinc. *Archives of Biochemistry and Biophysics* **2016**, 611 (Supplement C), 20–29.

- (184) Becker, J. S.; Zoriy, M.; Matusch, A.; Wu, B.; Salber, D.; Palm, C.; Becker, J. S. Bioimaging of Metals by Laser Ablation Inductively Coupled Plasma Mass Spectrometry (LA-ICP-MS). *Mass Spectrometry Reviews* **29** (1), 156–175.
- (185) Paunesku, T.; Vogt, S.; Maser, J.; Lai, B.; Woloschak, G. X-Ray Fluorescence Microprobe Imaging in Biology and Medicine. *Journal of Cellular Biochemistry* **99** (6), 1489–1502.
- (186) Donner, E.; Howard, D. L.; Jonge, M. D. de; Paterson, D.; Cheah, M. H.; Naidu, R.; Lombi, E. X-Ray Absorption and Micro X-Ray Fluorescence Spectroscopy Investigation of Copper and Zinc Speciation in Biosolids. *Environ. Sci. Technol.* **2011**, *45* (17), 7249–7257.
- (187) Zhao, F.-J.; Moore, K. L.; Lombi, E.; Zhu, Y.-G. Imaging Element Distribution and Speciation in Plant Cells. *Trends in Plant Science* **2014**, *19* (3), 183–192.
- (188) Frederickson, C. J.; Kasarskis, E. J.; Ringo, D.; Frederickson, R. E. A Quinoline Fluorescence Method for Visualizing and Assaying the Histochemically Reactive Zinc (Bouton Zinc) in the Brain. *J. Neurosci. Methods* **1987**, *20* (2), 91–103.
- (189) Zalewski, P. D.; Forbes, I. J.; Betts, W. H. Correlation of Apoptosis with Change in Intracellular Labile Zn(II) Using Zinquin [(2-Methyl-8-p-Toluenesulphonamido-6-Quinolyloxy)Acetic Acid], a New Specific Fluorescent Probe for Zn(II). *Biochemical Journal* **1993**, *296* (2), 403–408.
- (190) Anderson, C. T.; Kumar, M.; Xiong, S.; Tzounopoulos, T. Cell-Specific Gain Modulation by Synaptically Released Zinc in Cortical Circuits of Audition. *eLife Sciences* **2017**, *6*, e29893.
- (191) Que, E. L.; Bleher, R.; Duncan, F. E.; Kong, B. Y.; Gleber, S. C.; Vogt, S.; Chen, S.; Garwin, S. A.; Bayer, A. R.; Dravid, V. P.; et al. Quantitative Mapping of Zinc Fluxes in the Mammalian Egg Reveals the Origin of Fertilization-Induced Zinc Sparks. *Nat Chem* **2015**, *7* (2), 130–139.
- (192) Taylor, K. M.; Hiscox, S.; Nicholson, R. I.; Hogstrand, C.; Kille, P. Protein Kinase CK2 Triggers Cytosolic Zinc Signaling Pathways by Phosphorylation of Zinc Channel ZIP7. *Sci Signal* **2012**, *5* (210), ra11.
- (193) Roh, H. C.; Collier, S.; Guthrie, J.; Robertson, J. D.; Kornfeld, K. Lysosome-Related Organelles in Intestinal Cells Are a Zinc Storage Site in *C. Elegans*. *Cell Metab.* **2012**, *15* (1), 88–99.
- (194) Kukic, I.; Kelleher, S. L.; Kiselyov, K. Zn²⁺ Efflux through Lysosomal Exocytosis Prevents Zn²⁺-Induced Toxicity. *J. Cell. Sci.* **2014**, *127* (Pt 14), 3094–3103.

- (195) Rivera, O. C.; Hennigar, S. R.; Kelleher, S. L. Loss of ZnT2-Mediated Zinc Transport Leads to Cytoplasmic Zinc Accumulation and Impairs Mammary Gland Involution. *The FASEB Journal* **2016**, *30* (1_supplement), 1224.14-1224.14.
- (196) Hennigar, S. R.; Seo, Y. A.; Sharma, S.; Soybel, D. I.; Kelleher, S. L. ZnT2 Is a Critical Mediator of Lysosomal-Mediated Cell Death during Early Mammary Gland Involution. *Scientific Reports* **2015**, *5*, 8033.
- (197) Rivera-Fuentes, P.; Lippard, S. J. SpiroZin1: A Reversible and PH-Insensitive, Reaction-Based, Red-Fluorescent Probe for Imaging Biological Mobile Zinc. *ChemMedChem* **2014**, *9* (6), 1238–1243.
- (198) Rivera-Fuentes, P.; Wrobel, A. T.; Zastrow, M. L.; Khan, M.; Georgiou, J.; Luyben, T. T.; Roder, J. C.; Okamoto, K.; Lippard, S. J. A Far-Red Emitting Probe for Unambiguous Detection of Mobile Zinc in Acidic Vesicles and Deep Tissue. *Chem Sci* **2015**, *6* (3), 1944–1948.
- (199) Qin, Y.; Miranda, J. G.; Stoddard, C. I.; Dean, K. M.; Galati, D. F.; Palmer, A. E. Direct Comparison of a Genetically Encoded Sensor and Small Molecule Indicator: Implications for Quantification of Cytosolic Zn²⁺. *ACS Chem. Biol.* **2013**, *8* (11), 2366–2371.
- (200) Qin, Y.; Sammond, D. W.; Braselmann, E.; Carpenter, M. C.; Palmer, A. E. Development of an Optical Zn²⁺ Probe Based on a Single Fluorescent Protein. *ACS Chem. Biol.* **2016**, *11* (10), 2744–2751.
- (201) Fudge, D. H.; Black, R.; Son, L.; LeJeune, K.; Qin, Y. Optical Recording of Zn²⁺ Dynamics in the Mitochondrial Matrix and Intermembrane Space with the GZnP2 Sensor. *ACS Chem. Biol.* **2018**, *13* (7), 1897–1905.
- (202) Plum, L. M.; Rink, L.; Haase, H. The Essential Toxin: Impact of Zinc on Human Health. *Int J Environ Res Public Health* **2010**, *7* (4), 1342–1365.
- (203) Andreini, C.; Banci, L.; Bertini, I.; Rosato, A. Counting the Zinc-Proteins Encoded in the Human Genome. *J. Proteome Res.* **2006**, *5* (1), 196–201.
- (204) Prasad, A. S.; Miale, A.; Farid, Z.; Sandstead, H. H.; Schulert, A. R. Zinc Metabolism in Patients with the Syndrome of Iron Deficiency Anemia, Hepatosplenomegaly, Dwarfism, and Hypogonadism. *J. Lab. Clin. Med.* **1963**, *61*, 537–549.
- (205) Aggett, P. J. Acrodermatitis Enteropathica. *J. Inherit. Metab. Dis.* **1983**, *6 Suppl 1*, 39–43.

- (206) Costello, L. C.; Feng, P.; Milon, B.; Tan, M.; Franklin, R. B. Role of Zinc in the Pathogenesis and Treatment of Prostate Cancer: Critical Issues to Resolve. *Prostate Cancer Prostatic Dis.* **2004**, *7* (2), 111–117.
- (207) Costello, L. C.; Franklin, R. B. Cytotoxic/Tumor Suppressor Role of Zinc for the Treatment of Cancer: An Enigma and an Opportunity. *Expert Rev Anticancer Ther* **2012**, *12* (1), 121–128.
- (208) Geraki, K.; Farquharson, M. J.; Bradley, D. A. Concentrations of Fe, Cu and Zn in Breast Tissue: A Synchrotron XRF Study. *Phys. Med. Biol.* **2002**, *47* (13), 2327.
- (209) Jin, R.; Bay, B.; Tan, P.; Tan, B. K. Metallothionein Expression and Zinc Levels in Invasive Ductal Breast Carcinoma. *Oncology Reports* **1999**, *6* (4), 871–876.
- (210) Daniels, W. M. U.; Hendricks, J.; Salie, R.; van Rensburg, S. J. A Mechanism for Zinc Toxicity in Neuroblastoma Cells. *Metab Brain Dis* **2004**, *19* (1–2), 79–88.
- (211) Feng, P.; Li, T.-L.; Guan, Z.-X.; Franklin, R. B.; Costello, L. C. Direct Effect of Zinc on Mitochondrial Apoptogenesis in Prostate Cells. *The Prostate* **2002**, *52* (4), 311–318.
- (212) Lemire, J.; Mailloux, R.; Appanna, V. D. Zinc Toxicity Alters Mitochondrial Metabolism and Leads to Decreased ATP Production in Hepatocytes. *Journal of Applied Toxicology* **2008**, *28* (2), 175–182.
- (213) Untergasser, G.; Rumpold, H.; Plas, E.; Witkowski, M.; Pfister, G.; Berger, P. High Levels of Zinc Ions Induce Loss of Mitochondrial Potential and Degradation of Antiapoptotic Bcl-2 Protein in in Vitro Cultivated Human Prostate Epithelial Cells. *Biochemical and Biophysical Research Communications* **2000**, *279* (2), 607–614.
- (214) Kambe, T.; Hashimoto, A.; Fujimoto, S. Current Understanding of ZIP and ZnT Zinc Transporters in Human Health and Diseases. *Cell. Mol. Life Sci.* **2014**, *71* (17), 3281–3295.
- (215) Lee, J.-Y.; Kim, J.-H.; Hong, S. H.; Lee, J. Y.; Cherny, R. A.; Bush, A. I.; Palmiter, R. D.; Koh, J.-Y. Estrogen Decreases Zinc Transporter 3 Expression and Synaptic Vesicle Zinc Levels in Mouse Brain. *J. Biol. Chem.* **2004**, *279* (10), 8602–8607.
- (216) Bafaro, E.; Liu, Y.; Xu, Y.; Dempsey, R. E. The Emerging Role of Zinc Transporters in Cellular Homeostasis and Cancer. *Signal Transduction and Targeted Therapy* **2017**, *2*, 17029.

- (217) Hasan, R.; Rink, L.; Haase, H. Zinc Signals in Neutrophil Granulocytes Are Required for the Formation of Neutrophil Extracellular Traps. *Innate Immun* **2013**, *19* (3), 253–264.
- (218) Brieger, A.; Rink, L.; Haase, H. Differential Regulation of TLR-Dependent MyD88 and TRIF Signaling Pathways by Free Zinc Ions. *J. Immunol.* **2013**, *191* (4), 1808–1817.
- (219) Singh, J.; Itahana, Y.; Parrinello, S.; Murata, K.; Desprez, P. Y. Molecular Cloning and Characterization of a Zinc Finger Protein Involved in Id-1-Stimulated Mammary Epithelial Cell Growth. *J. Biol. Chem.* **2001**, *276* (15), 11852–11858.
- (220) Dawid, I. B.; Breen, J. J.; Toyama, R. LIM Domains: Multiple Roles as Adapters and Functional Modifiers in Protein Interactions. *Trends Genet.* **1998**, *14* (4), 156–162.
- (221) Sum, E. Y. M.; O'Reilly, L. A.; Jonas, N.; Lindeman, G. J.; Visvader, J. E. The LIM Domain Protein Lmo4 Is Highly Expressed in Proliferating Mouse Epithelial Tissues. *J. Histochem. Cytochem.* **2005**, *53* (4), 475–486.
- (222) Boudreau, N.; Sympton, C. J.; Werb, Z.; Bissell, M. J. Suppression of ICE and Apoptosis in Mammary Epithelial Cells by Extracellular Matrix. *Science* **1995**, *267* (5199), 891–893.
- (223) Rio, M. C.; Lefebvre, O.; Santavicca, M.; Noël, A.; Chenard, M. P.; Anglard, P.; Byrne, J. A.; Okada, A.; Régnier, C. H.; Masson, R.; et al. Stromelysin-3 in the Biology of the Normal and Neoplastic Mammary Gland. *J Mammary Gland Biol Neoplasia* **1996**, *1* (2), 231–240.
- (224) Picciano, M. F.; Guthrie, H. A. Copper, Iron, and Zinc Contents of Mature Human Milk. *Am J Clin Nutr* **1976**, *29* (3), 242–254.
- (225) Kelleher, S. L.; Lönnerdal, B. Zn Transporter Levels and Localization Change Throughout Lactation in Rat Mammary Gland and Are Regulated by Zn in Mammary Cells. *J. Nutr.* **2003**, *133* (11), 3378–3385.
- (226) Love, M. I.; Huber, W.; Anders, S. Moderated Estimation of Fold Change and Dispersion for RNA-Seq Data with DESeq2. *Genome Biology* **2014**, *15*, 550.
- (227) Pfaffl, M. W. A New Mathematical Model for Relative Quantification in Real-Time RT-PCR. *Nucleic Acids Res* **2001**, *29* (9), e45–e45.
- (228) Kim, D.; Pertea, G.; Trapnell, C.; Pimentel, H.; Kelley, R.; Salzberg, S. L. TopHat2: Accurate Alignment of Transcriptomes in the Presence of Insertions, Deletions and Gene Fusions. *Genome Biology* **2013**, *14*, R36.

- (229) Anders, S.; Pyl, P. T.; Huber, W. HTSeq—a Python Framework to Work with High-Throughput Sequencing Data. *Bioinformatics* **2015**, *31* (2), 166–169.
- (230) Fiedler, B. L.; Van Buskirk, S.; Carter, K. P.; Qin, Y.; Carpenter, M. C.; Palmer, A. E.; Jimenez, R. Droplet Microfluidic Flow Cytometer For Sorting On Transient Cellular Responses Of Genetically-Encoded Sensors. *Anal. Chem.* **2017**, *89* (1), 711–719.
- (231) Ball, R. K.; Friis, R. R.; Schoenenberger, C. A.; Doppler, W.; Groner, B. Prolactin Regulation of Beta-Casein Gene Expression and of a Cytosolic 120-Kd Protein in a Cloned Mouse Mammary Epithelial Cell Line. *EMBO J* **1988**, *7* (7), 2089–2095.
- (232) Danielson, K. G.; Oborn, C. J.; Durban, E. M.; Butel, J. S.; Medina, D. Epithelial Mouse Mammary Cell Line Exhibiting Normal Morphogenesis in Vivo and Functional Differentiation in Vitro. *PNAS* **1984**, *81* (12), 3756–3760.
- (233) Gr, M.; D, G.-P.; N, C.; Bm, M.; D, T.; Ne, H. Growth, Differentiation and Survival of HC11 Mammary Epithelial Cells: Diverse Effects of Receptor Tyrosine Kinase-Activating Peptide Growth Factors. *Eur J Cell Biol* **1996**, *70* (2), 97–105.
- (234) Cella, N.; Cornejo-Uribe, R. R.; Montes, G. S.; Hynes, N. E.; Chammas, R. The Lysosomal-Associated Membrane Protein LAMP-1 Is a Novel Differentiation Marker for HC11 Mouse Mammary Epithelial Cells. *Differentiation* **1996**, *61* (2), 113–120.
- (235) Chammas, R.; Taverna, D.; Cella, N.; Santos, C.; Hynes, N. E. Laminin and Tenascin Assembly and Expression Regulate HC11 Mouse Mammary Cell Differentiation. *J Cell Sci* **1994**, *107* (4), 1031–1040.
- (236) D, T.; B, G.; Ne, H. Epidermal Growth Factor Receptor, Platelet-Derived Growth Factor Receptor, and c-ErbB-2 Receptor Activation All Promote Growth but Have Distinctive Effects upon Mouse Mammary Epithelial Cell Differentiation. *Cell Growth Differ* **1991**, *2* (3), 145–154.
- (237) Cella, N.; Groner, B.; Hynes, N. E. Characterization of Stat5a and Stat5b Homodimers and Heterodimers and Their Association with the Glucocorticoid Receptor in Mammary Cells. *Mol. Cell. Biol.* **1998**, *18* (4), 1783–1792.
- (238) Doppler, W.; Villunger, A.; Jennewein, P.; Brduscha, K.; Groner, B.; Ball, R. K. Lactogenic Hormone and Cell Type-Specific Control of the Whey Acidic Protein Gene Promoter in Transfected Mouse Cells. *Mol Endocrinol* **1991**, *5* (11), 1624–1632.
- (239) Li, S.; Rosen, J. M. Nuclear Factor I and Mammary Gland Factor (STAT5) Play a Critical Role in Regulating Rat Whey Acidic Protein Gene Expression in Transgenic Mice. *Mol. Cell. Biol.* **1995**, *15* (4), 2063–2070.

- (240) Lodish, H.; Berk, A.; Zipursky, S. L.; Matsudaira, P.; Baltimore, D.; Darnell, J. Microtubule Dynamics and Motor Proteins during Mitosis. *Molecular Cell Biology* 4th edition **2000**.
- (241) Sept, D. Microtubule Polymerization: One Step at a Time. *Current Biology* **2007**, 17 (17), R764–R766.
- (242) Tsuchiya, M.; Koizumi, Y.; Hayashi, S.; Hanaoka, M.; Tokutake, Y.; Yonekura, S. The Role of Unfolded Protein Response in Differentiation of Mammary Epithelial Cells. *Biochem. Biophys. Res. Commun.* **2017**, 484 (4), 903–908.
- (243) Galon, J.; Franchimont, D.; Hiroi, N.; Frey, G.; Boettner, A.; Ehrhart-Bornstein, M.; O'shea, J. J.; Chrousos, G. P.; Bornstein, S. R. Gene Profiling Reveals Unknown Enhancing and Suppressive Actions of Glucocorticoids on Immune Cells. *The FASEB Journal* **2002**, 16 (1), 61–71.
- (244) Tu, Y.; Chen, C.; Pan, J.; Xu, J.; Zhou, Z.-G.; Wang, C.-Y. The Ubiquitin Proteasome Pathway (UPP) in the Regulation of Cell Cycle Control and DNA Damage Repair and Its Implication in Tumorigenesis. *Int J Clin Exp Pathol* **2012**, 5 (8), 726–738.
- (245) Nakayama, K. I.; Nakayama, K. Ubiquitin Ligases: Cell-Cycle Control and Cancer. *Nature Reviews Cancer* **2006**, 6 (5), 369–381.
- (246) Lee, S.; Hennigar, S. R.; Alam, S.; Nishida, K.; Kelleher, S. L. Essential Role for Zinc Transporter 2 (ZnT2)-Mediated Zinc Transport in Mammary Gland Development and Function during Lactation. *J Biol Chem* **2015**, 290 (21), 13064–13078.
- (247) Mengheri, E.; Murgia, C.; Vignolini, F.; Nobili, F.; Gaetani, S. Metallothionein Gene Is Expressed in Developing Rat Intestine and Is Induced by Zinc but Not by Corticosteroids. *J. Nutr.* **1993**, 123 (5), 817–822.
- (248) Dindia, L.; Faught, E.; Leonenko, Z.; Thomas, R.; Vijayan, M. M. Rapid Cortisol Signaling in Response to Acute Stress Involves Changes in Plasma Membrane Order in Rainbow Trout Liver. *Am. J. Physiol. Endocrinol. Metab.* **2013**, 304 (11), E1157-1166.
- (249) Tasker, J. G.; Di, S.; Malcher-Lopes, R. Minireview: Rapid Glucocorticoid Signaling via Membrane-Associated Receptors. *Endocrinology* **2006**, 147 (12), 5549–5556.
- (250) Stahn, C.; Buttgereit, F. Genomic and Nongenomic Effects of Glucocorticoids. *Nature Reviews Rheumatology* **2008**, 4 (10), 525–533.

- (251) Wang, C.; Liu, Y.; Cao, J.-M. G Protein-Coupled Receptors: Extranuclear Mediators for the Non-Genomic Actions of Steroids. *Int J Mol Sci* **2014**, *15* (9), 15412–15425.
- (252) Gupta, N.; Mayer, D. Interaction of JAK with Steroid Receptor Function. *JAKSTAT* **2013**, *2* (4).
- (253) McCormick, N.; Velasquez, V.; Finney, L.; Vogt, S.; Kelleher, S. L. X-Ray Fluorescence Microscopy Reveals Accumulation and Secretion of Discrete Intracellular Zinc Pools in the Lactating Mouse Mammary Gland. *PLOS ONE* **2010**, *5* (6), e11078.
- (254) Lechner, J.; Welte, T.; Tomasi, J. K.; Bruno, P.; Cairns, C.; Gustafsson, J.; Doppler, W. Promoter-Dependent Synergy between Glucocorticoid Receptor and Stat5 in the Activation of Beta-Casein Gene Transcription. *J. Biol. Chem.* **1997**, *272* (33), 20954–20960.
- (255) Krężel, A.; Maret, W. The Biological Inorganic Chemistry of Zinc Ions. *Arch Biochem Biophys* **2016**, *611*, 3–19.
- (256) Qiu, M.; Shentu, Y.; Zeng, J.; Wang, X.; Yan, X.; Zhou, X.; Jing, X.; Wang, Q.; Man, H.; Wang, J.; et al. Zinc Mediates the Neuronal Activity-Dependent Anti-Apoptotic Effect. *PLoS One* **2017**, *12* (8).
- (257) Dittmer, P. J.; Miranda, J. G.; Gorski, J. A.; Palmer, A. E. Genetically Encoded Sensors to Elucidate Spatial Distribution of Cellular Zinc. *J. Biol. Chem.* **2009**, *284* (24), 16289–16297.
- (258) Hwang, J. J.; Lee, S.-J.; Kim, T.-Y.; Cho, J.-H.; Koh, J.-Y. Zinc and 4-Hydroxy-2-Nonenal Mediate Lysosomal Membrane Permeabilization Induced by H₂O₂ in Cultured Hippocampal Neurons. *J. Neurosci.* **2008**, *28* (12), 3114–3122.
- (259) Eichelsdoerfer, J. L.; Evans, J. A.; Slaugenhaupt, S. A.; Cuajungco, M. P. Zinc Dyshomeostasis Is Linked with the Loss of Mucopolidosis IV-Associated TRPML1 Ion Channel. *J. Biol. Chem.* **2010**, *285* (45), 34304–34308.
- (260) Qin, Y.; Dittmer, P. J.; Park, J. G.; Jansen, K. B.; Palmer, A. E. Measuring Steady-State and Dynamic Endoplasmic Reticulum and Golgi Zn²⁺ with Genetically Encoded Sensors. *PNAS* **2011**, *108* (18), 7351–7356.
- (261) Park, J. G.; Qin, Y.; Galati, D. F.; Palmer, A. E. New Sensors for Quantitative Measurement of Mitochondrial Zn²⁺. *ACS Chem. Biol.* **2012**, *7* (10), 1636–1640.
- (262) Miranda, J. G.; Weaver, A. L.; Qin, Y.; Park, J. G.; Stoddard, C. I.; Lin, M. Z.; Palmer, A. E. New Alternately Colored FRET Sensors for Simultaneous Monitoring of Zn²⁺ in Multiple Cellular Locations. *PLoS One* **2012**, *7* (11).

- (263) Hessels, A. M.; Chabosseau, P.; Bakker, M. H.; Engelen, W.; Rutter, G. A.; Taylor, K. M.; Merx, M. EZinCh-2: A Versatile, Genetically Encoded FRET Sensor for Cytosolic and Intraorganelle Zn²⁺ Imaging. *ACS Chem. Biol.* **2015**, *10* (9), 2126–2134.
- (264) Vinkenborg, J. L.; Nicolson, T. J.; Bellomo, E. A.; Koay, M. S.; Rutter, G. A.; Merx, M. Genetically Encoded FRET Sensors to Monitor Intracellular Zn²⁺ Homeostasis. *Nat Meth* **2009**, *6* (10), 737–740.
- (265) Chabosseau, P.; Tuncay, E.; Meur, G.; Bellomo, E. A.; Hessels, A.; Hughes, S.; Johnson, P. R. V.; Bugliani, M.; Marchetti, P.; Turan, B.; et al. Mitochondrial and ER-Targeted ECALWY Probes Reveal High Levels of Free Zn²⁺. *ACS Chem. Biol.* **2014**, *9* (9), 2111–2120.
- (266) Chung, H.; Yoon, Y. H.; Hwang, J. J.; Cho, K. S.; Koh, J. Y.; Kim, J.-G. Ethambutol-Induced Toxicity Is Mediated by Zinc and Lysosomal Membrane Permeabilization in Cultured Retinal Cells. *Toxicol. Appl. Pharmacol.* **2009**, *235* (2), 163–170.
- (267) Taylor, K. M.; Vichova, P.; Jordan, N.; Hiscox, S.; Hendley, R.; Nicholson, R. I. ZIP7-Mediated Intracellular Zinc Transport Contributes to Aberrant Growth Factor Signaling in Antihormone-Resistant Breast Cancer Cells. *Endocrinology* **2008**, *149* (10), 4912–4920.
- (268) Suh, S. W.; Gum, E. T.; Hamby, A. M.; Chan, P. H.; Swanson, R. A. Hypoglycemic Neuronal Death Is Triggered by Glucose Reperfusion and Activation of Neuronal NADPH Oxidase. *J Clin Invest* **2007**, *117* (4), 910–918.
- (269) Jayaraman, A. K.; Jayaraman, S. Increased Level of Exogenous Zinc Induces Cytotoxicity and Up-Regulates the Expression of the ZnT-1 Zinc Transporter Gene in Pancreatic Cancer Cells. *The Journal of Nutritional Biochemistry* **2011**, *22* (1), 79–88.
- (270) Chandler, P.; Kochupurakkal, B. S.; Alam, S.; Richardson, A. L.; Soybel, D. I.; Kelleher, S. L. Subtype-Specific Accumulation of Intracellular Zinc Pools Is Associated with the Malignant Phenotype in Breast Cancer. *Molecular Cancer* **2016**, *15*, 2.
- (271) Wiggins, H. L.; Wymant, J. M.; Solfa, F.; Hiscox, S. E.; Taylor, K. M.; Westwell, A. D.; Jones, A. T. Disulfiram-Induced Cytotoxicity and Endo-Lysosomal Sequestration of Zinc in Breast Cancer Cells. *Biochem Pharmacol* **2015**, *93* (3), 332–342.
- (272) Taniguchi, M.; Fukunaka, A.; Hagihara, M.; Watanabe, K.; Kamino, S.; Kambe, T.; Enomoto, S.; Hiromura, M. Essential Role of the Zinc Transporter

- ZIP9/SLC39A9 in Regulating the Activations of Akt and Erk in B-Cell Receptor Signaling Pathway in DT40 Cells. *PLOS ONE* **2013**, *8* (3), e58022.
- (273) Rohrer, J.; Schweizer, A.; Russell, D.; Kornfeld, S. The Targeting of Lamp1 to Lysosomes Is Dependent on the Spacing of Its Cytoplasmic Tail Tyrosine Sorting Motif Relative to the Membrane. *J. Cell Biol.* **1996**, *132* (4), 565–576.
- (274) Wang, C.-C.; Ng, C. P.; Lu, L.; Atlashkin, V.; Zhang, W.; Seet, L.-F.; Hong, W. A Role of VAMP8/Endobrevin in Regulated Exocytosis of Pancreatic Acinar Cells. *Dev. Cell* **2004**, *7* (3), 359–371.
- (275) Lippert, U.; Ferrari, D. M.; Jahn, R. Endobrevin/VAMP8 Mediates Exocytotic Release of Hexosaminidase from Rat Basophilic Leukaemia Cells. *FEBS Lett.* **2007**, *581* (18), 3479–3484.
- (276) Loo, L. S.; Hwang, L.-A.; Ong, Y. M.; Tay, H. S.; Wang, C.-C.; Hong, W. A Role for Endobrevin/VAMP8 in CTL Lytic Granule Exocytosis. *Eur. J. Immunol.* **2009**, *39* (12), 3520–3528.
- (277) Polgár, J.; Chung, S.-H.; Reed, G. L. Vesicle-Associated Membrane Protein 3 (VAMP-3) and VAMP-8 Are Present in Human Platelets and Are Required for Granule Secretion. *Blood* **2002**, *100* (3), 1081–1083.
- (278) Wang, C.-C.; Ng, C. P.; Shi, H.; Liew, H. C.; Guo, K.; Zeng, Q.; Hong, W. A Role for VAMP8/Endobrevin in Surface Deployment of the Water Channel Aquaporin 2. *Mol. Cell. Biol.* **2010**, *30* (1), 333–343.
- (279) Bolte, S.; Cordelières, F. P. A Guided Tour into Subcellular Colocalization Analysis in Light Microscopy. *J Microsc* **2006**, *224* (Pt 3), 213–232.
- (280) Ehrlich, M.; Boll, W.; van Oijen, A.; Hariharan, R.; Chandran, K.; Nibert, M. L.; Kirchhausen, T. Endocytosis by Random Initiation and Stabilization of Clathrin-Coated Pits. *Cell* **2004**, *118* (5), 591–605.
- (281) Yoshimori, T.; Yamamoto, A.; Moriyama, Y.; Futai, M.; Tashiro, Y. Bafilomycin A1, a Specific Inhibitor of Vacuolar-Type H(+)-ATPase, Inhibits Acidification and Protein Degradation in Lysosomes of Cultured Cells. *J. Biol. Chem.* **1991**, *266* (26), 17707–17712.
- (282) Montanini, B.; Blaudez, D.; Jeandroz, S.; Sanders, D.; Chalot, M. Phylogenetic and Functional Analysis of the Cation Diffusion Facilitator (CDF) Family: Improved Signature and Prediction of Substrate Specificity. *BMC Genomics* **2007**, *8*, 107.
- (283) Lu, M.; Chai, J.; Fu, D. Structural Basis for Autoregulation of the Zinc Transporter YiiP. *Nat. Struct. Mol. Biol.* **2009**, *16* (10), 1063–1067.

- (284) Grass, G.; Otto, M.; Fricke, B.; Haney, C. J.; Rensing, C.; Nies, D. H.; Munkelt, D. FieF (YiiP) from *Escherichia Coli* Mediates Decreased Cellular Accumulation of Iron and Relieves Iron Stress. *Arch. Microbiol.* **2005**, *183* (1), 9–18.
- (285) Shusterman, E.; Beharier, O.; Shiri, L.; Zarivach, R.; Etzion, Y.; Campbell, C. R.; Lee, I.-H.; Okabayashi, K.; Dinudom, A.; Cook, D. I.; et al. ZnT-1 Extrudes Zinc from Mammalian Cells Functioning as a Zn²⁺/H⁺ Exchanger. *Metallomics* **2014**, *6* (9), 1656–1663.
- (286) Ohana, E.; Hoch, E.; Keasar, C.; Kambe, T.; Yifrach, O.; Hershfinkel, M.; Sekler, I. Identification of the Zn²⁺ Binding Site and Mode of Operation of a Mammalian Zn²⁺ Transporter. *J. Biol. Chem.* **2009**, *284* (26), 17677–17686.
- (287) Cho, K. S.; Yoon, Y. H.; Choi, J. A.; Lee, S.-J.; Koh, J.-Y. Induction of Autophagy and Cell Death by Tamoxifen in Cultured Retinal Pigment Epithelial and Photoreceptor Cells. *Invest. Ophthalmol. Vis. Sci.* **2012**, *53* (9), 5344–5353.
- (288) Lee, S.-J.; Cho, K. S.; Koh, J.-Y. Oxidative Injury Triggers Autophagy in Astrocytes: The Role of Endogenous Zinc. *Glia* **2009**, *57* (12), 1351–1361.
- (289) Hwang, J. J.; Kim, H. N.; Kim, J.; Cho, D.-H.; Kim, M. J.; Kim, Y.-S.; Kim, Y.; Park, S.-J.; Koh, J.-Y. Zinc(II) Ion Mediates Tamoxifen-Induced Autophagy and Cell Death in MCF-7 Breast Cancer Cell Line. *Biometals* **2010**, *23* (6), 997–1013.
- (290) Hennigar, S. R.; Lanz, M. C.; Kelleher, S. L. TNF α Redistributes ZnT2 to Accumulate Zinc in Lysosomes and Activate Autophagic Cell Death in Mammary Epithelial Cells. *The FASEB Journal* **2013**, *27* (1_supplement), 234.3-234.3.

Appendix A

Protocol and Data Analysis for RT-(q)PCR

Workflow:

RNA > DNase I Treatment-> Pure RNA without DNA->RT Reaction-> 1st cDNA -> qPCR, or regular PCR Amplification

(1) DNase I treatment:

20 μ L = 4ug RNA + 2 μ L 10x rxn buffer with MgCl₂ + 2 μ L Dnase I (1unit) + 1 μ L RNaseOUT + Nuclease-free H₂O up to 20 μ L.

Incubate at 37 degree for 30min.

Add 4 μ L 50mM EDTA and incubate at 65 degree C for 10min to deactivate DNase.

Final [RNA] = 200ng/ μ l

(2) Reverse Transcription rxn: generate first-strand cDNA.

40 μ L reaction:

10x Buffer RT: 4 μ L

dNTP (5mM): 4 μ L

OligodT Primer (20uM): 2 μ L (1uM final concentratioin)

RnaseOUT (RNase Inhibitor): 2 μ L

Rnase-free H₂O: 2 μ L

RNA: 24ul (200 ng/ μ L)

OT E: 2 μ L

Final [RNA] = 100 ng/ μ L

Incubate at 37 degree for 60min. It is important to not to over-incubate reaction mix at 37 degree. cDNA can be stored at -20 or -80 degree C freezer for one week.

(3) qPCR:

96-well: 25ul /well

25 μ L = 12.5 μ L 2x SYBR Green PCR Master Mix

10 μ L cDNA (10x dilution of RT rxn mix)

2.5 μ L primer mix

Control: no template control. Replace cDNA with water or RT rxn mix without RT enzyme as templates.

(4) Regular PCR

1 μ L cDNA

0.3 μ L Casein 3 Fwd (10mM)

0.3 μ L Casein 3 Rev (10mM)

0.3 μ L dNTP (10uM)

10x PFU buffer: 1 μ L

PFU: 0.25 μ L

H₂O: up to 10 μ L

PCR running condition:

94 °C, 2min

94 °C, 30s

55 °C, 2min

72 °C, 40s

30 cycles of step 2-4,

72 °C, 10min

Table A. A. 1 Primers sequences for RT-(q)PCR

Gene name	Application	Forward Primer Sequence (5' to 3') [Final Concentration]	Reverse Primer Sequence (5' to 3') [Final Concentration]	Product Size (bp)
ACTB	RT-PCR, RT-qPCR	AGCCATGTACGTAGCCATCC [50 nM]	CTCTCAGCTGTGGTGGTGAA [50 nM]	228
RPS9	RT-PCR, RT-qPCR	ATTTACCCTGGCCAAGATCC [50 nM]	AGCTTCATCTTGCCCTCATC [50 nM]	141
CSN2	RT-PCR, RT-qPCR	TCACTCCAGCATCCAGTCACA [50 nM]	GGCCCAAGAGATGGCACCA [50 nM]	126
WAP	RT-PCR, RT-qPCR	CCGTGCCCAATGAAGATAGA [50 nM]	GCTGCTCACTGAAGGGTTAT [50 nM]	125
ZIP14	RT-qPCR	CGGTCCCAGACAACAAGATT [250 nM]	TGGCTTGTGGTGTGAAATGT [250 nM]	116
MT1	RT-qPCR	CTCCGTAGCTCCAGCTTCAC [250 nM]	AGGAGCAGCAGCTCTTCTTG [250 nM]	137
MT2	RT-qPCR	CAAACCGATCTCTCGTCGAT [200 nM]	CATTGCAATTGTTTGCATTTG [200 nM]	121

Quantification of gene expression using qPCR

Quantitative analysis of relative expression ratio (R) of target genes normalized to reference genes was performed with the Pfaffl method as previously described. Basically, the ratio R is calculated using this equation:

$$R = \frac{E(\text{target})^{\Delta CT, \text{target}(\text{control-sample})}}{E(\text{ref})^{\Delta CT, \text{ref}(\text{control-sample})}}$$

The explanation of each term in this equation refers to the following table A. A. 2. In my experiment, target genes are CSN2, WAP, ZIP14, MT1 and MT2; reference genes are ACTB and RPS9. CT value represents cycle threshold, which is the number of cycles for signals to reach a certain threshold.

Table A. A. 2

E (target)	The amplification efficiency of a target gene
E (ref)	The amplification efficiency of a reference gene
$\Delta CT, \text{target}(\text{control} - \text{sample})$	The CT value of a target gene under the control condition minus the CT value of the target gene under the experimental condition (sample)
$\Delta CT, \text{ref}(\text{control} - \text{sample})$	The CT value of a reference gene under the control condition minus the CT value of the reference gene under the experimental condition (sample)

To determine the amplification efficiency (E), a standard curve was generated by plotting the CT value of each qPCR reaction with a 10-fold serial dilution of template against the \log_{10} (dilution of template). A best-fit linear trend line was created and the

slope was acquired from this curve. E is calculated with this equation $E = 10^{[-1/\text{slope}]}$. For example, in the Figure A.A. 1, the slope of the standard curve of RPS9 reaction with 10^1 , 10^{-2} , 10^{-3} template DNA dilution is plugged in the reaction: $E = 10^{(-1/3.4285)} = 1.95$. The E for each gene amplification was calculated in the same way and is shown in the following table A. A. 3.

Figure A. A. 1 Standard curve of RPS9 qPCR reaction.

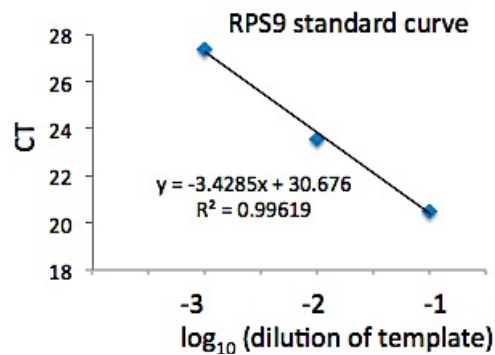


Table A. A. 3 Amplification efficiency for each gene

Gene	E	Gene	E
ACTB	1.87	ZIP14	1.93
RPS9	1.95	MT1	1.85
CSN2	1.98	MT2	2.09
WAP	2.01		

Appendix B

Top down- or up-regulated GO_BP terms in D 24 hr and D day6 samples

	Downregulated D 24hr	Downregulated D day6	Upregulated D 24hr	Upregulated D ay6
GO terms	P value	P value	P value	P value
Cell cycle	1.1248E-38	1.07845E-34	N.A.	0.999987016
Mitotic nuclear division	5.81226E-41	4.94414E-31	N.A.	N.A.
Cell division	7.84258E-38	1.22833E-28	N.A.	0.9999997
DNA replication	0.000108638	1.473E-06	N.A.	0.999426461
Cell proliferation	5.36786E-05	1.47598E-06	N.A.	0.416502521
Cellular response to DNA damage stimulus	9.12157E-07	6.57441E-06	N.A.	0.999505486
DNA repair	1.89778E-05	0.000602517	N.A.	0.999999162
Microtubule depolymerization	0.000696981	3.0701E-05	N.A.	N.A.
Microtubule-based movement	0.001604039	6.22704E-05	N.A.	N.A.
Positive regulation of cell migration	0.001604039	6.31641E-05	0.026546031	0.016206726

Inactivation of MAPK activity	0.010033256	0.000523448	N.A.	N.A.
Immune system process	N.A.	N.A.	1.74744E-06	1.32724E-06
Ion transport	0.093900291	0.006916626	0.005627542	1.66105E-05
Transmembrane transport	0.688077966	0.498319959	0.009488001	0.000418027
transport	0.863100023	0.739469543	0.16573244	0.000920184
Endoplasmic reticulum unfolded protein response	0.777724116	0.500368196	0.635770253	8.17695E-05
Cellular Zinc ion homeostasis	N.A.	0.759064037	N.A.	0.003105688
Response to peptide hormone	0.898601296	0.923048512	0.004098764	0.003375759
Positive regulation of protein phosphorylation	0.501946639	0.427429421	0.038933446	0.011894421
Response to glucocorticoid	0.676827102	0.025670645	0.204797608	0.011964716
Positive regulation of MAP kinase activity	0.815867794	0.225104366	0.102051472	0.012876377

Activation of MAPK activity	0.085063661	0.011731548	0.798179211	0.013075637
Fatty acid biosynthetic process	0.007686002	0.330744683	0.789479583	0.000335685
Lipid metabolic process	0.176263644	0.383066201	0.618051992	0.013087877
Glucose metabolic process	N.A.	0.898464477	0.761072107	0.017428649

Top down- and up-regulated zinc genes in D day6 sample

	Downregulated D day6	Upregulated Dday6
GO terms	p-value	p-value
Nucleic acid binding	6.81047E-10	0.004259146
DNA binding	1.55444E-07	0.090933838
Protein binding	5.95714E-06	0.270930119
Metallopeptidase activity	8.56237E-11	1.37174E-07
Peptidase activity	3.35924E-05	0.000322465
Ligase activity	6.17158E-05	0.039316772
Ubiquitin protein transferase activity	0.000473424	0.088130209
Ubiquitin protein ligase activity	0.007067595	0.274090331

Transcription regulatory region DNA binding	0.000851443	0.119316506
Transcription factor activity, sequence-specific DNA binding	0.003403323	0.03819728
Hydrolase activity	0.010137491	8.5E-05
Nucleotide diphosphatase activity	N.A	0.000156852
Phosphodiesterase I activity	N.A	0.02047772
Zinc ion transmembrane transporter activity	N.A	0.005684898

Appendix C

ICP-MS Protocol

For ICP-MS you need to create standard curves of two internal standards (Y and Ga) as well as a standard curve of your metal of interest (Zn). This way you can normalize the amount of Zn to the internal standard you spike into the experimental samples. A typical ICP-MS experiment should include samples as shown in this table:

ICP-MS standard curve set-up					
All samples should be made in the same volume of chelex-treated water and nitric acid as your samples					
Sample	Description	Y	Ga	Zn	other
1	Y and Ga	5 ppb	5 ppb	-	
2	Standard	10 ppb	10 ppb	-	
3	curve	25 ppb	25 ppb	-	
4	Zn Standard Curve	5 ppb	5 ppb	25 ppb	
5		5 ppb	5 ppb	100 ppb	
6		5 ppb	5 ppb	200 ppb	
7	Blank	-	-	-	your water + nitric acid
8		5 ppb	5 ppb	-	prepped cells
9	Experimental Samples	5 ppb	5 ppb	-	prepped cells
10		5 ppb	5 ppb	-	prepped cells
etc		5 ppb	5 ppb	-	prepped cells

To prepare samples:

- (1) Collect $\sim 10 \times 10^6$ cells from cell culture dish: trypsinize cells, spin down cells at 1000rpm, 5min.
- (2) Re-suspend cells in 2ml of phosphate-free HBSS buffer, count cells, transfer cells to metal-free conical tubes, spin down cells again at 1000rpm, 5min.
- (3) Discard supernatant. Cells can be frozen here. To continue the procedure, dry cells in the heat block (50 degree C) overnight in a fume hood.

(4) Next day, add 200ul nitric acid (trace-metal grade) to the cell pellet to digest the cells. (200ul nitric acid is enough to digest 10 million cells. You can always adjust the volume as necessary). To lyse cells, heat sample in hot water bath (80-100 degree C) for 30 min.

(5) Add desired amount of internal control element to the sample (5 ppb Y and Ga in each sample).

(6) After samples cool down, add 6400ul of Chelex H2O to each sample to make the final the HNO₃ concentration as ~2%.

* Final concentration of HNO₃ matters as the matrix of sample would affect mass spec. 2%-6% HNO₃ is recommended.

Data Analysis using the example in the above table:

1. Generate Y and Ga standard curve:

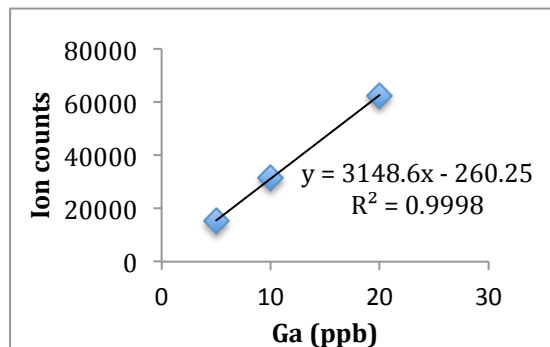
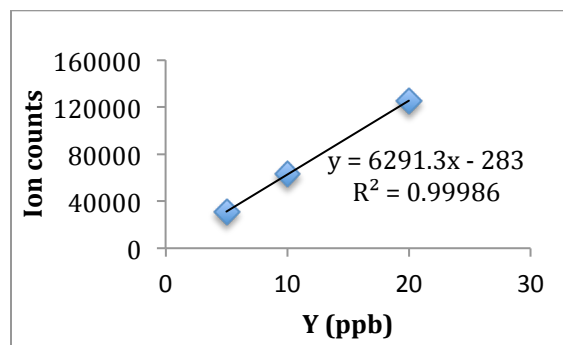
Sample (1): Blank+5 ppb Ga + 5 ppb Y

Sample (2): Blank+10 ppb Ga + 10 ppb Y

Sample (3): Blank + 20 ppb Ga + 20ppb Y

*All ion counts should subtract the background ion counts (readout from sample (7)).

Standard curve is generated by plotting ion counts against ppb.



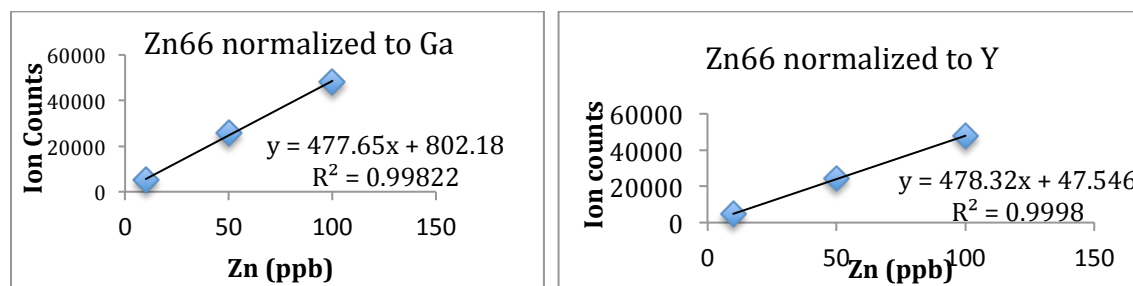
2. Generate zinc standard curve.

Sample (4): Blank + 5ppb Y+5ppb Ga + 25ppb Zn

Sample (5): Blank + 5ppb Y+5ppb Ga + 100ppb Zn

Sample (6): Blank + 5ppb Y+5ppb Ga + 200ppb Zn

First , calculate measured ppb units of Y and Ga from the Y and Ga counts in samples using the standard curves generated above. Then normalize all Zn ion counts to 5ppb Y and 5ppb Ga, respectively. Second, Zn standard curve is generated by plotting Zn ion counts with added Zn ppb.



Sample (8)-Sample (10): measure Zinc level in your cell samples

Sample (8): Cell sample1 rep#1 + 5ppb Ga+ 5ppb Y

Sample (9): Cell sample1 rep#2 + 5ppb Ga+ 5ppb Y

Sample (10): Cell sample X rep#1 + 5ppb Ga+ 5ppb Y

.

.

To convert Zn (ppb) to [Zn] per cell, first, ppb was converted to molar concentration (M): 1 ppb Zn = 1 gram (g) of Zn / 109 grams (g) of water = 15 nM (Zn atomic mass: 65.38 g/mol, 1 g of water = 1 mL of water); next, with the known volume of the sample, 15 nM was converted to total mols of Zn (Zn mols). Zn (mols) per cell was

acquired by dividing total Zn (mols) by the total cell number. To calculate [Zn] per cell, divide the Zn (mols) per cell by single cell volume (L). Single cell dimension was measured using light microscopy: length: 20 μm ; width: 15 μm ; height: 10 μm . Single cell volume = 20 μm x 15 μm x 10 μm = 3000 μm^3 = 3 x 10⁻⁹ cm³ = 3 x 10⁻⁹ mL = 3 x 10⁻¹² L.

Materials:

- (1) Trace-metal grade Nitric Acid: *02650 FLUKA*, Nitric acid. CAS number: 7696-372.
 - (2) Chelex H₂O: Add chelex beads to a big jar of MiliQ H₂O and stir overnight. The next day, filter H₂O. Chelex beads can be re-used.
 - (3) Y standard solution (10ppm): 125 mL - IV-STOCK-53-125ML, Inorganic Ventures.
 - (4) Ga standard solution (1000ppm): Gallium for ICP - CGGA1-125ML, Inorganic Ventures.
 - (5) Zn standard solution (1000ppm): VWR. VWR catalog #: RCMSZN1KN-100
-

Appendix D

Promoter Reporter Assay of Response of ZIP14, MT1 and MT2

Promoters to Lactogenic Hormones

The promoter reporter assay designed to test the promoter activity in response to hormone treatment was performed using the Secrete-Pair™ Dual Luminescence Assay Kit (GeneCopoeia™) following the manufacturer's instructions. The ZIP14 and MT2 promoters were amplified from the HC11 cell genome using the [xxxx](#) kit. The MT1 promoter was synthesized by IDT®. All promoters were inserted into the multiple cloning site 1 (MCS1) of the pEZX-LvGA01 vector (GeneCopoeia™, catalog No. ZX107) 5' upstream of the *Gaussia* Luciferase (GLuc) ORF. This vector also constitutively expresses an internal control reporter, SEAP (secreted alkaline phosphatase). Both GLuc and SEAP can be secreted into cell media upon being synthesized. The promoter activity is reported using the ratio of GLuc signal to the SEAP signal. Detailed information about promoter sequences: For ZIP14, the 1850-bp promoter sequence includes a 1349-bp fragment upstream of the TSS and a 500-bp fragment downstream of the TSS; For MT1, the 1209-bp promoter sequence includes a 956-bp fragment upstream of the TSS and a 122-bp fragment downstream of the TSS; For MT2, the 1301-bp promoter sequence includes a 1000-bp fragment upstream of the TSS and a 300-bp fragment downstream of the TSS. The TSS position was acquired from the Eukaryotic Promoter Database (EPD). HC11 cell lines stably expressing promoter

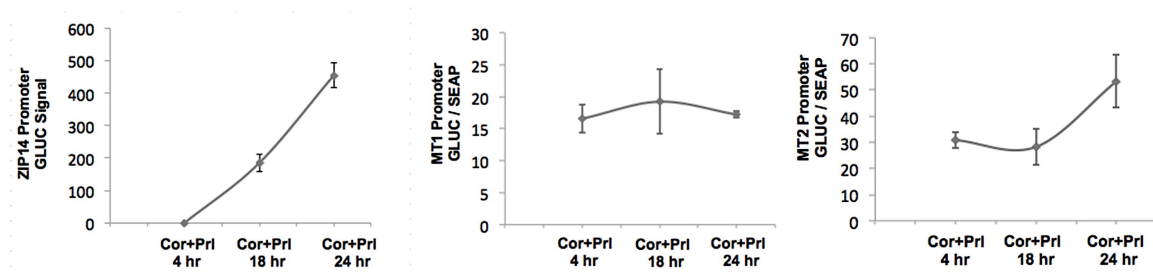
constructs were generated using lentiviral transduction and selected for successful transduction by puromycin.

To determine the promoter activity in response to lactogenic hormone treatment, 4×10^5 HC11 stable cells were plated in a 35 mm dish in the proliferation media (2 mL) for 3 days and then cultured in the resting media (2 mL) for one more day. Cells were then treated with the vesicle (resting, R), cortisol (cor), prolactin (prl) or lactogenic hormones (cor+prl) for 24 hr. For luciferase analysis, 200 μ L of media was collected at 4, 18 and 24 hr post hormone treatment. 200 μ L of fresh media was added back to cell culture to compensate for the volume change after media collection. All samples were frozen at -20 °C use. The GLuc and SEAP catalyzed luminescence reactions were performed using the Secrete-Pair™ Dual Luminescence Assay Kit (GeneCopoeia™) following the manufacturer's instructions. Luminescence was recorded using a BioTek Synergy H1 hybrid plate reader (gain: 200; integration time: 3 sec). 2 biological replicates were utilized at each time point and 3 technical replicates were measured for each biological replicate.

However, HC11 cells expressing ZIP14 promoter reporter construct did not express SEAP. The GLUC luminescence was used to represent the ZIP14 promoter activity instead of the dual luminescence. First, the promoter activity upon lactogenic hormone treatment was determined at different time points. ZIP14 and MT2 promoter response increased up to 24 hr post hormone treatment whereas MT1 promoter response transiently increased at 18 hr post hormone treatment but slightly decreased at 24hr (Figure A.C.1 (A)). To analyze the effect of each lactogenic hormone on promoter activity, promoter activity of resting, cor, prl and cor+prl cells was analyzed at

24 hr post hormone treatment (Figure A.D.1 (B)). Individual or the combination of hormones did not activate promoter compared to the vehicle group.

(A)



(B)

